UNCLASSIFIED

AD NUMBER

AD816318

NEW LIMITATION CHANGE

TO

Approved for public release, distribution unlimited

FROM

Distribution authorized to DoD only; Administrative/Operational Use; JUN 1967. Other requests shall be referred to Commanding General, U.S. Army Electronics Command, Attn: AMSEL-KL-PE, Fort Monmouth, NJ.

AUTHORITY

USAEC ltr, 1 May 1968

THIS PAGE IS UNCLASSIFIED

AD

AD816318

TECHNICAL REPORT ECOM-03743-10

HYDROCARBON-AIR FUEL CELL

SIXTH SEMI-ANNUAL REPORT

By

C. E. HEATH *M. BELTZER*

E. H. OKRENT *B. BROYDE*

P. DUBY

JUNE 1967

AD816318

ECOM

UNITED STATES ARMY ELECTRONICS COMMAND • FORT MONMOUTH, N. J.

CONTRACT DA 36-039 AMC-03743 (E)

ESSO RESEARCH AND ENGINEERING COMPANY
GOVERNMENT RESEARCH LABORATORY
Linden, N. J.

DISTRIBUTION STATEMENT

Each transmittal of this document outside the Department of Defense must have prior approval of CG, U. S. Army Electronics Command, Fort Monmouth, N. J. ATTN: AMSEL-KL-PE

NOTICES

DISCLAIMERS

The findings in this report are not to be construed as an official Department of the Army position, unless so designated by other authorized documents.

The citation of trade names and names of manufacturers in this report is not to be construed as official Government indorsement or approval of commercial products or services referenced herein.

DISPOSITION

Destroy this report when it is no longer needed. Do not return it to the originator.

Technical Report ECOM-03743-10 June 1967

HYDROCARBON-AIR FUEL CELL

Sixth Semi-Annual Report
1 August 1966 - 31 December 1966
Report No. 10

Contract No. DA 36-039 AMC-03743(E)
Task No. 1C622001A053-04

Prepared by

Carl E. Heath
Eugene H. Okrent
Morton Beltzer
Barret Broyde
Paul Duby

Esso Research and Engineering Company
Government Research Laboratory
Linden, New Jersey

For

Electronic Components Laboratory
United States Army Electronics Command, Fort Monmouth, N. J.

Distribution Statement

Each transmittal of this document outside the Department of Defense must have prior approval of CG, U.S. Army Electronics Command, Fort Monmouth, New Jersey
ATTN: AMSEL-KL-PE

SUMMARY

The research discussed in this report is a continuation of studies aimed at determining the feasibility of a direct hydrocarbon-air fuel cell capable of widespread military application. The high platinum catalyst requirements of current generation systems is the major obstacle to systems development. Consequently, these investigations have emphasized the search for non-noble metal electrocatalysts, the improvement in noble metal utilization through modification of electrode and catalyst structure, and the development of intermediate temperature electrolyte systems.

Task A, Non-Noble Electrocatalysts

Previous studies considered acid resistant transition metal oxides and carbides as potential non-noble electrocatalysts. In view of the promising results reported in the previous semi-annual report, emphasis has shifted away from the eta phase carbide studies in favor of the more promising tungsten bronzes and metal-tungsten oxides. Studies aimed at defining the range of catalytically active metal-tungsten oxides have shown that a wide variety of materials can form electrochemically active anode and cathode systems. All of the rare earth bronzes that possess a magnetic moment show both anodic and cathodic activity, while lutecium, which is non-magnetic, shows only the oxygen activity typical of the conductive tungsten oxide systems. Thus, it appears that the injected ion must have a magnetic moment to retain anodic activity. All of the first row transition element (except Cu, Sc, Co) tungsten oxides show both anodic and cathodic activity. However, the response does not follow the Tafel equation.

Oxygen performance on the other hand yielded good Tafel slopes, and all mixed oxides and bronzes showed oxygen activity. These systems appear to be more active cathodes than they are anodes. However, this appears to be a property of the conductive tungsten oxides in general.

$Ni_{0.237}WO_3$ gave the best hydrogen performance (8-9 ma/cm^2) at 0.6 volts polarized) in 3.7 M sulfuric acid. Methanol activity was also observed (50 ma/cm^2 at 0.6 volts polarized) but open circuit polarization was quite poor. However, no other hydrocarbon activity has been detected thus far.

The metal-tungsten oxygen system was also evaluated as potential oxygen cathodes and butane anodes in 275°C pyrophosphoric acid electrolytes. No significant corrosion was observed with these materials even though $Fe_{0.2}WO_3$ could sustain 100 ma/cm^2 on oxygen. However, the polarization on oxygen is high due to a poor open circuit potential. Several of the other metal-tungsten oxides could sustain significant oxygen currents but none were any better than $Fe_{0.2}WO_3$. No unequivocal hydrocarbon activity has been observed in this electrolyte as yet.

Task B, Noble Metal Catalysis

Supported platinum catalysts continue to show promise of significant hydrocarbon activity improvements in both low and intermediate temperature electrolytes. The initial target for this program is a liquid or gaseous hydrocarbon electrode capable of 150 ma/cm^2 with less than 2 mg/cm^2 of noble metal. These studies have shown that improvements can best be obtained through alteration in platinum deposition selectivity and increased platinization. In this latter regard, the multiple absorption procedure continues to be a potent tool for increasing platinization without significant loss in catalyst utilization.

Attempts to improve platinization selectivity through the use of intermediate porosity carbon supports met with only partial success. Although these preparations gave the best performance of any previously prepared synthetic carbon support, butane utilization was only 10 ma/mg Pt. Thus it appears that a distribution of macro and micropores is required for good hydrocarbon activity.

Efforts to alter platinum deposition selectivity by varying adsorbate composition failed to produce any marked change in crystallite size. However, these studies led to the development of a new Co-Pt catalyst system. Indeed, a Co-Pt on FC-30 carbon has shown significant utilization in electrolytes ranging in temperature from 150 to 275°C. Although performance at 150°C is comparable to our best platinized carbon 80 ma/cm^2 at 3.2 mg/cm^2, utilization at elevated temperatures have reached as high as 44 ma/mg at 200°C for thick 23 mil electrodes. A reduction in thickness to 13 or 14 mils resulted in more than double the current capability. For example, a 1.8 mg Pt/cm^2 electrode sustained 200 ma/cm^2 at 0.45 polarized at 200°C (110 ma/mg Pt). Increasing the temperature caused some loss in performance but even at 275°C the electrode sustained 75 ma/mg Pt.

Task C, New Electrolytes

Hydrocarbon electrodes are limited by activation rather than diffusion phenomena. Higher temperature operation, within the constraints of engineering practical field batteries, should significantly improve fuel cell power densities for both non-noble metal and platinum catalyzed electrodes. Pyrophosphoric acid has been shown to be an effective electrolyte for the electrochemical oxidation of butane, hexane, octane and decane. However, fuel humidification is important, and it appears that the optimum water-fuel ratio will vary with carbon number. Octane half cell data indicates that system power densities as high as 100 mw/cm^2 at 0.45 volts/cell can be obtained with humidification using high loaded electrodes. This electrolyte system is also potentially useful in hydrocarbon reformer fuel cell systems since no carbon monoxide poisoning is noted at the 250-275°C operating temperature even with 10% carbon monoxide in the reformer gas effluent. The absence of CO poisoning is also noted with low loaded supported platinum catalysts.

The enhanced anodic and cathodic performance observed has led to an assessment of overall systems capability to determine if these improvements are reflected in system weight and catalyst economy. This study indicates that a butane or octane-air system can be designed with a significant reduction in catalyst loading (1400 vs 61 gm/kw) at a weight increase of only 14 lbs/kw. On the other hand, an approximate ten fold reduction in catalyst loading (454 to 56.2 gms/kw) in the reformer air fuel cell requires a two fold weight increase (58.4 to 101.0 lbs/kw). Thus, in this electrolyte, low catalyst loaded direct hydrocarbon systems may have a weight advantage over comparable reformer systems. It is interesting to note that from a catalyst standpoint, both low catalyst loaded systems (reformer and direct) are within a factor of three of the military target of 20 gm Pt/kw. Development of these systems concepts will continue.

The phosphate melt continues to show promise as an alternate intermediate temperature electrolyte for hydrocarbon-air systems. Tests with unsupported (50 mg/cm^2) anodes and cathodes indicate that a butane-oxygen system performance of 100 ma/cm^2 is possible. However, low catalyst density carbon supported anodes and cathodes do not show the anticipated utilization improvements. Raney Ni-Co alloy catalyst show some hydrogen activity (10 ma/cm^2) in this electrolyte with no evidence of corrosion. This bodes well for potential development of more active non-noble anode catalyst systems. Attempts to prepare active catalysts based upon silver and silver-silver oxides systems have thus far been unsuccessful even when the alkalinity of the electrolyte was increased by cesium carbonate addition. Work on both non-noble anode and cathode catalysts for this system will continue.

CONTENTS

Section		Page
1	INTRODUCTION	1
2	EXPERIMENTAL STUDIES AND DISCUSSION	2
	2.1 Task A, Non-Noble Electrocatalyst	2
	Phase 1 - Metal-Tungsten-Oxygen System Electrocatalysts	2
	Phase 2 - Other Bronze Systems	9
	Phase 3 - Electrochemical Evaluation Studies Metal-Tungsten-Oxide and Related Catalysts	12
	Phase 4 - Intermediate Temperature Electrolyte Performance	22
	Phase 5 - High Surface Area Alloys	26
	Phase 6 - Conclusions	27
	2.2 Task B, Noble Metal Catalysis	30
	Phase 1 - Supported Platinum Catalysts	30
	Phase 2 - Electrode Structure Studies	39
	Phase 3 - Conclusions	44
	2.3 Task C, New Electrolytes	46
	Phase 1 - Pyrophosphoric Acid Electrolyte Studies	46
	Phase 2 - Preliminary Systems Evaluation - Intermediate Temperature (Pyrophosphoric Acid) Fuel Cell	50
	Phase 3 - Mixed Alkali-Metal Dihydrogen Phosphate Melts	55
	Phase 4 - Conclusions	65
3	REFERENCES	67
A	Appendices for Task A	71
B	Appendices for Task B	76
C	Appendices for Task C	82

Appendix		Page
A-1	Anodic Activity of the Rare Earth Tungsten Bronzes	71
A-2	X-Ray Lines of $Cr_{0.05}WO_3$	73
A-3	Anodic Activity of the Active Transition Metals in the Transition Metal-Tungsten-Oxygen System	74
A-4	Slurry Electrode Cells	76
A-5	Corrosion of $TiWO_3$ By Voltage Scan	77
A-6	Corrosion of $Mo_{0.2}WO_3$ By Voltage Scan	78
A-7	Corrosion of $W_{0.2}WO_3$ By Voltage Scan	79
B-1	Butane Performance Carbon Supported Catalysts	80
B-2	Butane Performance of Experimental Sucrose Carbons	83
B-3	Potential Absorbates	84
B-4	Performance of Porous Teflon Supported Electrodes	85
C-1	Octane Performance in Pyrophosphoric Acid with Pre-metered Feed	86
C-2	Schematic Feed Preparation System--Pyrophosphoric Acid Tests	87
C-3	Weights of Various Fuel Cell Components Weight Burden Per Stack	88
C-4	Summary Sheet-Butane Air Fuel Cell	89
C-5	Summary Sheet-Octane-Air	90
C-6	Hydrogen Generator Weights	91
C-7	Summary Sheet Reformer-Air Fuel Cell	92

ILLUSTRATIONS

Figure		Page
A-1	Anodic Activity of $Ce_{0.1}WO_3$, H_2 Fuel	4
A-2	Anodic Activity of $Ni_{0.237}WO_3$-Hydrogen and Methanol	8
A-3	Cathodic Activity of $W_{18}O_{49}$ and Typical Metal-Tungsten-Oxygen Catalyst ($Mn_{0.2}WO_3$)	9
A-4	Voltage Scan of $Fe_{0.2}WO_3$ in a Slurry Cell	15
A-5	Polarization of a Slurry as H_2 Electrode	16
A-6	Polarization of $Ti_{0.2}WO_3$-Slurry and Porous Electrode	17
A-7	Corrosion of $Ti_{0.2}WO_3$ by Voltage Scan	18
A-8	Voltage Scans of Various Mixed Oxides	20
A-9	Voltage Scans of Various Mixed Oxides	20
A-10	Hydrogen Activity of $Ti_{0.2}WO_3$ by Voltage Scan	21
A-11	Oxygen Activity of $Ti_{0.2}WO_3$ by Voltage Scan	21
A-12	Iron Tungsten Bronze Exhibits Oxygen Activity	24
A-13	Oxygen Activity of Various Oxide Bronzes at 275°C in Pyrophosphoric Acid	25
A-14	Correlation of Hydrogen Activity and Magnetic Moment	27
A-15	Active Metal-Tungsten Oxide Catalysts	28
B-1	Optimization of Fluid Bed Ozonizer	33
B-2	Effect of Ozone Treatment on Platinization and Crystallite Size - Fluid Bed Ozonization	34
B-3	Effect of Foraminant Content on Platinization and Surface Area	36
B-4	Butane Performance of Sucrose Carbons	36
B-5	Effect of Loading and Thickness on Butane Performance	40
B-6	Effect of Electrolyte and Temperature on Butane Performance	41
B-7	Butane Performance-Low Loaded Anodes	42
C-1	Hydrocarbon Activity in Pyrophosphoric Acid	47
C-2	Predicted Performance Pyrophosphoric Acid	51
C-3	Predicted Performance Pyrophosphoric Acid Cell	51
C-4	Schematic Noncondensing Vapor Feed Hydrocarbon Fuel Cell	53
C-5	Performance of Butane Oxygen System	

TABLE

Table		Page
A-1	Effect of Lanthanum Content on Structure La_xWO_3 Bronze	5
A-2	X-Ray Powder Diffraction Lines of $La_{0.15}WO_3$	5
A-3	d-Spacings of $CeTiO_{2.5}$ and $Nd_{0.8}TiO_3$	11
A-4	Cathodic Activity of $Zn_2Mo_3O_8$	12
A-5	Resistance of Nickel-Tungsten Oxide Electrodes	13
A-6	Resistance Measurements $Ni_{0.237}WO_3$ Kordesch Bridge	14
A-7	Initial Corrosion of Some Transition Metal Tungsten Oxygen Catalysts	18
A-8	Corrosion Resistance Metal-Tungsten Oxides and Related Compounds	23
B-1	Effect of Double Adsorption on Limiting Butane Performance	31
B-2	Effect of Adsorption and Reduction Conditions on Butane Performance	32
B-3	Platinum Crystallite Size and Utilization, Sucrose Carbons	35
B-4	Butane Performance of Platinum Salts	37
B-5	Effect of Carbon Type and Platinization Level on Butane Performance	39
B-6	Platinum Utilization-Low Loaded Carbon Supported Co-Pt Anode (Butane, FC-30 Carbon)	43
B-7	Performance of Catalyzed Carbon Anodes and Cathodes	43
B-8	Comparison of Porous Teflon Substrates	44
C-1	Properties of Pyrophosphoric Acid Electrolytes	46
C-2	Comparative Activity Reformer Effluent vs Pure Hydrogen	49
C-3	Hydrogen or Reformer Gas Cell (250-275°C Pyrophosphoric Acid)	52
C-4	Hydrocarbon Performance 275°C Pyrophosphoric Acid Cell	52
C-5	Weight and Platinum Requirements Hydrocarbon-Air Fuel Cell	54
C-6	Weight and Platinum Requirements Reformer-Air Fuel Cell System	55
C-7	Performance of Butane on Catalyzed Carbon-Phosphate Melt at 250°C	57
C-8	Performance of Oxygen on Catalyzed Carbon Electrodes, Phosphate Melt at 250°C	58
C-9	Performance on Chem-Cell Electrode Phosphate Melt at 250°C	58
C-10	Hydrogen Activity-Raney Nickel-Cobalt Alloy	59
C-11	Silver Cathode Active in Phosphate Melt	60
C-12	Buffering Capacity of Modified (Alkaline) Phosphate Melt - 250°C	61
C-13	Oxygen Performance-Modified Phosphate Melt (Sintered Silver Electrodes, 250°C)	61
C-14	Oxygen Activity on Sintered Ag/Ag_2O Electrodes at 250°C	62
C-15	Oxygen Activity of Borohydride Co-reduced Silver-Group B Metal Cathodes	63
C-16	Cathode Activity of Borohydride Reduced Silver Salts of Group IV and V Anions	63
C-17	Oxygen Performance of High Temperature (800°C) Hydrogen Reduced Silver Salts of Group IV and V Anions	64

SECTION 1

INTRODUCTION

The objective of these investigations is to determine the feasibility of a direct hydrocarbon-air fuel cell capable of widespread military application. Such fuel cells must use fuels which react to carbon dioxide, must be reasonably available, and pose no unusual corrosion, toxicity, or handling problems. Also, the cell must use a CO_2-rejecting electrolyte and operate at temperatures consistent with reasonable start-up characteristics. The system should be thermally self-sustaining without excessive loss in efficiency. Other desired requirements include high electrical output per unit volume and weight, high efficiency, long life, high reliability, reasonable cost, particularly, catalyst cost, and ruggedness.

Previous studies have established that a direct liquid hydrocarbon-air fuel cell system is feasible provided that the noble metal catalyst requirement is substantially reduced through improvements in utilization or replacement by non-noble metal systems. Current work is aimed at substantially reducing the platinum requirement through improved electrode and catalyst structures. In addition, non-noble platinum substitutes are being actively sought. Improved catalyst effectiveness could be attained through intermediate (150-300°C) temperature systems. Electrolyte and systems studies aimed at evaluating the overall power density and systems requirements are under way.

The program is thus divided into three parts, referred to as Task A through C in this report. Task A describes studies on non-noble metal catalysts and Task B, research on noble metal catalyst utilization improvement. Task C discusses new electrolyte research.

SECTION 2

EXPERIMENTAL STUDIES AND DISCUSSION

2.1 Task A, Non-Noble Electrocatalysts

Present hydrocarbon fuel cell systems either utilize the hydrocarbon fuel directly or reform it to produce hydrogen which is subsequently electrochemically oxidized. Both systems use expensive components and catalysts. Direct systems require acidic carbon dioxide rejecting electrolytes, thus necessitating acid resistant catalysts, the most effective ones being platinum group metals. Although the reformer system can potentially use non-noble catalysts when combined with an alkaline electrolyte cell, palladium diffusors are required.

Development of a practical hydrocarbon fuel cell system depends upon reducing the cost of these expensive components by replacing the platinum group metals with either more effective or less expensive materials. The development of active non-noble metal catalysts offers one route towards this goal.

Previous studies considered the acid resistant transition metal oxides and carbides as potential non-noble electrocatalysts. During this report period emphasis has shifted away from the eta phase carbide studies in favor of the more promising tungsten bronze and transition metal-tungsten oxides since some of these materials have shown promising anodic and cathodic activity. Studies were conducted to define the range of electrochemically active tungsten bronze and metal tungsten-oxygen systems. In addition, all the other bronze forming metals were considered as replacements for the tungsten oxide system. This study included transition metal and rare earth bronzes based upon the vanadium, titanium, mobium, tantalum and molybdenum oxide systems.

Some of the more active of the metal-tungsten-oxygen materials were examined as hydrocarbon anodes and oxygen cathodes for the intermediate temperature (275°C) electrolyte, pyrophosphoric acid.

Phase 1 - Metal-Tungsten-Oxygen System Electrocatalysts

Potential non-noble hydrocarbon electrocatalysts must meet two principle electrochemical requirements. They must be conductive and stable in carbon dioxide rejecting electrolytes. The tungsten bronzes and mixed metal-tungsten oxides meet these requirements. These materials provide a means of incorporating a catalytic transition element into a corrosion resistant matrix. Previous work (9) has shown that some transition and post-transition metal-tungsten-oxygen systems are active as anode and cathode catalysts. Consequently, current studies emphasized defining the range of potential catalystic systems and, where possible, illustrating the mechanism reponsible for activity.

This study included both the mixed metal tungsten oxides and the true tungsten bronzes. The true tungsten bronzes are compounds with the general formula A_xWO_3 with characteristic simple crystal structure. The mixed oxides, on the other hand, show no well defined crystal forms by X-ray diffraction. However, they do have all the other bronze characteristics including intense color and electronic conduction.

Part a - Tungsten Bronzes as Anode Catalysts

Rare earth tungsten bronzes have been reported and characterized in the literature (10,11). One of these materials, $Eu_{0.1}WO_3$, had previously shown activity as a hydrogen anode (16). Consequently, a number of rare earth tungsten bronzes were examined as potential catalysts. Two new tungsten bronzes containing group IIb elements were also examined.

All of the rare earth and the group IIIb bronzes were prepared by thoroughly mixing the required portions of the rare earth or group IIIb oxide powder with powdered tungsten metal and tungsten trioxide to give the desired stoichiometry. The mix was pelletized and sealed into a quartz tube under 5×10^{-4} torr. The tubes were heated in either a Leco or a Lindberg tube furnace at 1100° for 72 hours. In some cases the pellets were ground and pressed again every 24 hours but it was found that this did not change the results. The pellets remained intact during the heating. Less than 25 mg were lost from the pellets during the preparation, indicating that the resulting stoichiometry was quite close to that of the mix. Preparations normally were made in 9-10 gm batches.

The products of the above preparations were examined for homogeneity both by microscopy and by X-ray powder methods. No materials were obtained that showed inhomogeneity in one method of examination, but not the other. X-ray studies were made with a Norelco X-ray Diffractometer type 12045-6 modified for use with an Advance Metals Research Corporation curved crystal focusing monochromator model 3-202. The copper K_α lines were detected with a Norelco Scintillation Counter attachment type 52245.

The resulting tungsten bronzes were fabricated into a standard sintered Teflon bonded electrode supported on tantalum screen, using the minimum Teflon content consistent with structural stability (5 wt%). These porous electrodes were evaluated in 3.7 M sulfuric acid at 90°C. Current measurements (at constant potential) were made with either nitrogen, hydrogen, or oxygen passing across the face of the electrode. A conventional half cell was used for these evaluations. A graphite rod was used as the counter electrode to prevent contamination with noble metals. The current densities obtained with these structures are quite low. However, as indicated previously (9), these performance levels are probably due to a poor electrode structure, since repeat electrodes yielded different current capabilities. The reported current densities obtained for one catalyst should not be compared with that of another. Performance data is useful only in establishing the existence or lack of existence of activity, not its absolute level.

Thus far, all the rare earth tungsten bronzes synthesized in this laboratory have shown activity as anodes with hydrogen as the fuel. These include: $Ce_{0.04}WO_3$, $Ce_{0.1}WO_3$; $Sm_{0.1}WO_3$; $Eu_{0.1}WO_3$; $Gd_{0.1}WO_3$; $Dy_{0.1}WO_3$; $Ho_{0.1}WO_3$ and $Yb_{0.1}WO_3$. Hydrogen activity data is summarized in Appendix A-1. As indicated in Figure A-1, $Ce_{0.1}WO_3$ does not appear to show Tafel behavior during anodic hydrogen dissolution. This behavior is typical of all of the rare earth bronzes tested.

Two new Group IIIb tungsten bronzes, one containing lanthanum and the other yttrium have been prepared and characterized. These materials are acid resistant, electrically conductive, have a wide range of compositions and are intensely colored. They therefore can be classified as bronzes (12).

Figure A-1

Anodic Activity of $Ce_{0.1}WO_3$, H_2 Fuel

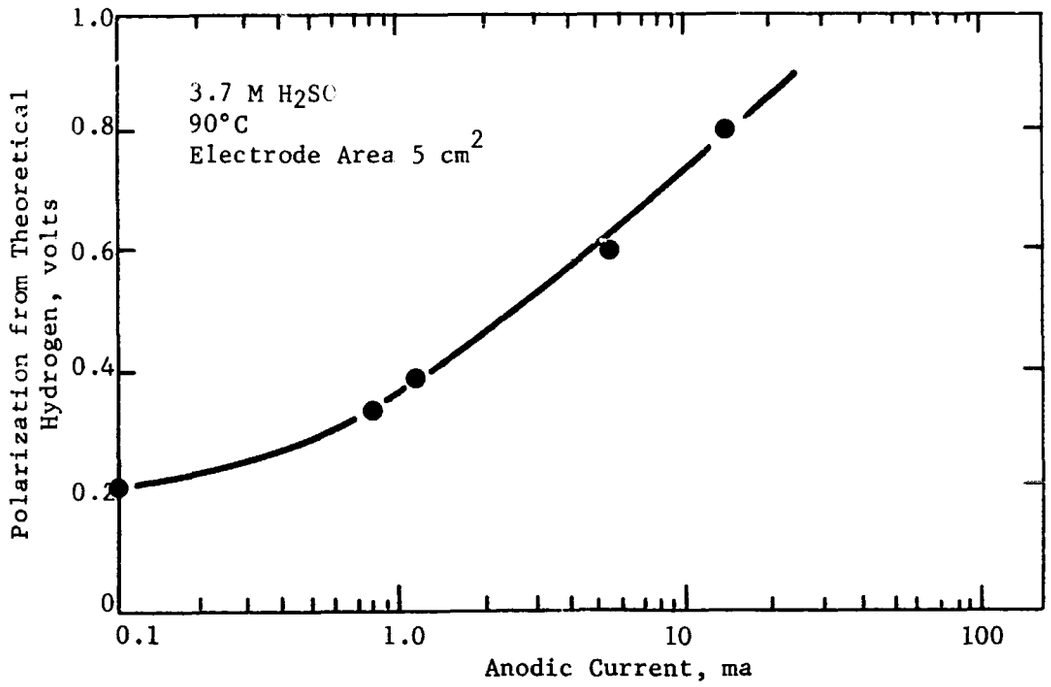

While the rare earth bronzes showed activity as anode catalysts, the Group IIIb tungsten bronzes were not active anode catalysts. However, as indicated in part b, they did show the cathodic activity typical of tungsten bronzes. These new tungsten bronzes were studied to see if activity could be obtained by varying their transition metal content and structure.

A homogeneous cubic perovskite-type structure was found for the lanthanum tungsten bronze La_xWO_3, where x is between 0.08 and 0.19. Powder X-ray diffraction data show that the cubic lattice parameter increases from 3.829°A to 3.845°A in this region. Below x = 0.08 a tetragonal structure also appears, and at x = 0.02 it occurs as a pure form with lattice parameters of a = 7.52°A and c = 3.89°A. Above x = 0.19, two additional phases are present. One has the same X-ray pattern as $La_2W_3O_{12}$ (13), while the other gives an X-ray diffraction pattern similar to WO_2 (14). Table A-1 summarizes the various La_xWO_3 phases observed, while Table A-2 presents the indexing of $La_{0.15}WO_3$, which is representative of the cubic forms of lanthanum and yttrium tungsten bronzes.

Y_xWO_3 also exists in tetragonal and cubic forms. However, the range of x yielding homogeneous cubic structures is narrower for this material than for lanthanum tungsten bronze. Above x = 0.15, WO_2 appears. No yttrium tungstate

structure(13,15) could be detected, even at the stoichiometric value of x = 0.2. Scandium does not form a tungsten bronze under the preparative condition employed here. A mixture of $W_{18}O_{49}$ (16) and $W_{20}O_{58}$ (17) was found by X-ray examination.

Table A-1

Effect of Lanthanum Content on Structure La_xWO_3 Bronze

Composition Range x, mole	Structure	Lattice Spacing °A	Lattice Spacing C°A
x = 0.02	Pure tetragonal	7.52	3.89
$0.02<x<0.08$	Tetragonal plus cubic		
$0.08\leq x<0.19$	Pure cubic	3.829 to 3.845	-
$x>0.19$	$La_2W_3O_{12}$ and WO_2		-

Table A-2

X-Ray Powder Diffraction Lines of $La_{0.15}WO_3$

a = 3.838°A

d_{obsd}	I	hkl	d_{calc}	d_{obsd}	I	hkl	d_{calc}
3.840	vs	100	3.838	1.108	m	222	1.108
2.715	vs	110	2.714	1.064	m	320	1.064
2.216	s	111	2.216	1.026	ms	321	1.026
1.919	vs	200	1.919	0.9595	w	400	0.9595
1.717	vs	210	1.717	0.9306	m	410	0.9309
1.567	vs	211	1.567	0.9042	m	411	0.9045
1.357	s	200	1.357	0.8801	w	331	0.8805
1.279	s	300	1.279	0.8580	m	420	0.8582
1.214	s	310	1.214	0.8369	m	421	0.8374
1.157	m	311	1.157	0.8180	w	332	0.8183

The transition from tetragonal to cubic structure observed with the lanthanum and yttrium tungsten bronzes is the same type of behavior recently reported for the rare earth tungsten bronzes (10). For some of the rare earth tungsten bronzes reported in the literature a tetragonal form was found at low concentrations of the rare earths, while at higher concentrations, a cubic perovskite-type structure was found with all the readily available rare earth elements. Magnetic studies showed that the rare earth was present in a trivalent form. It would appear that both yttrium and lanthanum also form tungsten bronzes in their trivalent states. This is to be expected as these elements normally exist in a trivalent state and further have essentially the same radii as the rare earths in the 12-coordinated position of the perovskite lattice. For example, Geller (18) has found that relative radii of Y^{+3}, Eu^{+3}, and La^{+3} in the A position of perovskites to be, 1.281 Å, 1.304 Å, and 1.346 Å, respectively. The cubic lattice parameters for the corresponding tungsten bronze preparations are in the same order. $Y_{0.1}WO_3$ has a parameter of 3.802 Å; $Eu_{0.1}WO_3$ was found to have a lattice constant of 3.815 Å (10), while $La_{0.1}WO_3$ synthesized in this laboratory has a cubic parameter of 3.834 Å.

The color of La_xWO_3 varies from green at x = 0.02 to blue at x = 0.10 and finally to red-purple at x = 0.19. The last color indicates that the lanthanum is present in its trivalent state. A red-purple color is characteristic of a free electron concentration of approximately 0.6 electrons per tungsten atom in the case of the sodium tungsten bronzes (19).

Unfortunately, none of the Group IIIb tungsten bronze preparations showed any anodic activity even with wide variations in metal content. Chromium also forms a tungsten bronze. A tetragonal structure was obtained when chromium metal was heated with tungsten trioxide at 1100° for 72 hours in an evacuated quartz tube. The composition limits of this system have not been determined yet. Appendix B-2 gives the X-ray lines obtained for $Cr_{0.05}WO_3$ prepared in this manner. The chromium tungsten bronzes are active catalysts for the oxidation of hydrogen. Their behavior is similar to that found for the rare earth tungsten bronzes. This bronze has not been reported previously.

Cadmium tungsten bronzes have only recently been reported (20). These authors found that cadmium metal and tungsten trioxide, when heated together, form a bronze structure. Work in our laboratories has shown that the same results can be obtained with cadmium oxide, tungsten, and tungsten trioxide. This later preparative procedure is safer since pressure build up (and explosion hazard) in the evacuated quartz ampules is minimized. Neither method of preparation yielded materials with anodic activity.

The following tungsten bronzes were examined during this period and failed to show activity as anodes: sodium tungsten bronze, barium tungsten bronze, and copper tungsten bronze. The sodium tungsten bronze was prepared by electrolyzing a melt of sodium-tungstate and tungsten trioxide (11) using graphite anodes. If noble metal electrodes are used, anodic activity can be observed. However, this is probably due to noble metal dissolution in the melt and subsequent deposition on the growing bronze crystal. The barium (22,23) and copper (24) tungsten bronzes preparations were accomplished as described in the literature. Several attempts at preparing a silver tungsten bronze by solid state reactions were not successful although one has been reported in the literature (25).

Although mechanism studies have not been completed on these systems, it does appear that one requirement that a tungsten bronze must meet in order to be active as an anode, is that its inserted ion must possess a rather high magnetic moment. The rare earth tungsten bronzes (10), except for the one containing lutetium,

all possess magnetic moments. A lutetium tungsten bronze is in preparation here and should not show any anodic activity. The alkali metal tungsten bronzes do not have high magnetic moments (19,20). It would appear that barium and cadmium enter the tungsten bronze lattice as divalent ions and therefore neither would have a magnetic moment. No magnetic data are available yet on the lanthanum and yttrium tungsten bronzes, but if they are trivalent, then they would not be magnetic. Copper tungsten bronzes also have low magnetic moments (27).

The mechanism of the anode reaction is not clear, and the role of the magnetic material is uncertain. A high magnetic moment should catalyze the dissociation of hydrogen. Indeed, it has been found that the sodium tungsten bronzes which possess a weak magnetic moment are active in deuterium-H_2 exchange, ortho-para conversion of hydrogen (28) and formic acid decomposition (29). It appears that the alkali metal tungsten bronzes cannot dissociate hydrogen in acid media and therefore they are not active anode electrocatalysts. Perhaps a higher magnetic moment is required.

Part b - Transition Metal-Tungsten-Oxygen Anode Catalysts

While the rare earth tungsten bronzes are potent electrocatalysts, the rare earth constituent is rather expensive. Even if the active constituent is present in trace amounts, as in $Ce_{0.04}WO_3$, the catalyst might still be a costly one. Previous work with the nickel-tungsten oxygen system showed that corrosion resistant, active anode catalysts could be obtained from materials made from the nickel system. The nature of the active species is unclear at present. However, it may be that the transition metal is incorporated into a number of tunnel structures (10). This would account for its acid stability.

Preparative procedures were the same as those used in the rare earth studies except that lower temperatures were usually employed. Performance evaluation data obtained with Teflon bonded electrodes are summarized in Appendix A-3.

In an effort to expand the number of potential low cost catalysts, other transition metal and post-transition metal tungsten oxygen systems were examined. No tungsten bronze structures were observed, but many mixed oxide systems were found to be catalytically active and acid stable, including those containing titanium, vanadium, chromium, manganese, iron, nickel, zinc, and zirconium. No activity was found for the cobalt-tungsten-oxygen system (Co_xWO_3). At $x = 0.2$, the material was inert; at $x = 0.25$, severe corrosion was encountered. This is surprising since cobalt lies between iron and nickel in the periodic table and both these elements form active systems.

The nickel-tungsten-oxygen system (M_xWO_3) was thoroughly studied in the region $0 < x \geq 1$. It was found that preparations made from any of the following (a) nickel metal and tungsten trioxide, (b) nickel oxide, tungsten metal and tungsten trioxide, and (c) nickelic oxide, tungsten and tungsten trioxide all behave the same way. They all show activity when the value of $x \geq 0.237$, and are not active when $x \leq 0.2$. The X-ray spectra of the compositions $Ni_{0.2}WO_3$ and $Ni_{0.237}WO_3$ are identical and the active component has not been identified as yet. At higher nickel contents WO_2 appears. This material is not acid stable (large corrosion currents are found under nitrogen) so that it is not responsible for the catalytic effect.

The performance of a typical $Ni_{0.237}WO_3$ electrode is shown in Figure A-2. This electrode was prepared by sintering the $Ni_{0.237}WO_3$ on to a porous tantalum disc. Notice that $Ni_{0.237}WO_3$ is not only active on hydrogen, it is also able to oxidize methanol at reasonable current densities. Hydrogen activity commences quite close to theoretical potential. However, no methanol activity is detected until 0.26 volts polarization. Tafel behavior was not observed with either fuel even though oxygen activity (Part c) does seem to follow a Tafel equation.

Figure A-2

Anodic Activity of $Ni_{0.237}WO_3$ - Hydrogen and Methanol

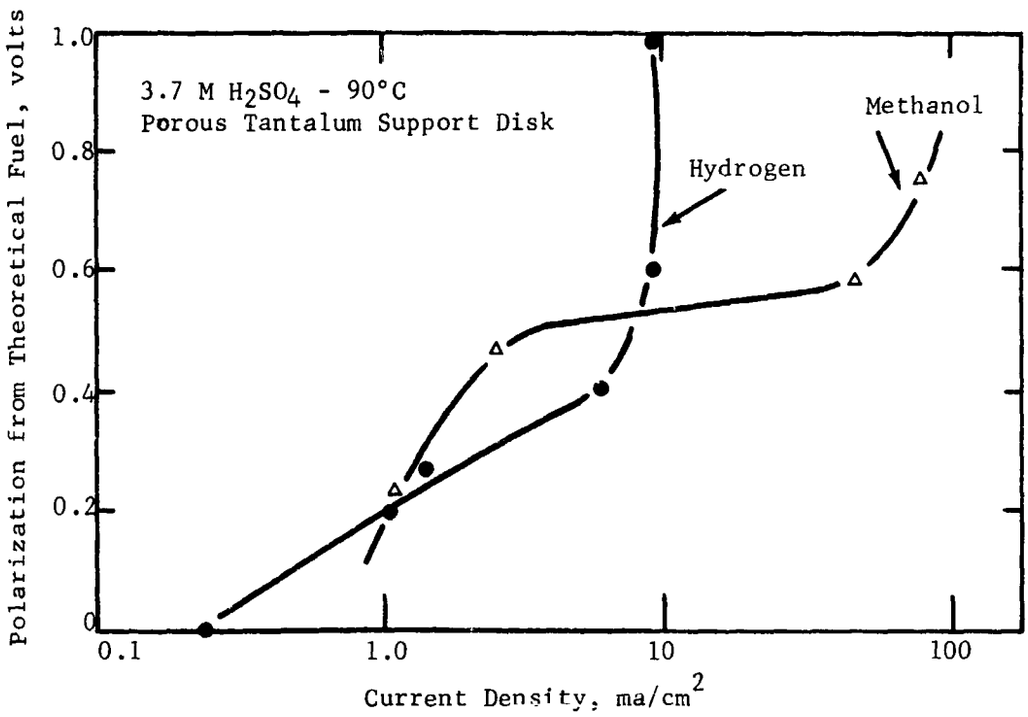

Many transition and post-transition metal-tungsten-oxygen systems do not show anodic activity. These include Co_xWO_3 ($0 \leq x < 0.3$), $Nb_{0.2}WO_3$, $Mo_{0.2}WO_3$, Cd_xWO_3 ($0.05 < x < 0.4$), $Hf_{0.2}WO_3$, and $Ta_{0.2}WO_3$. Niobium, molybdenum and tantalum form oxides with tungsten in which the metal substitates for the tungsten in the oxide. Consequently, these materials do not form tunnel compounds (34), and this structure may be required for activity (9).

Part c - Cathodic Activity
Metal-Tungsten Oxygen Systems

Thus far, all of the acid resistant, electrically conductive metal-tungsten-oxygen and tungsten oxide systems prepared in this laboratory are active cathode catalysts. Tungsten oxides such as $W_{18}O_{49}(WO_{2.72})$ (35) and $W_{20}O_{58}(WO_{2.9})$ (33) show the same type of behavior as that given by tungsten bronzes and the transition metal

and post-transition metal-tungsten-oxygen systems. All these systems have the ability to electrochemically reduce oxygen, although not all of them are active anodic catalysts. Tafel behavior is shown by all these systems when operating cathodically, even though Tafel behavior is not observed anodically. Each electrode preparation has a different apparent Tafel slope, due to differences in electrode fabrication which could arise from conductivity problems. Figure A-3 compares the behavior of the tungsten oxide $W_{0.1}WO_3$ ($W_{18}O_{49}$) with a typical transition metal-tungsten oxide catalyst. Notice that both materials yield approximately the same Tafel slope, although the limiting currents differ significantly.

Figure A-3

Cathodic Activity of $W_{18}O_{49}$ and Typical Metal-Tungsten-Oxygen Catalyst ($Mn_{0.2}WO_3$)

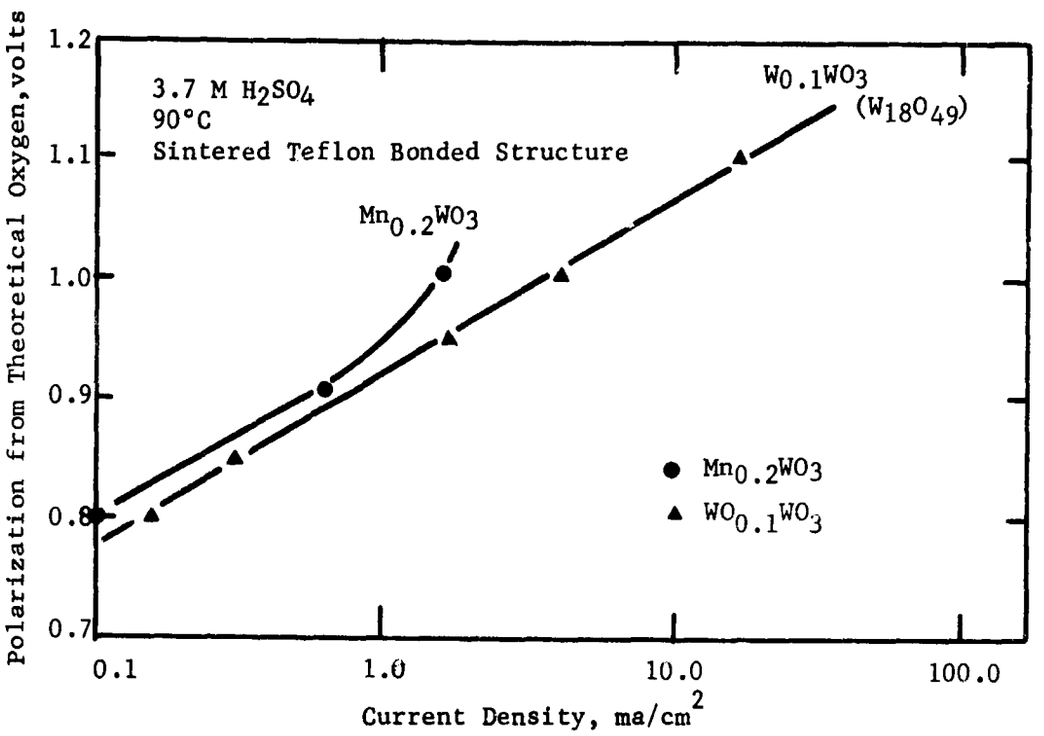

The tungsten oxides are all stoichiometric compounds (35) so that the oxygen activity cannot arise from having oxygen atoms fill vacancies in the bulk lattice. However, there may be oxygen deficiencies on the surface and these would be important in the oxygen reduction reaction. The fact that all tungsten bronzes and mixed oxides show this reaction indicates that it is a property of tungsten-oxygen systems that are electrically conductive.

Phase 2 - Other Bronze Systems

Although the tungsten bronzes are better known, vanadium, molybdenum, titanium, tantalum, and niobium all form oxide bronze systems (41). Many of these were prepared to see if they showed promise as electrocatalysts.

Part a - Vanadium Bronzes

Vanadium bronzes were discovered at the turn of the century (41-43). Alkali metal vanadium bronzes have been extensively studied and characterized (44,45) and a silver vanadium bronze has also been reported (51,52). These materials are in general much less conductive but more magnetic (54) than the tungsten bronzes, and are known catalysts for hydrocarbon reactions (55). All these materials were prepared in our laboratories. Unfortunately, they all had poor acid stability in 3.7 M sulfuric acid at 90°C. With the possible exception of a sodium vanadium bronze, none of these compounds showed any activity in this medium. Sodium vanadium bronzes prepared from sodium sulfate and vanadium pentoxide (56) showed about 0.1 ma/cm^2 of activity for the oxidation of hydrogen at 0.94 volts from the theoretical hydrogen potential. However, the material was slowly corroded under these conditions.

A strontium vanadium bronze, $SrVO_{2.5}$, (55) has a perovskite-type crystal structure that is quite different from that of the other vanadium bronzes and it was hoped that better performance could be obtained from this compound. It was found that the electrical conductivity of $SrVO_{2.5}$ was comparable to that of the tungsten bronzes but that it was inert electrochemically. Further, it was slowly attacked by acid.

Some mixed oxides of molybdenum and vanadium are known (56-60). Both V_2MoO_8 and $VMoO_5$ were prepared in quartz ampoules sealed at 10^{-3} torr (60). These materials are not good conductors, showed no electrochemical activity, and were slowly attacked by dilute sulfuric acid at 90°C. They are classified with the vanadium bronzes rather than with the molybdenum bronzes (Part c), because they both have these properties in common.

Part b - Titanium Bronzes

Only the sodium (61,62,63), lanthanium (64), and strontium (55) titanium bronzes have been reported. The latter two were prepared here and found to be conductive and acid stable in 3.7 M sulfuric acid at 90°. They showed no activity for either hydrogen or oxygen. The lack of cathodic activity is a bit surprising for if these systems are analogous to the tungsten bronzes there should have been some oxygen activity. The lack of anodic activity is not surprising, for the lanthanum tungsten bronze and the alkaline earth tungsten bronzes are not active in the oxidation of hydrogen. For this reason, the sodium titanium bronze was not prepared. Rather, it was decided to prepare some rare earth titanium bronzes.

By substituting cerium for strontium in the $SrTiO_{2.5}$ structure, we have obtained an X-ray pattern similar to that found for the strontium titanium bronze, except that the cubic parameter is 3.963 Å, rather than 3.90 Å (55). This increase in size is surprising for the radius of the cerium ion should be smaller than that of strontium. The value for the radius of lanthanum, which is larger than that of cerium, is about 1.35 Å (18) while that of strontium is 1.37 Å (55).

The neodymium analog of $La_{0.8}TiO_3$ (64) has also been prepared. Its lattice constant is 3.860 Å, a bit smaller than that reported for $La_{0.8}TiO_3$. This is to be expected from the relative radii of the two ions (18). The range of homogeneity of the cerium titanium bronze has not been determined. It is probably close to that of the lanthanum system. Presumably all the rare earths and probably yttrium can form phases analagous to $SrTiO_{2.5}$ and $La_{(2/3+x)}TiO_3$. Table A-3 contains the X-ray data found for the $CeTiO_{2.5}$ and $Nd_{0.8}TiO_3$ structures.

Table A-3

d Spacings of $CeTiO_{2.5}$ and $Nd_{0.8}TiO_3$

hkl	d Spacing	
	$CeTiO_{2.5}$	$Nd_{0.8}TiO_3$
100	3.970	3.865
110	2.803	2.730
111	2.288	2.228
200	1.982	1.930
210	1.772	1.726
211	1.618	1.576
220	1.401	1.365
300	1.318	1.287
310	1.253	1.221
311	1.195	1.163
222	1.144	1.114

While these new compounds were conductive and acid resistant, they showed no hydrogen activity even at high polarizations. They were also unable to act as catalysts for the reduction of oxygen under the conditions studied.

Part c - Niobium, Tantalum and Molybdenum Bronzes

The only niobium bronzes reported in the literature are those containing alkaline earth metals. The alkaline earth metal is undoubtedly present in a divalent state so these bronzes would have a small magnetic moment, if any at all. Thus, they would not be expected to show any anodic activity.

Both $Sr_{0.8}NbO_3$ (66) and $Ba_5Nb_4O_{13}$ (67) were prepared as the literature directed except that niobium metal rather than niobium dioxide was used as the reducing agent. The bronzes were blue and excellent conductors of electricity. They were stable in sulfuric acid at 90°C. Alas, they were not only inactive as anodes but also as cathodes.

The fact that these materials were completely inert led to the conclusion that the niobium bronzes were not promising electrocatalysts. For this reason no effort was made at introducing a rare earth ion into the niobium bronze lattice as a substitute for strontium as was done with the titanium bronzes. The alkali titanoniobiates (68) are not electrical conductors and therefore were not investigated.

Only the barium and strontium tantalum bronzes have been reported (67,69,70). Efforts at preparing $Ba_{0.5}TaO_{2.5}$ and $Ba_5Ta_4O_{13}$, starting from $BaCO_3$ that had been fired at 1100°C for six hours, were not successful. $Ba_{0.5}TaO_{2.5}$ was prepared from BaO_2 that had been heated in a vacuum furnace at 1200°C and 10^{-5} torr for four hours. This tantalum bronze is inert electrochemically and the tantalum bronzes were not pursued further. The tantalum tungsten bronzes (71) may show useful cathodic properties and will be investigated further.

Molybdenum bronzes have been reported (72,73) and characterized (74,75,76) recently. They should be active cathode catalysts as they are in Group VIB of the periodic table just as tungsten is.

Non-conductive oxides of molybdenum of the formula $M^{II}Mo_3O_8$ have been synthesized (77,78), where M is a transition or post-transition metal. The molybdenum exists in clusters (79) and the transition metal is in octahedral and tetrahedral holes (80). Several of these materials have been prepared and fabricated into electrodes. They all showed cathodic activity despite the high resistance of 10^7 ohms/pellet. Thus far, $Fe_2Mo_3O_8$, $Co_2Mo_3O_8$ and $Zn_2Mo_3O_8$ have been studied. Typical data is given in Table A-4 for $Zn_2Mo_3O_8$.

Table A-4

Cathodic Activity of $Zn_2Mo_3O_8$

(90°C, 3.7 M H_2SO_4, 5 cm^2 Electrodes)

Volts from Theoretical Oxygen Potential	Cathodic ma/5 cm^2	Gas
1.0	0.01	N_2
1.0	0.60	O_2
0.9	0.01	N_2
0.9	0.12	O_2
0.8	0.00	N_2
0.8	0.03	O_2

Studies of the tungsten and molybdenum bronzes and mixed oxides of transition, post-transition, rare earth and actinide metals with these two groups VIB metals will be continued.

Phase 3 - Electrochemical Evaluation Studies
Metal-Tungsten-Oxide and Related Catalysts

The electrochemical activity of the metal-tungsten-oxygen system has been adequately demonstrated, but the current capability remains very low. Furthermore, problems with the electrode and catalyst microstructure led to poorly reproducible results which can complicate catalyst evaluation. Two techniques have been investigated, which look promising for catalyst screening: the slurry electrode system and the voltage scan technique.

The slurry electrode system (6) was examined as a potential tool for evaluating catalyst activity independent of the physical structure factors discussed in Part a. The only requirement for reproducibility and reliability in comparing different catalysts is that they behave similarly as a suspension in the electrolyte, which implies only similar particle size and density. These requirements are satisfied when comparing various mixed tungsten oxides. The slurry electrode appears to be a reliable tool for testing their electrochemical activity.

The voltage-scan (8,9) technique is also a powerful tool for investigating electrochemical catalysts. The application of this technique to tungsten bronzes and mixed oxides is especially advantageous in that it can provide information on catalyst activity, corrosion, and basic electrode processes.

Part a - Electrode Structure Problems

Previous studies (9) have indicated that the low current capability of these metal-tungsten-oxygen catalysts was due to their comparatively low surface area and poor interparticle bonding with low conductivity. The amount of activity obtained from these catalysts varied markedly from electrode to electrode. The screening electrodes studied were generally prepared using Teflon bonded 200-325 mesh ground catalyst powder with low intrinsic surface areas (7-8 m^2/gm). The reproducibility of these electrode structures was poor, and different electrodes fabricated following the same procedure yielded widely differing activities.

Recent work by Bockris (36) sheds some light on our "effective" catalyst surface area. These authors have shown that the reduction of oxygen on single crystal of sodium tungsten bronze yields 10 ma/cm^2 of geometric surface at about 0.25 volts from reversible hydrogen potential. This indicates that the Teflon bonded ground powder electrodes have an effective surface area of at most 10 cm^2/gm of catalyst, since 100 ma/gm is the highest current level attained at this potential. This amounts to a factor of over 100 reduction of the measured B.E.T. surface area. Thus, it appears that very little catalyst is functioning electrochemically in the finished electrode, because of poor electrical coupling to the tantalum collector. Work reported previously (29) indicated that grinding to 325 mesh or smaller decreased the conductivity markedly. This small amount of contact probably arises from the poor electrical bonding between tungsten bronze particles. While the conductivity of single crystals of sodium tungsten bronzes (37) is of the order of 10^4 mhos, that of pressed powders is much lower (38). In our electrodes it appears that only those catalyst particles that are in direct contact with the current collector are active. The rest of the catalyst is inactive, since it is electrically insulated from the current collector by other tungsten bronze particles or the Teflon used to form the structure. Further evidence for poor electrical contact between the catalyst and the current collector is that the prepared electrodes have a resistance of about 1000 ohms between the tantalum screen and the tungsten bronze.

To clarify this point, an examination of the IR characteristics of nickel-tungsten-oxide electrodes was made by photographing the voltage time trace generated by the application of a constant current and measuring the IR directly with a Kordesch bridge. The first method was used with two electrodes, one prepared with an inactive material, $Ni_{0.2}WO_3$, the other with $Ni_{0.237}WO_3$. These data are summarized in Table A-5.

Table A-5

Resistance of Nickel-Tungsten Oxide Electrodes

Catalyst	Resistance, ohms	Polarization from H_2 Theory, volts
$Ni_{0.2}WO_3$	2.0	0.5
$Ni_{0.237}WO_3$	0.5-1.0	0.2

These measurements suggest that electronic resistance depends upon polarization. This result was substantiated by measurements with the Kordesch Bridge, Table A-6.

Table A-6

Resistance Measurements $Ni_{0.237}WO_3$
Kordesch Bridge

Current, ma	Polarization from Theoretical H_2, volts	IR, mv
40	0.23	55
40	0.54	100
40	0.70	140

As a result of all these effects the evaluation of performance of any given catalyst or even the comparison of different catalyst is difficult, and under some circumstances, catalytic activity could be obscured entirely.

Part b - Slurry Electrode System

Although the slurry electrode gives poorer catalyst utilization than a good porous electrode, it offers the significant advantage in that the electrode structure is no longer a factor in comparative testing. The experiments, discussed below, indicate that a slurry electrode, with mixed metal-tungsten oxides as catalysts, behaves in the same way and is almost as efficient as the rather poor porous electrodes fabricated from the same materials. However, it appears that the slurry is more reproducible than the porous electrode and therefore is worth considering for catalyst screening.

The experimental cell was similar to the one used previously when the slurry system was investigated for platinum catalysts (5). The current collector, however, was a tantalum screen (12 x 6 in - 50 x 50 mesh) folded several times and rolled up inside the cell. Appendix A-4 illustrates cell configurations used in this study. Cell A was equipped with a helicoidal stirrer and gas was introduced through a gas dispersion tube at the bottom of the vessel. Cell B had no stirrer and the gas was bubbled through a porous disk pressed between Teflon gaskets. In both cases, the auxiliary electrode was a platinum screen protected by a porous fritted cylinder. The Luggin junction and the reference electrode were the same as usual and the tip of the Luggin was within one or two millimeters of the tantalum screen.

Experiments were performed in 3.7 M sulfuric acid at about 90°C. Three mixed oxide catalysts were tested. The first two powders, $Ni_{0.237}WO_3$ and $Fe_{0.2}WO_3$, were passed through a 325 mesh screen and 1gm was added to the electrolyte in the cell. The third catalyst, $Ti_{0.2}WO_3$, was prepared by grinding the raw material in a colloid mill and making a slurry with 1gm of solid per 100 ml water. Sulfuric acid was then added to the slurry to obtain the required concentration. In addition, a run was made with platinum powder prepared by reduction of ammonium chloroplatinate with potassium borohydride and screening the precipitate through 325 mesh.

The two 325 mesh powders were tested in Cell A. The rate of mechanical stirring was not a significant factor and the agitation caused by the gas bubbles was sufficient to maintain a stable system. The stirrer was used, accordingly, mostly at the beginning of a series of experiments in order to put the catalyst in suspension. The colloid milled powder was tested in Cell B and it remained in suspension indefinitely without any mechanical stirring. The platinum powder was also tested in Cell B and, although it had a tendency to agglomerate, some measurements could be made.

The slurry electrode behaves as a stable and reproducible electrochemical system. This fact is best shown by the reproducible voltage scans cycles which were reported (Figure A-4) and which are similar to the curves obtained with porous electrodes (Figure A-6).

Figure A-4

Voltage Scan of $Fe_{0.2}WO_3$ in a Slurry Cell

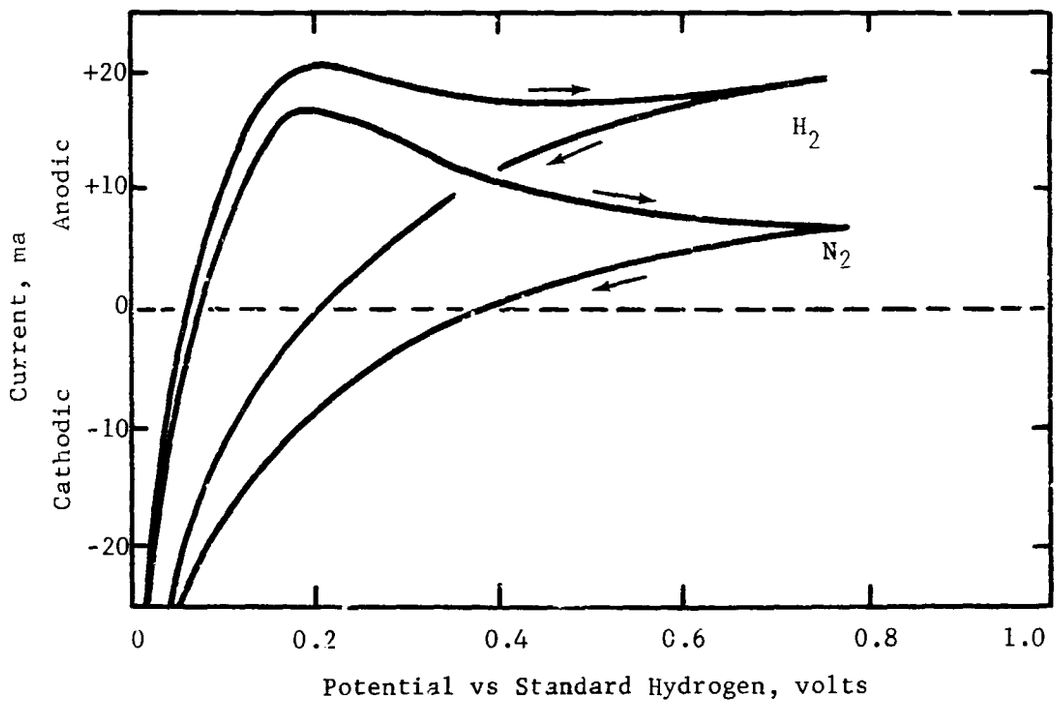

Reproducible polarization curves were obtained when using $Fe_{0.2}WO_3$ as a hydrogen anode or cathode. Figure A-5 compares this activity with that of platinum. Both materials are active at low polarization, but while the platinum curve is almost symmetrical, $Fe_{0.2}WO_3$ is about 100 times more active as a cathode than as it is an anode. The shape of those curves shows that the platinum slurry electrode has an important ohmic polarization. By comparison with platinum, the shape of the $Fe_{0.2}WO_3$ curve indicates that the resistance varies with polarization; it decreases towards more cathodic potentials, and it still decreases further with time during cathodic operation.

Figure A-5

Polarization of a Slurry as H_2 Electrode

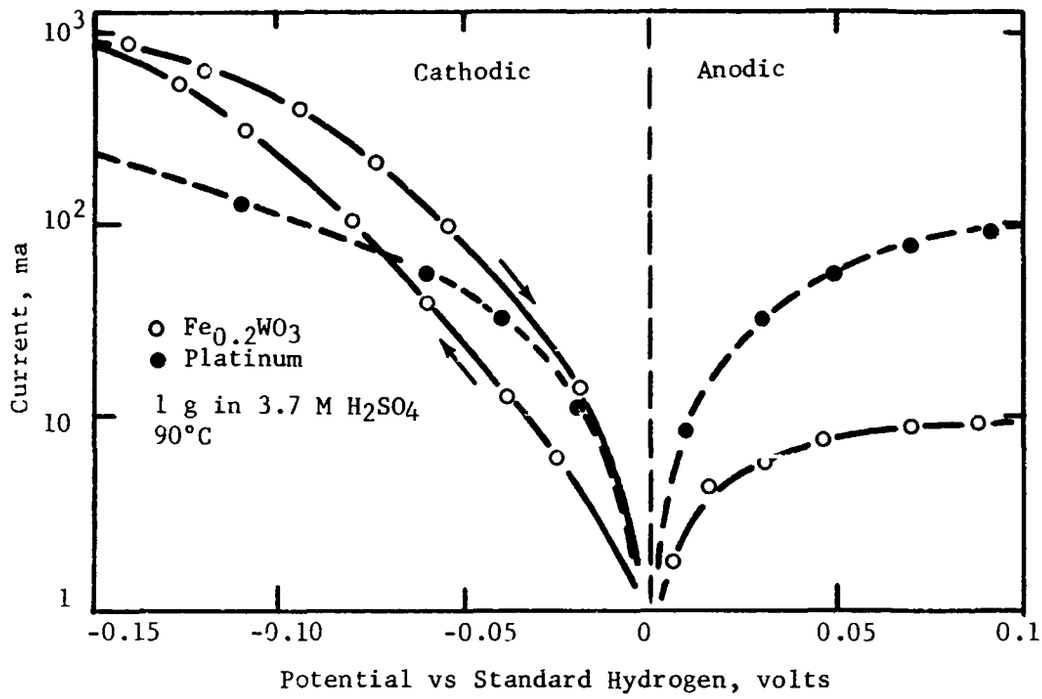

$Ti_{0.2}WO_3$ showed a behavior similar to $Fe_{0.2}WO_3$. This is illustrated in Figure A-6, which compares the hydrogen and oxygen performance obtained with a slurry electrode to that of a comparable porous electrode system. These curves clearly indicate that the slurry behavior is the same as that of the porous electrode.

Further studies are required to determine the most efficient conditions for slurry cell operation and test conditions for quantitative catalyst testing. However, the present study has established that the slurry system responds in the same manner as a porous electrode without the problems of electrode fabrication.

Figure A-6

Polarization of $Ti_{0.2}WO_3$ -
Slurry and Porous Electrode

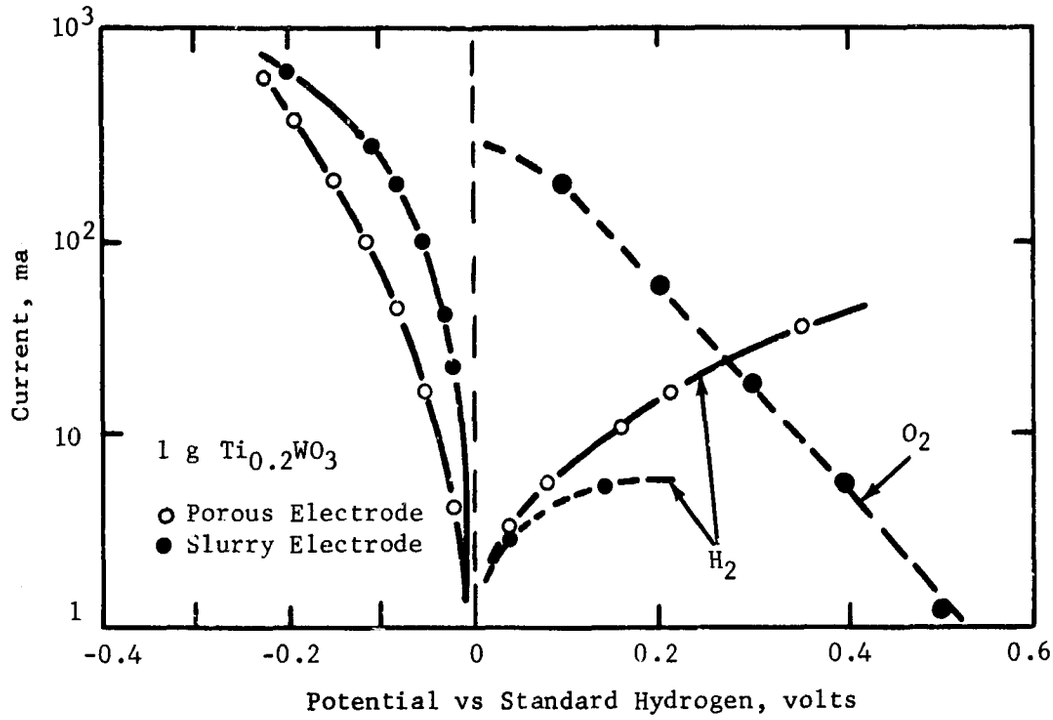

Part c - Voltage Scan Analysis
Metal-Tungsten-Oxygen System

Previous studies (9) have shown that the voltage scan procedure can provide insight into the behavior of the metal-tungsten-oxygen catalysts. These scans can be interpreted to explain initial corrosion behavior and steady state oxidation reduction cycles. In addition, hydrogen or oxygen activity can be demonstrated unambiguously.

Voltage scan measurements were made using the previously described electrodes in 3.7 M sulfuric acid at 90°C. Slow scans (7.2 millivolt/sec) were run between 0 and 1.5 volts vs standard hydrogen potential, with repeat scans run to determine the extent of corrosion, if any.

The initial corrosion behavior of a $Ti_{0.2}WO_3$ electrode is shown in Figure A-7. This response is typical of the initial corrosion curves obtained in this study. The various curves (in numerical order) represent successive voltage scans with nitrogen passing over the electrode. Two anodic peaks are generally observed, one large double peak extending between 100 and 400 millivolts vs standard hydogen, and a second "corrosion" peak between 400 and 700 millivolts. Notice that the first peak reached steady state after the second scan, while the second peak decreases

continually with each subsequent scan and then disappears. The disappearance of the second peak and the establishment of a well defined peak at 100-400 mv marks the end of detectable corrosion. Corrosion curves for $TiWO_3$, $Mo_{0.2}WO_3$ and $W_{0.2}WO_3$ are shown in Appendix A-5, 6, 7.

Figure A-7

Corrosion of $Ti_{0.2}WO_3$ by Voltage Scan

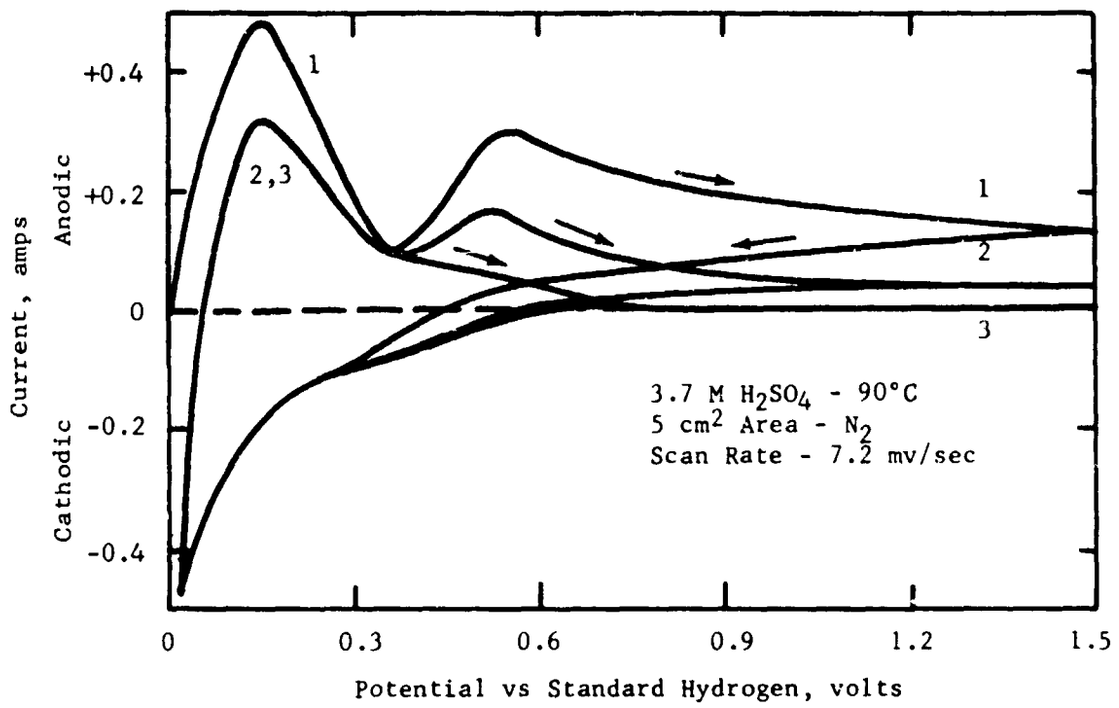

The initial currents of the metal-tungsten oxygen catalyst can be compared qualitatively in order of increasing initial corrosion (Table A-7). This

Table A-7

Initial Corrosion of Some
Transition Metal-Tungsten Oxygen Catalysts

Corrosion Detected	Materials
None	$W_{0.1}WO_3$
Slight	$Fe_{0.2}WO_3$, $Ti_{0.2}WO_3$
Significant	$W_{0.2}WO_3$, $W_{0.3}WO_3$
Very Significant	$TiWO_3$, $Mo_{0.2}WO_3$

ordering seems to be correspond to increasing tungsten-oxygen ratio or addition of active metal. This may be due to irreversible oxidation of the tungsten and tungsten oxide to higher oxides or tungstates since X-ray examination of the $TiWO_3$ electrodes before and after use, shows a weakening of the W and WO_2 lines along with the appearance of as yet unidentified lines. Furthermore, a comparison of the X-ray patterns indicates that WO_2 is present in $W_{0.2}WO_3$ and $W_{0.3}WO_3$, but absent in the more corrosion resistant $W_{0.1}WO_3$.

In any event, the corrosion totally disappears after the passage of a very insignificant amount of current. The steady state response (after corrosion is completed) of these electrodes can be attributed to reversible oxidation-reduction of the catalyst surface layer. All of the electrodes tested show a response similar to that previously reported for $Ni_{0.237}WO_3$ (9). They are characterized by an oxidation-reduction peak with maximum between 0.1 and 0.3 volts versus standard hydrogen. However, the shape and position varies slightly from one material to another; possibly due to oxidation state. Figure A-8 illustrates the effect of varying tungsten oxidation state on the shape and position of the characteristic peak, while Figure A-9 shows the same kind of response for three transition metal tungsten oxide catalysts. Three types of anodic peaks have been observed: Type I ($W_{0.1}WO_3$, $Ti_{0.2}WO_3$, and $Nb_{0.2}WO_3$) is characterized by a very sharp peak with a maximum at 0.13 volts anodic versus standard hydrogen, Type II ($Fe_{0.2}WO_3$, $Mo_{0.2}WO_3$, $W_{0.2}WO_3$ and $W_{0.3}WO_3$) are unsymmetrical peaks with slight displacement towards anodic potentials, and Type III ($TiWO_3$ and W), a symmetrical broad peak.

The anodic reactions, shown in Figures A-8 and A-9, are reversible and the cathodic process occurs at about the same potential. The anodic and cathodic coulombs are approximately equal, indicating a reversible oxidation reduction process such as:

$$H_xWO_3 \rightleftharpoons H_{(x-y)}WO_3 + y\,H^+ + ye, \quad 0<y\leq x\leq 0.33 \ .$$

The existence of hydrogen bronzes such as $H_{0.1}WO_3$ and $H_{0.33}WO_3$ are reported in the literature (84).

Activity as hydrogen electrodes can also be demonstrated in the voltage scan by comparing the oxidation reduction curve under nitrogen with its behavior in the presence of hydrogen. This is illustrated in Figure A-10 for a $Ti_{0.2}WO_3$ catalyst. Notice that the entire hydrogen curve is displaced upward from the reference (nitrogen) case (to more anodic currents). This is similar to the curve reported previously for $Ni_{0.237}WO_3$ (9). Figure A-11, illustrates the activity of this same $Ti_{0.2}WO_3$ catalyst operating as an oxygen cathode, the peaks being shifted downward towards more cathodic current.

From these observations, a mechanism of hydrogen oxidation involving chemical reduction of the catalyst material with hydrogen followed by electrochemical re-oxidation of the reduced species can be postulated. A similar mechanism (i.e, chemical oxidation of the catalyst species followed by electrochemical reduction) could also account for the oxygen activity, since cathodic activity is observed over the same potential range with these catalysts.

Figure A-8

Voltage Scans of Various Mixed Oxides

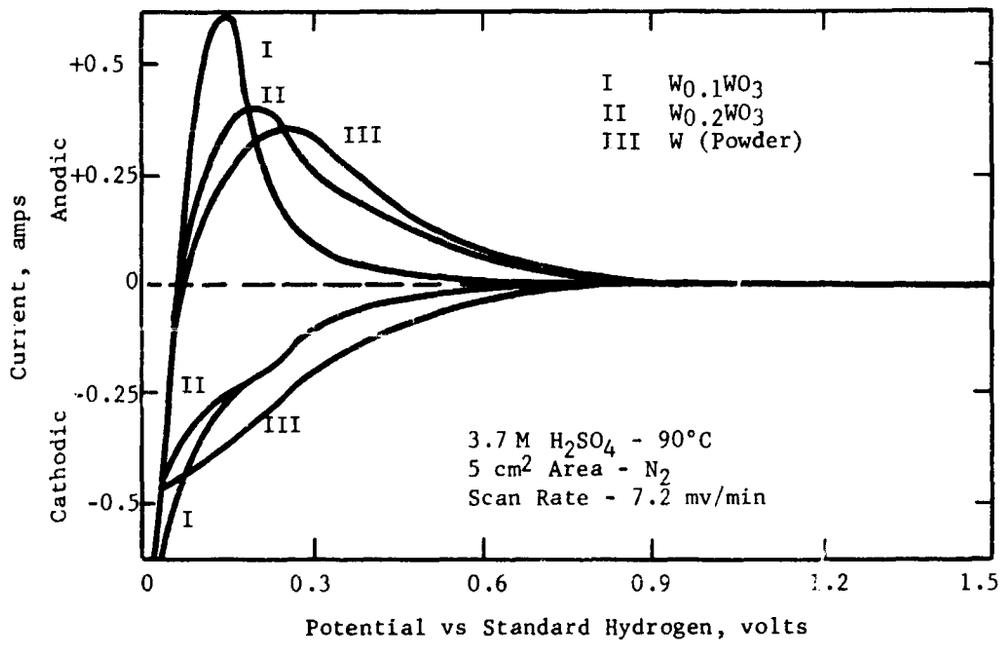

Figure A-9

Voltage Scans of Various Mixed Oxides

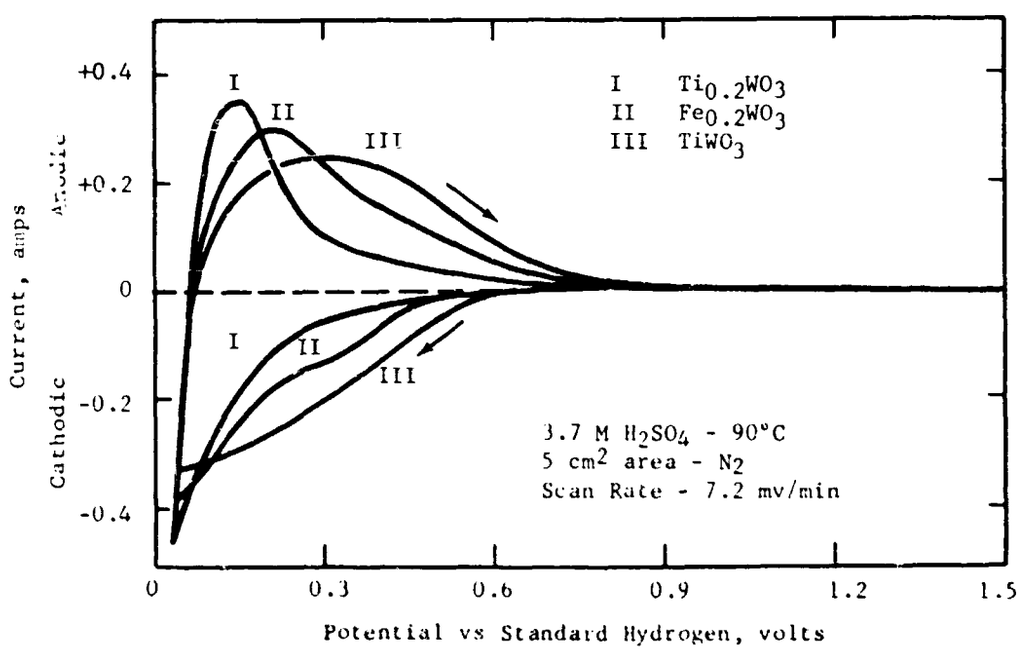

Figure A-10

Hydrogen Activity of $Ti_{0.2}WO_3$ by Voltage Scan

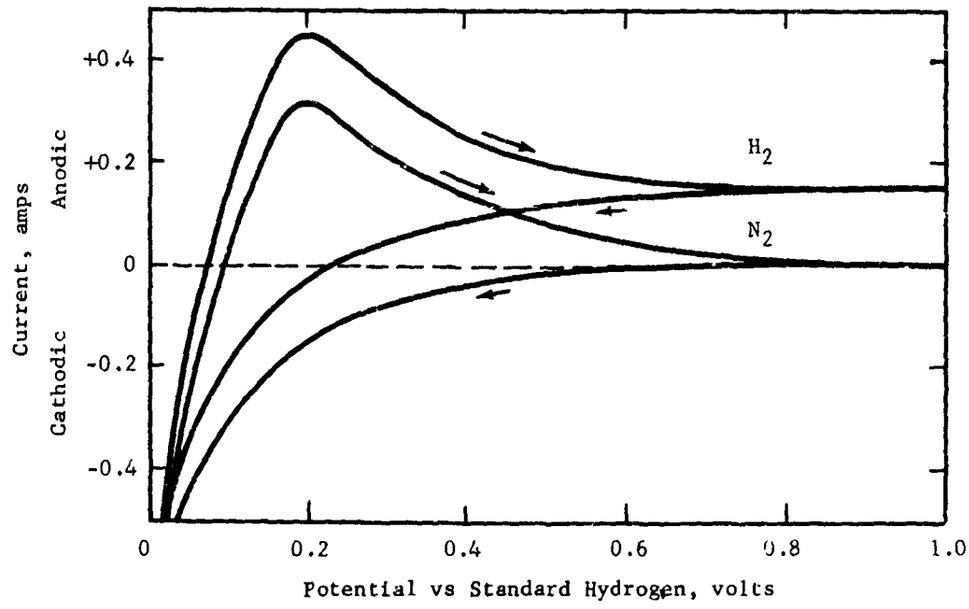

Figure A-11

Oxygen Activity of $Ti_{0.2}WO_3$ by Voltage Scan

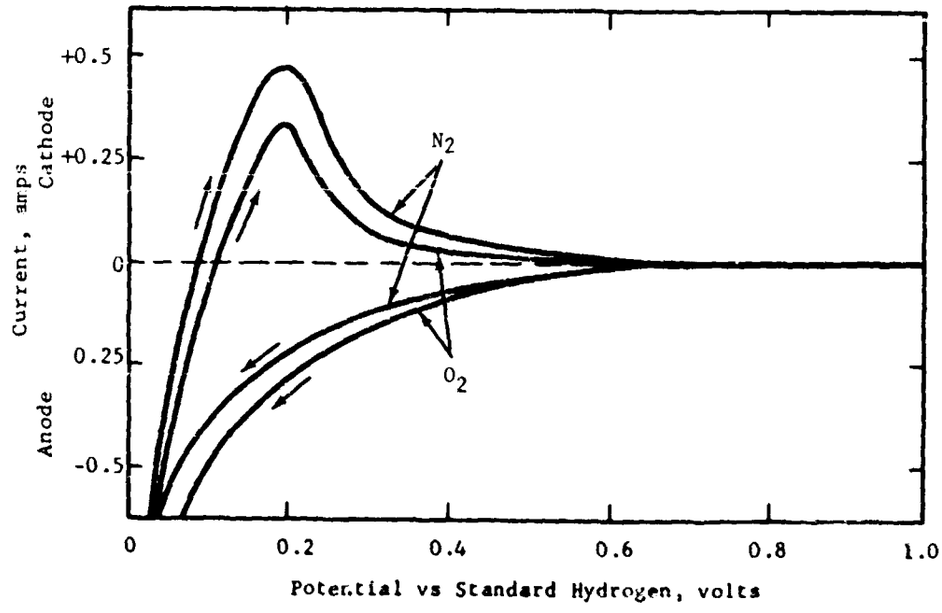

Further support for this mechanism is given by the following experiment. A mixture of 20 mole percent platinum and 80 mole percent $W_{18}O_{49}$ was made into an electrode and a voltage scan was run. The characteristic peaks (82) of platinum could not be detected, indicating that the tungsten-oxygen redox system was strong enough to supress the platinum peaks.

The existence of two peaks in the anodic part of the voltage scan indicates that a two-site surface may be present (39). The nature of the sites is different in anode catalysts from that in cathode catalysts, for not all cathode catalysts can oxidize hydrogen.

Part c - Catalyst Activation Effects

A large number of metal-tungsten-oxide and tungsten bronze catalysts have shown anodic and cathodic activity without any prior anodic or cathodic activation treatment. In some cases hydrogen activity could be substantially increased by evolving hydrogen or dissolving oxygen. However, this effect could only be noted when an oxygen evolving platinum counter electrode was used. Graphite, tungsten, and tantalum counter electrodes failed to cause catalyst activation. Furthermore, the $Ni_{0.237}WO_3$ catalyst could not be activated anodically or cathodically. Since this activation could lead to improved performance a limited study was initiated to determine the source of this effect.

This study has shown that platinum counter electrode disintegration under severe anodic polarization was responsible for these effects. Chemical analysis of an activated $W_{0.2}WO_3$ catalyst showed that this electrode contained 0.05% (0.1 mg/cm^2) platinum after cathodization. This level of platinum is not detectable by X-ray or voltage scan techniques (see Part b). Furthermore, activation was not observed when a Teflon bonded platinum counter electrode operating near hydrogen potentials was used as a counter electrode, thus tending to support a platinum dissolution or transport mechanism.

Further tests showed that this platinum activation could only be accomplished when the platinum counter electrode was in the same compartment as the non-noble catalyst. When the counter electrode was separated from the non-noble metal anode by an ion permeable membrane (Permion P-1010) no activation was observed. Thus, it appears that electrophoretic transport from the disintegrating counter electrode is the most probable source of the platinum deposited during cathodization. No further work is planned in this area.

Phase 4 - Intermediate Temperature Electrolyte Performance

As indicated (Phase 1), a large number of tungsten bronze and transition metal-tungsten oxides exhibit activity as electrocatalysts for hydrogen. In view of this activity, evaluation in the intermediate temperature (275°C) pyrophosphoric acid electrolyte was initiated to determine if the activities of these materials could be increased at higher operating temperature to yield enhanced performance levels despite their inherent low surface areas. These studies included evaluation of corrosion resistance, cathode activity and hydrocarbon performance.

Part a - Corrosion Studies

Most of the transition metal-tungsten-oxides and bronzes exhibited substantial corrosion resistance in 275°C pyrophosphoric acid. Although extended corrosion life studies were not conducted, the six hour electrode evaluation was

sufficient to give a reliable indication of corrosion resistance. For example, a contact time of five minutes in this medium is more than sufficient to completely corrode massive amounts of tantalum metal. During testing, the metal-tungsten-oxide and oxide bronze electrodes are subject to both chemical and electrochemical corrosion forces. It would be expected, therefore, that the severity of the conditions and the contact time would be enough to demonstrate the corrosion resistant properties of these systems.

None of the metal-tungsten oxide electrodes tested showed any physical effects associated with corrosion. Furthermore, electrolyte analysis indicated that little if any corrosion occurred with the metal-tungsten-oxides. However, corrosion was detected with the vanadium bronzes. These results are shown in Table A-8.

Table A-8

Corrosion Resistance Metal-Tungsten Oxides and Related Compounds

(275°C, Pyrophosphoric Acid)

Electrode	Run As	Test Results
$Ni_{0.237}WO_3$	Cathode	Negative for Ni, W barely detectable.
$Ni_{0.237}WO_3$	Anode	Trace Ni, no W.
$Ce_{0.1}WO_3$	Cathode	Negative for all elements.
$Co_{0.2}WO_3$	Cathode	Negative for all elements.
$Mn_{0.2}WO_3$	Cathode	Trace, Mn, no W.
$In_{0.2}WO_3$	Cathode	Trace In, no W.
$Sr_{0.8}NbO_3$	Cathode	Trace Sr, Nb (not indicated).
$Ag_{0.01}WO_3$	Cathode	Barely detectable amount of Ag initially, negative tests for all elements with continued use.
$Fe_{0.2}WO_3$	Cathode	Trace Fe, W barely detectable with continued use, amount of Fe found smaller, W barely detectable.
MoO_5V	Cathode	Corrodes--vanadate colors electrolyte.
$Na_{0.33}V_2O_5$	Cathode	Corrodes--vanadate colors electrolyte.
$Ag_{0.33}V_2O_5$		Corrodes--vanadate colors electrolyte.

It is doubtful that there is any significance to the differences obtained when an electrode is run as an anode or cathode. Excluding catalytic considerations, the lack of corrosion of the metal tungsten-oxide systems in pyrophosphoric acid at 275°C is a promising development.

Part b - Cathode Performance

The oxygen performance of various transition metal-tungsten-oxygen and related bronzes was investigated in 275°C pyrophosphoric acid electrolyte using sintered Teflon bonded electrodes containing 3 wt % Teflon and 185 mg catalyst/cm^2. Heavily gold plated platinum screens were used as the electrode support to rule out any spurious sources of activity.

A Raney gold electrode prepared with this plated screen (catalyst density 150 mg/cm^2) was tested first to establish the oxygen activity of gold in this medium. Should the oxygen activity exhibited by the "bronze" structures exceed that of the Raney gold electrode, activity can be unequivocably assigned to the bronzes since the gold support could not possibly be comparable to Raney gold.

As shown in Figure A-12, the Raney gold electrode does exhibit some oxygen activity which is comparable to that of the $Fe_{0.2}WO_3$ electrode at low (5 ma/cm^2) current densities. At higher current densities the bronze electrode is considerably better. Furthermore, replacing the oxygen with nitrogen resulted in a 200 mv increase in polarization (at 10 ma/cm^2). After ten minutes the polarization was still increasing. Upon returning to oxygen, the $Fe_{0.2}WO_3$ electrode rapidly recovered its original performance level.

Figure A-12

Oxygen Activity of Iron Tungsten Bronze System

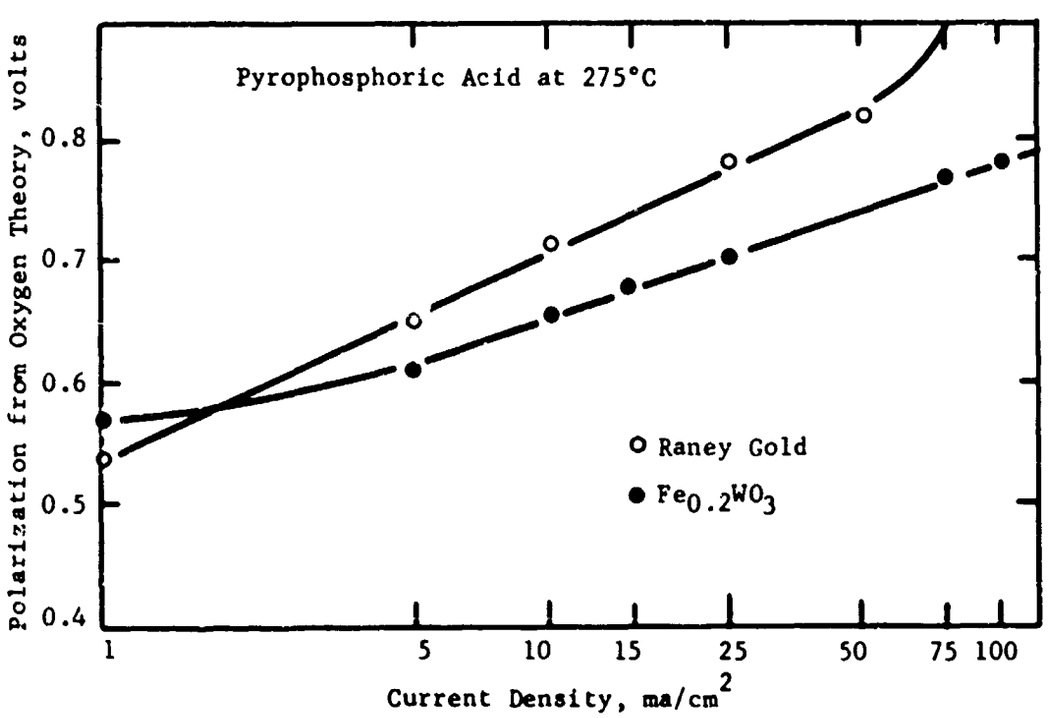

As shown in Figure A-12, the iron tungsten bronze structure supports current densities as high as 100 ma/cm^2, although polarizations at all current levels was severe. This was chiefly due to the large open circuit polarization of 0.53 volts. In part, this polarization may be due to the inherently lower catalytic activity of the bronze relative to platinum. It may also reflect a large mixed potential due to the presence of iron, as any competing anodic reaction that iron may undergo such as: $Fe^{o} \longrightarrow Fe^{+2} + 2\,\mathcal{E}$ and $Fe^{+2} \longrightarrow Fe^{+3} + 1\,\mathcal{E}$ could have a higher exchange current than the oxygen dissolution reaction on this catalyst. This could readily pull the oxygen potential down. The iron tungsten bronze electrode did not show any physical signs of corrosion. No coloration was imparted to the electrolyte, which had a trace of iron, but no tungsten compounds. The corrosion stability of the oxide bronze electrodes is discussed in Part a.

Additional oxide bronzes were screened as catalysts for cathodic activity. Open circuit polarizations were high with three exceptions, the sodium, molybdenum, and silver vanadium bronze electrodes, which were essentially unpolarized at open circuit. The current capability of these systems was poor, however. Other metal-tungsten-oxides such as the cobalt, nickel, and cerium tungsten bronze exhibited oxygen activities comparable to $Fe_{0.2}WO_3$. The performances of some of these systems is shown in Figure A-13, the detailed performance data of all the oxide bronze systems screened is given in Appendix A-8.

Figure A-13

Oxygen Activity of Various Oxide Bronzes at 275°C in Pyrophosphoric Acid

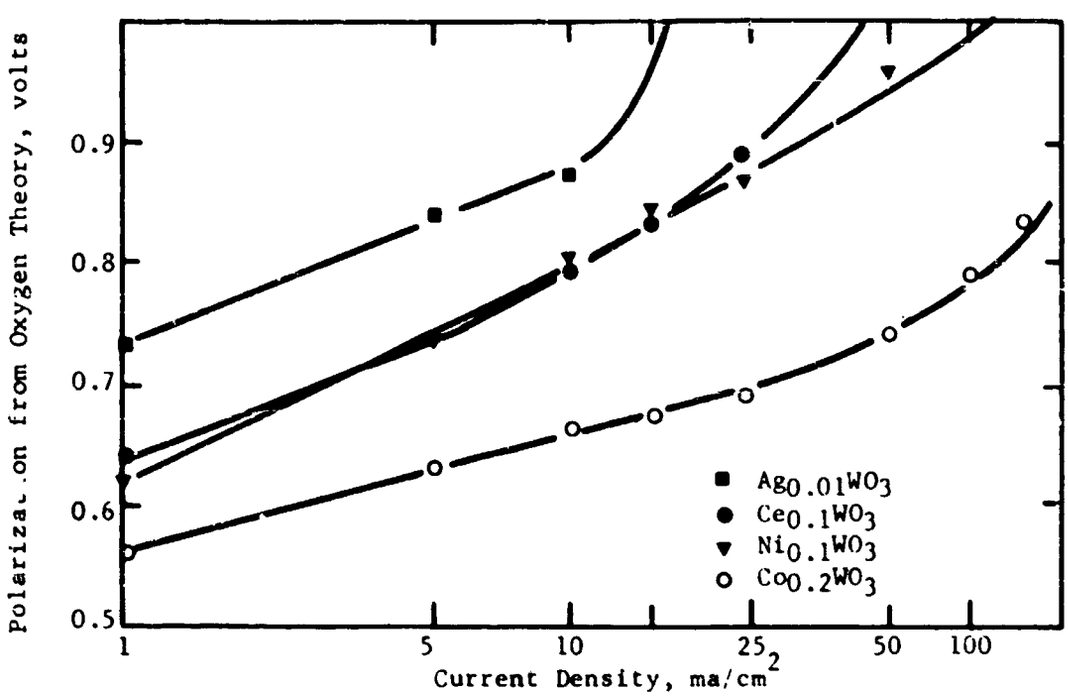

The sodium, molybdenum, and silver vanadium bronzes were the only systems to exhibit appreciable corrosion. Only brief contact times (15 minutes) were necessary for the electrolyte to become greenish yellow. This color could be reproduced by dissolving sodium vanadate in hot pyrophosphoric acid.

Part c - Hydrocarbon Performance

A number of tungsten bronze systems were tested as catalysts for the oxidation of butane in pyrophosphoric acid. Some of these structures had exhibited activity as oxygen catalysts in this medium. Butane was pre-humidified with 60 or 80°C water before entering the anode chamber. Open circuit polarizations ranged from 0.10 to 0.5 volts. All the electrodes were polarized over 1 volt at a current density of 1 ma/cm^2 when steady state was achieved. The electrodes tested include: $Ag_{0.1}WO_3$, $Ce_{0.1}WO_3$, $Ni_{0.1}WO_3$, $Co_{0.2}WO_3$, $In_{0.2}WO_3$, $W_{0.1}WO_3$ and $Sr_{0.8}NbO_3$. Some of the electrodes such as the last one listed polarized over a volt almost immediately while others such as the $W_{0.1}WO_3$ electrode polarized slowly, taking almost one hour to polarize to one volt at 1 ma/cm^2 (details in Appendix A-9).

A nickel tungsten bronze, $Ni_{0.1}WO_3$ was also tested on methanol at 275°C in pyrophosphoric acid. This particular catalyst exhibited a polarization of 0.55 volts on methanol at a current of 10 ma/cm^2 in 3.7 M sulfuric acid at 90°C. A nitrogen carrier gas sparged through water at 80°C and then through boiling methanol was used to carry the fuel to the anode. Methanol activity at 275°C was poor, an estimated 0.46 volts polarized at open circuit, and over one volt at 1 ma/cm^2. Direct methanol injection at a current density of 1 ma/cm^2 brought about a temporary 0.4 volt improvement. No improvements were obtained by injection at higher current densities.

The electrolyte became dark brown, resembling phosphoric or pyrophosphoric acid solutions that have contacted ethylene for some time. The degradation of methanol is probably caused by the bronze catalyst since the brown color is not observed when platinum is used as the catalyst in pyrophosphoric acid (85).

Phase 5 - High Surface Area Alloys

Research to determine how to apply the electronic theory of metals and semi-conductors to catalyst development was initiated during the previous report period. As a first step towards this goal, a series of high surface area alloys of known magnetic properties were prepared with a view towards obtaining a correlation of activity with bond occupancy. Included in this study were solid solution alloys of nickel containing copper, cobalt and iron.

As indicated in the Fifth Semi-Annual Report, only the nickel copper and nickel cobalt alloy actually formed (8). X-ray data indicated that the iron nickel alloys were mechanical mixtures of Fe_3O_4 and Ni. All of these alloys were tested on hydrogen in 6 M KOH at 90°C using an unsintered Teflon bonded electrode structure.

The data reported previously indicated that a correlation of hydrogen activity and magnetic moment (hence d-band occupancy) could be found. However, considerable scatter was observed due to lack of data on catalyst surface area and information on the effect of electrode structure on hydrogen activity. Now that catalyst surface area data are available, the performance information can be corrected to achieve a better correlation. The corrected correlation curve is shown in Figure A-14, which is a plot of corrected hydrogen limiting current versus magnetic moment (η_o). The correction was made by multiplying the observed current

density by the ratio of the surface area of the most active pure nickel catalyst to that of the various alloys. The iron-nickel alloys were not included in this correlation because X-ray data indicated that the desired alloys were not formed (Table B-10) (8).

An examination of Figure A-14 indicates that the observed correlation is quite good, only one Ni-Co alloy out of the nine successful alloys failed to fall on the correlation curve. Notice that the maximum hydrogen activity (170 ma/cm^2) still occurs 1.0 Bohr magnetons as shown in the last report. Since these materials are solid solution alloys of first row transition elements the correlation is equivalent to a correlation with d-band occupancy. Thus, it appears that it may be possible to ultimately establish what the optimum electronic configuration for hydrocarbon oxidation is.

Figure A-14

Correlation of Hydrogen Activity and Magnetic Moment

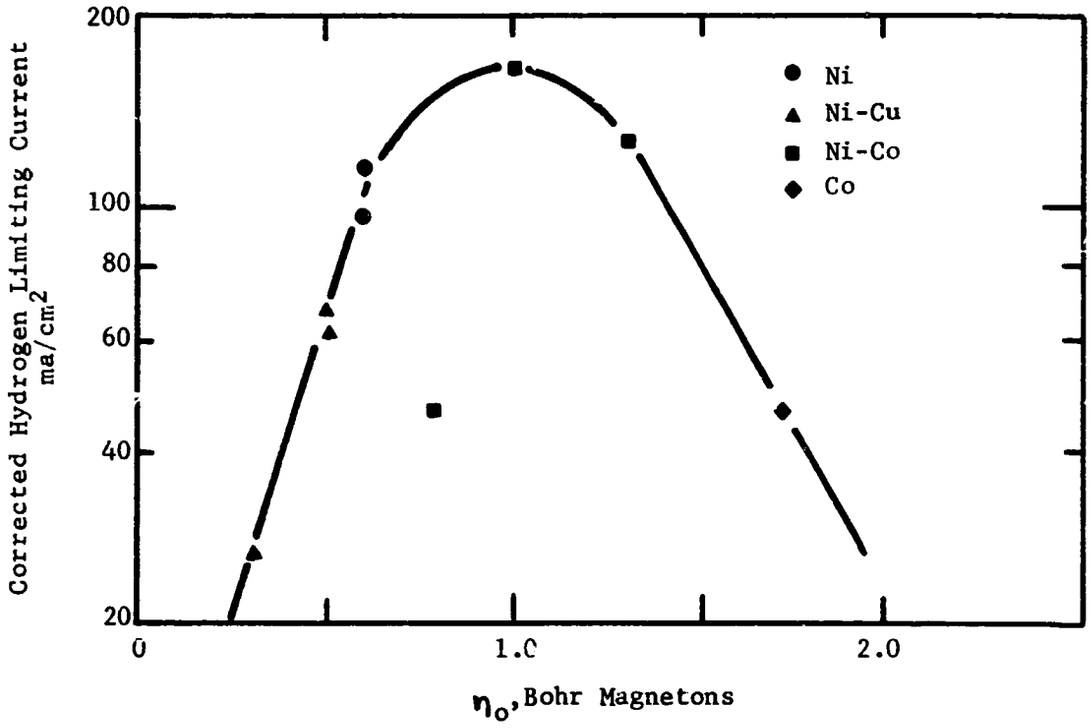

Phase 6 - Conclusions

Part a - Transition Metal-Tungsten-Oxide and Related Catalyst Systems

Studies aimed at defining the range of catalytically active tungsten bronze and transition metal-tungsten oxide catalysts have shown that a wide variety of materials can form electrochemically active anode and cathode systems. This is

illustrated in Figure A-15 which is a portion of the periodic table. In this figure, the materials active as both anodes and cathodes are represented by gray areas, while systems which show only cathodic activity are unshaded. Notice that all of the rare earth tungsten bronzes that possess a strong magnetic moment show both anodic and cathodic activity. Lutetium which is non-magnetic, shows only the oxygen activity typical of the tungsten oxide systems. Thus, it appears that the injected ion must have a magnetic moment in order to insure anodic activity. Indeed, all of the first row transition elements except scandium, cobalt,and copper show both anodic and cathodic activity. However, the absence of anodic activity with the cobalt-tungsten-oxide is quite surprising since both iron and nickel produce active anode catalysts. However, where hydrogen activity is detected,its current-voltage response does not follow the Tafel equation.

Oxygen performance,on the other, hand does yield good Tafel slopes, and all of these systems show oxygen activity. These systems appear to be more active cathodes than anodes. However, this appears to be a property of conductive tungsten oxides in general. The fact that all tungsten bronzes and mixed metal-tungsten-oxides (including $W_{0.1}WO_3$) show cathodic activity strongly indicates that oxygen activity is a property of the tungsten-oxygen systems that are electrically conductive.

$Ni_{0.237}WO_3$ gave the best hydrogen performance attained thus far, 8-9 ma/cm^2 at 0.6 volts polarized; again the response was not Tafel. Methanol activity was also observed with this system (50 ma/cm^2 at 0.6 volts polarized),but open-circuit polarization was quite poor. No other hydrocarbon activity has been detected thus far.

Figure A-15

Active Metal-Tungsten Oxide Catalysts

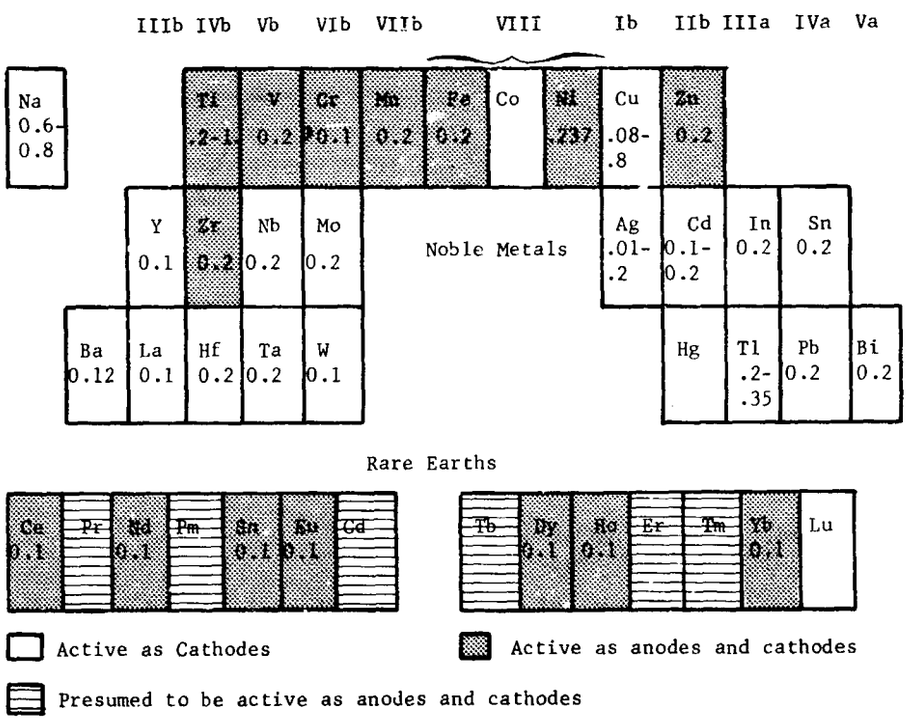

All of the other bronze forming metals were considered as potential bronze and mixed-oxide catalysts systems. With the exception of molybdenum, these materials show no promise as potential hydrocarbon electrocatalysts.

Part b - Electrochemical Evaluation Studies

Problems associated with the electrical bonding of finished electrodes prepared from ground metal-tungsten-oxygen catalysts powders has limited both the anodic and cathodic performance. Indeed, this poor bonding results in a reduction in effective catalyst surface area from its BET values of 7-8m^2/gm to its electrochemical value of 10 cm^2/gm. Furthermore, an analysis of the IR characteristics of the nickel-tungsten-oxygen system indicates that the conductivity of the finished electrode is potential dependent - resistance increasing with increased anodic polarization.

Attempts to eliminate this electrode structure problem by using the slurry electrode system were only partially successful. Although the slurry electrode is quite stable it behaves essentially like a high resistance porous electrode. Both voltage scan and steady state runs are comparable to interface maintaining electrodes. Only the electrode fabrication step is eliminated.

Voltage scan experiments with mixed metal-tungsten-oxides have shown that there are probably several intermediate oxidation-reduction states which take part in hydrogen-oxidation and oxygen reduction. From these observations, a hydrogen oxidation mechanism involving chemical reduction of the catalyst by hydrogen, followed by electrochemical re-oxidation is postulated. The reverse process (oxidation by oxygen-followed by electrochemical reduction) could also account for oxygen activity.

Part c - Intermediate Temperature Electrolyte Performance

The metal-tungsten-oxygen system was evaluated as potential cathodes and butane anodes in 275°C pyrophosphoric acid. This study has shown that $Fe_{0.2}WO_3$ can sustain up to 100 ma/cm^2. However, the polarization is high due to a poor open circuit potential. Several of the other metal-tungsten-oxides could sustain significant oxygen currents but none were any better than $Fe_{0.2}WO_3$. No unequivocal hydrocarbon activity has been observed as yet.

2.2 Task B, Noble Metal Catalysis

Current research on noble metal catalysis is aimed at increasing the platinization levels of carbon supported catalyst systems while retaining or improving overall platinum utilization. This increased platinization is required to accommodate these materials in thin (6-8 mil) optimized hydrocarbon anode structures while retaining sufficient platinum in the active zone to attain practical current densities. Platinization levels of 12 to 18% are required to meet the initial hydrocarbon anode target of 150 ma/cm^2 with a platinum loading of under 2 mg Pt/cm^2. Previous studies (9) have shown that alterations in platinum adsorption selectivity, through carbon dioxide or ozone treatment, can markedly improve catalyst utilization. Increased platinum contents could be obtained by a multiple adsorption technique without loss in catalyst utilization. Consequently, studies aimed at developing techniques for selectively activating or deactivating platinum adsorption sites through pre-treatment and platinum salt selection have received considerable attention. Alternately, adjusting platinum adsorption sites by producing narrow pore size distribution carbons was also investigated.

Incorporation of highly platinized carbon catalysts in suitable electrode structures will introduce new requirements since thin 1-3 mil conductive catalyst beds will ultimately be required. Therefore, potential future generation anode structures and electrolytes were also briefly examined using current generation supported catalysts.

Phase 1 - Supported Platinum Catalysts

Work reported previously has shown that for a given carbon type, platinum utilization is critically dependent on adsorbed crystallite size. Platinum utilization was best when deposited crystallites of less than 70°A were observed. Furthermore, surface area per-se did not appear to be an important factor since the 200 m^2/gm FC-30 carbon gave a better utilization response than either of the higher surface area FC-20 (700 m^2/gm) and FC 50 (450 m^2/gm) carbons tested. This indicated that some other factor such as pore size distribution was important. This program also showed that platinum crystallite size and,hence,utilization could be controlled by deactivation of macro-pore adsorption sites by ozone oxidation, thus favoring chemisorption on the less accessible 70-180°A pore sites. As indicated in Table B-1, application of this ozone oxidation procedure coupled with multiple platinum adsorptions has resulted in increased platinization without loss in limiting current utilization. However, the performance of the double adsorbed catalyst at 0.4 polarized was somewhat impaired.

Accordingly, alteration of platinization selectivity and multiple adsorption procedures were examined in an effort to achieve the higher performance levels required. Commercial FC-20 (200 m^2/gm) and 28% CO_2 treated FC-30 carbons were used in most of these studies. Two Regal carbons,XC-72 and 330R,were briefly examined. In addition, some successful intermediate porosity carbons were also prepared.

All of the catalyst preparations were evaluated in the sintered carbon Teflon emulsion electrode structure (7) using either Teflon 41BX (349°C, 1 minute, 2200 psig) or Teflon 42 BX (329°C, 1 minute, 2200 psig). The use of two different grade emulsions was necessitated by differences in quality control even with the improved Teflon 42BX system. Butane activity was determined using 14.7 M H_3PO_4 at 150 °C in the standard half cell described previously.

Table B-1

Effect of Double Adsorption on
Limiting Butane Performance

(FC-20 Carbon - 0.1 gms O_3/gm C,)
(150°C - 14.7M H_3PO_4)

Number of Adsorptions	Wt % Platinum	Loading, mg Pt/cm^2	Thickness, mils	Limiting Butane Utilization, ma/mg Pt (0.45-0.48 v Polar)
Single	5.9	2.5	23	22
Double	11.2	4.7	23	18
Double	11.2	3.2	15	25
Double	11.2	1.6	10	25

(1) Platinization procedure discussed in Part a

Part a - Catalyst Preparation Studies

Examination of a number of different platinization and activation procedures has shown that platinum adsorption from dilute solution can result in a utilization advantage over conventional methods such as impregnation or co-precipitation. This technique allows a number of degrees of freedom in platinization selectivity not attainable with the other procedures. For example, by proper selection of the platinum salt, concentration, adsorption time, substrate pretreatment,and pore size distribution,it is possible to direct the platinum to the less accessible pores which in turn results in smaller platinum crystallites and enhanced performance.

A room temperature adsorption procedure was adopted for this and subsequent studies (8). The platinum adsorption is accomplished by allowing the active sites on the carbon to partially reduce the platinum salt with subsequent deposition at that site. This reduction is accompanied by a decrease in pH and a loss of chlorine from the adsorbed salt. This is accomplished by contacting the pre-treated substrate (carbon) with 0.4 wt% platinum salt solution for 16 hours. This is sufficient to allow platinization of the most active sites but not long enough to produce saturation coverage. After adsorption, the excess salts are washed away, and the unactivated platinized carbon is washed and dried from methanol. If no subsequent re-adsorption is required,the catalyst is activated by a three hour carbon monoxide treatment at 425°C,followed by a three hour hydrogen reduction at 870°C.

When successive re-adsorption is required to increase platinization, an intermediate temperature (150 or 204°C) hydrogen treatment is required between re-adsorptions. All catalysts receive the high temperature CO and H_2 treat after final adsorption. Finished catalysts are then ball milled for four hours to improve platinum accessibility (8).

Previous studies have shown that the high temperature carbon monoxide and hydrogen treatment are required to attain maximum performance. However, these treatments were developed and optimized for catalysts with significantly lower platinization levels than those available at present, or contemplated for future preparation. Thus, a re-examination of this activation procedure will be required with highly platinized carbon catalysts. Preliminary experiments indicate that the effectiveness of the high temperature hydrogen treatment may depend upon how the platinum salt is initially deposited on the carbon substrate.

Table B-2

Effect of Adsorption and Reduction Conditions on Butane Performance (1)

(14.7 M H_3PO_4, 150°C,)
(FC-30 Carbon - 0.1 gm O_3/gm C)

Adsorption Condition		Reduction Temperature °C	
		760	870
Vigorous agitation	ma/cm^2	20	22
	Crystallite Size, Å	57	67
Mild agitation	ma/cm^2	13	2
	Crystallite Size, Å	90	90

(1) CO treat three hours at 425°C

Tests (summarized in Table B-2) indicate that reducing the reduction temperature 100°C had little effect on performance when contacting during the adsorption step was adequate, even though the 760°C material had a lower crystallite size. However, where contacting during adsorptions was poor, a marked performance deficit was observed at 820°C. This is not too surprising since the high temperature reduction was designed to perform two functions, (1) reduce the platinum salt and (2) cause some platinum migration and growth to improve conductivity, accessibility, and bonding. If the platinum salt is adsorbed in the small pores (when diffusion is favored by agitation), the crystallite growth will not be excessive. However, under stagnant or poorly agitated conditions, adsorption will occur in the larger pores and growth will be significant. In this latter case, lowering the reduction temperature could have an effect. X-ray crystallite size measurements obtained with the poorly agitated material did not reflect this anticipated difference. However, this may not be significant since X-ray crystallite measurements weight the largest crystallites and tend to ignore the smaller ones. In any event this will have to be given some additional examination when the 12-18% platinization target is achieved.

Part b - Fluid Bed Ozonization

Room temperature ozonization can significantly improve catalyst utilization through alteration of the initial platinum adsorption sites. As indicated earlier, platinum adsorption is due to a partial reduction of the platinum salt at active sites on the carbon support. Because of its high reactivity, ozone attack occurs at the relatively accessible sites in the macro-pores, oxidizing them and deactivating them for subsequent platinum reduction. Thus, the salt is forced to deposit on less accessible micro-pore sites.

These initial studies used a fixed bed reactor for the ozone treatment. In view of the reactivity of the ozone stream, it was felt that most of the ozone oxidation occurs in the lower portion of the reactor, resulting in an inhomogeneous material. Consequently, a series of experiments were conducted in a fluidized bed unit to insure good vertical mixing of the carbon and the O_3/O_2 stream. Unlike the fixed bed reactor, the hand ground FC-20 carbon had to be screened to 60 to 150 micron size prior to use, the fixed bed unit does not required this.

The resultant ozone treatment - utilization response curve, shown in Figure B-1, is similar to that obtained previously with the fixed bed unit, yielding an optimum utilization at an ozone treatment level near 0.1 gm O_3/gm of carbon. However, the entire utilization level was significantly poorer than that obtained previously in the fixed bed unit. The reason for this impaired performance is not clear. However, difficulties with the Teflon emulsion were encountered during this period and none of the catalysts evaluated during this period fared too well. Furthermore, it is difficult to see how a more controlled ozonization and a restricted particle size could reduce performance. These latter changes would only make for a more homogeneous catalyst. Details are summarized in Appendix B-1.

Figure B-1

Optimization of Fluid Bed Ozonizer

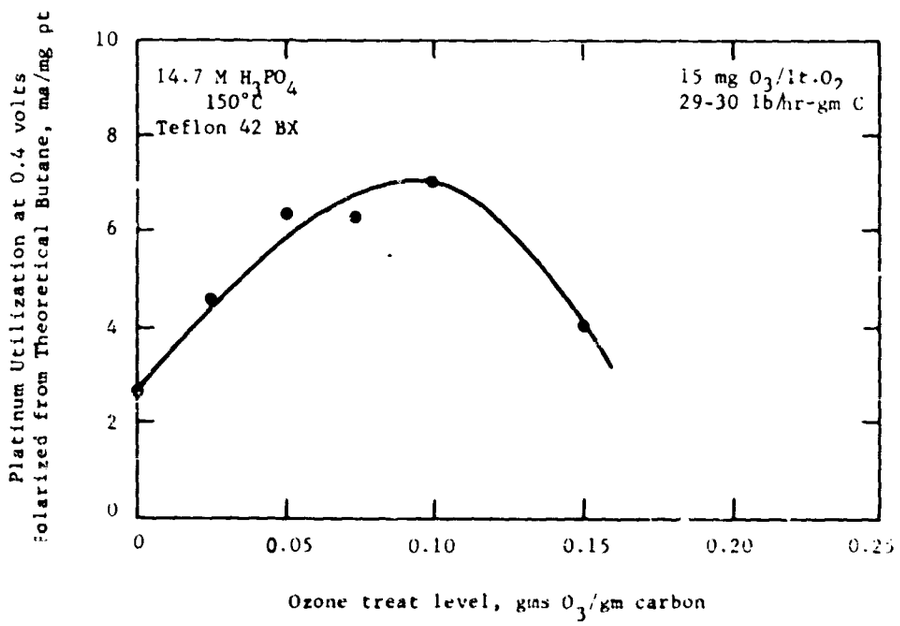

Indeed, the data on platinization and platinum crystallite size, Figure B-2, tend to confirm the proposed adsorption site deactivation mechanism for ozone action. Notice that the platinization level decreases with increasing ozone treatment, leveling off at about 4.4% between 0.1 and 0.15 gms O_3/gm C. This plateau appears to correspond to complete deactivation of the macro-pore adsorption sites. Thus, ozone treatments beyond 0.1 gm O_3/gm C are not required. Indeed, further ozone treatment could be deleterious since attack on micropores would begin. This reduction in platinization with increased ozone treatment was not observed with the FC-20 carbon when the fixed bed ozonizer was used. Instead a constant platinization level of 5.7% was obtained independent of ozone treat, a further indication of the lack of homogeneity in the fixed bed O_3 treatment.

Crystallite size was also found to decrease monatonically with increased ozone treat, reaching a minimum at 0.1 gms O_3/gm C, the point at which all of the macropore adsorption sites are presumed to be deactivated.

Figure B-2

Effect of Ozone Treatment on Platinization
And Crystallite Size - Fluid Bed Ozonization

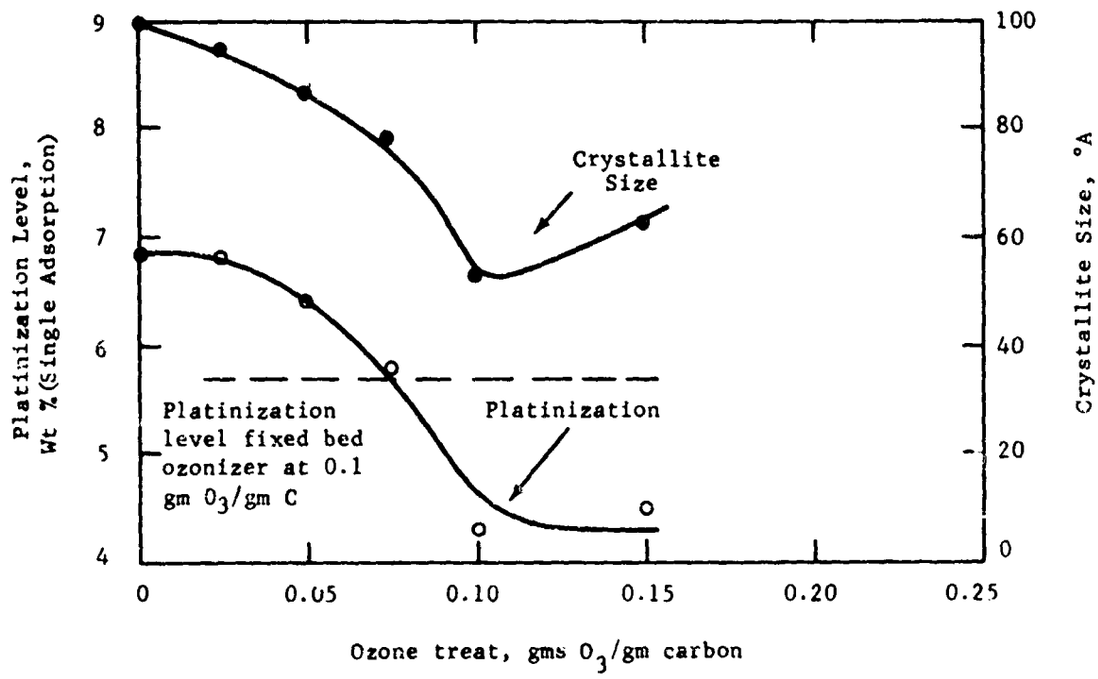

Part c - Intermediate Porosity Carbons

The extent of crystallite growth during hydrogen activation is dependent upon the initial location of the adsorbed platinum salt. Platinum located in the smallest pores show the least (sintering) growth on activation with hydrogen. For this reason the ideal support appears to be one with a maximum intermediate or transitional pore volume. Carbons with this required pore distribution are not generally available. However, they can be prepared using the method of Dubinin (86). In this procedure, a leachable foraminating agent such as $ZnCl_2$ or $FeCl_3$ is dispersed in a sucrose solution prior to evaporation. The resultant thick syrup is then carbonized at 800°C in a carbon dioxide atmosphere and the foraminant removed by leaching in 4NHCl at 65°C for thirty minutes and washing till free of chloride ion. Platinization was accomplished by standard adsorption ($(NH_4)_2 PtCl_6$) and activation procedures.

This technique was used to prepare a number of intermediate porosity carbons ranging in surface area from 200 to 1200 m^2/gm. The effect of foraminant content on surface area and platinization level (single adsorption) is shown in Figure B-3. As indicated, the surface area increases monatonically with $ZnCl_2$ content, while platinum content increases almost linearly with surface area above 600 m^2/gm. Despite these high surface areas the total pore volume was quite low, ranging from 0.03 to 0.05 cm^3/gm, with 35-50% of these pores in the 70 to 215°A range.

This low intermediate pore volume was quite discouraging. However, the performance observed was better than any synthetically prepared carbon thus far examined (Appendix B-2). The effect of foraminant content on butane performance and catalyst utilization is summarized in Figure B-4. Note that the platinum utilization remained fairly constant (10 ma/mg Pt) above 20 wt% $ZnCl_2$. The increased current density observed was only a reflection of increased platinum adsorption due to the higher carbon surface area. Attempts to use $FeCl_3$ as the foraminant produced poorer utilization.

The failure to produce improved platinum utilization through the use of "sucrose" carbons is probably due to the lack of pore volume. Conventional carbons generally have about the same amount of 70 to 215°A pores as did the sucrose carbons. However, their total pore volume (and hence fuel accessibility) is considerably higher, ranging near 1 cm^3/gm. Indeed, the platinized carbon with the smallest crystallite size gave the poorest performance. From these data it appears that a distribution of macro and micro pores is required for good hydrocarbon anode performance, but the correct pore distribution is yet to be defined.

Table B-3

Platinum Crystallite Size And Utilization, Sucrose Carbons

%$ZnCl_2$	Crystallite Size, °A	Utilization at 0.40 volts polarized, ma/mg
11	25	3
20	55	10
33	60-65	9.7

Figure B-4

Butane Performance of Sucrose Carbons
(Electrode Thickness: 23 mils)

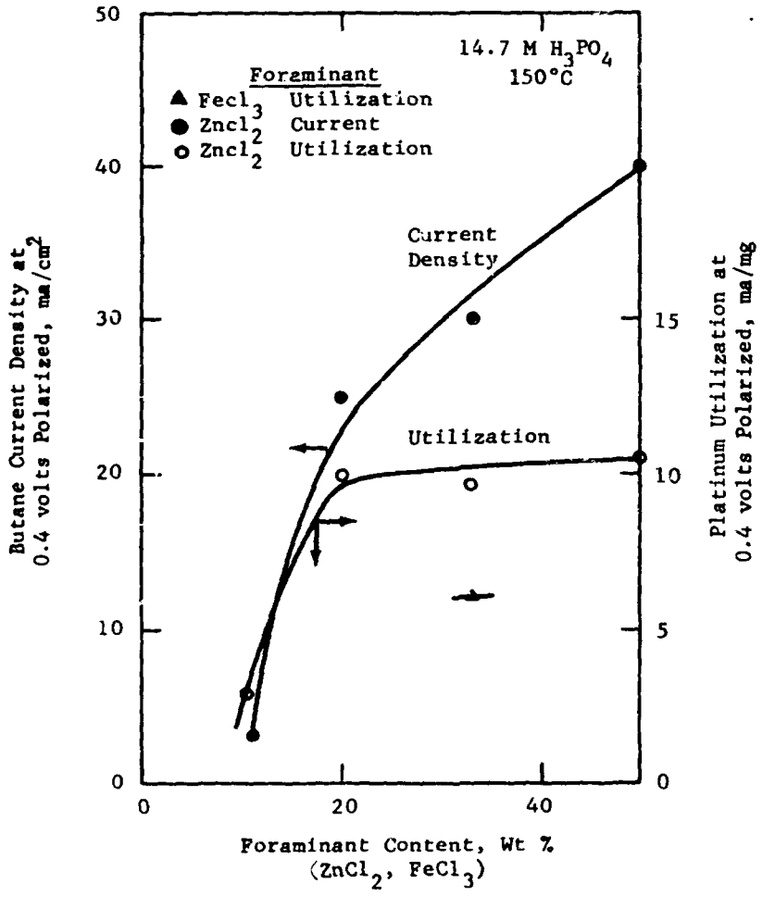

Figure B-3

Effect of Foraminant Content
on Platinization and Surface Area
(Sucrose Carbons)

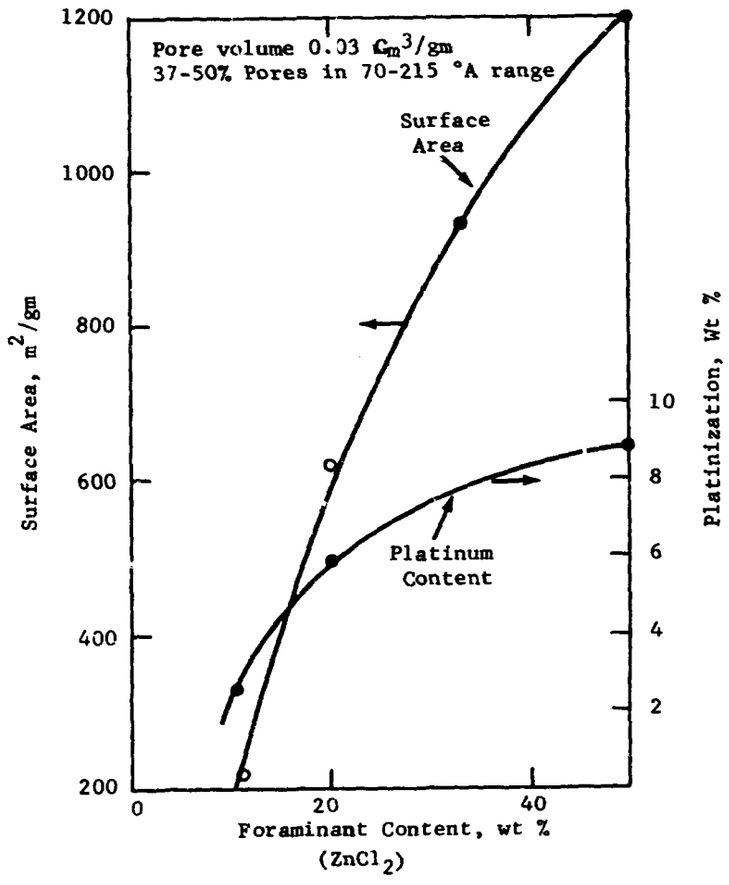

Part d - Alternate Platinum Salts

Platinum deposition selectivity can also be altered through a judicious selection of adsorbate salt. Consequently, a number of inorganic and organic platinum salts were screened as potential adsorbates. These salts are listed in Appendix B-3. Some of these salts were initially reduced as unsupported materials to check on their corrosion resistance prior to use as adsorbates. These tests indicated that the 50 Co-50 Pt alloy (atm.%) had excellent corrosion resistance in 3.7 M sulfuric and 14.7 M phosphoric acids. However, the 50 Ni-50 Pt alloy was not acid resistant. Therefore it was dropped from this initial survey because the nickel would have to be removed after catalyst preparation and the extent of removal could not be accurately determined.

The remaining salts were adsorbed from the appropriate solvent on to a well characterized FC-30 carbon support (172 m^2/gm, 28% CO_2 treated). This material was selected because of its availability since sufficient quantities of the best FC-30 carbon was not available. Activation was accomplished in the usual manner.

The butane performance of the three inorganic salts is summarized in Table B-4. These data indicate that using a neutral ammonium chloroplatinate (commercial) salt can result in a 60% improvement in platinum utilization. However, the performance deteriorated significantly with time and subsequent attempts to prepare active materials using other carbon supports produced materials with little or no activity. A 50% improvement in utilization was also obtained when cobalt chloroplatinate was used as the adsorbate. Repeat preparations also showed this improved utilization even when the multiple adsorption technique was employed. This 50 Co - 50 Pt alloy is interesting since it is the electronic analogue of the non-noble 25 Co - 75 Ni alloy which gave the best hydrogen activity. (Task A, Phase 5).

Table B-4

Butane Performance of Platinum Salts

(150°C - 14.7 M H_3PO_4)
(FC-30 Carbon)

Salt	Wt % Platinum	Catalyst Utilization, ma/mg Pt	
		at 0.4 v polarized	at limiting Current
NH_4OH Neutralized H_2PtCl_6(pH 6)	2.3	20	25
Cobaltous[1] Chloroplatinate	2.1	30	30
Commercial[2] $(NH_4)_2$ $PtCl_6$ neutral salt	1.4	32	32
Tetra amino platinum IV chloride	0	No adsorption	

(1) Active on repeats and with other carbons.

(2) Single preparation--all other carbons produced inactive materials.

In view of the improved performance of the cobalt platinum catalyst, studies were initiated to determine if this alloy was catalytically different from pure platinum. If this could be established it would provide the first experimental verification of our previous contention that platinum does not have the optimum electronic structure for hydrocarbon oxidation. Methanol oxidation provides a well characterized reaction for this examination. Methanol performance studies[90] demonstrated that Co-Pt is a uniquely different material in that it (a) gave a lower open circuit polarization, (b) higher Tafel slope (0.085 vs 0.06) and (c) a 160 mv reduction in polarization at 100 ma/cm^2 when compared to either commercial platinum black or comparably reduced material. Indeed, the methanol catalyst utilization was improved by 50% with this alloy. Part e will discuss more detailed studies of this alloy system.

Organo-platinum compounds were also considered as potential adsorbates since they might tend to favor adsorption sites which would normally see hydrocarbon in the finished electrode. Unfortunately results to date have been far from encouraging. A commercial salt, platinum trimethyl benzyl ammonium chloride, was successfully adsorbed (from benzene) on FC-30 carbon. However, the electrode yielded less than 2 ma/mg. X-ray analysis indicated that about half the adsorbate remained unreduced after the 870°C hydrogen treat.

Other thermally decomposable organo-platinum compounds were also briefly considered. $(CH_3)_3$ PtI was prepared by the method of Pope and Peachy [87]. However, thermal decomposition failed to yield an active catalyst. This method of preparation will be attempted again. Attempts to prepare the tetramethyl platinum salt have thus far been unsuccessful.

Part e - Cobalt-Platinum on Carbon Catalyst Studies

In view of the success with the Co-Pt on carbon catalysts, attempts were made to produce materials with increased platinization and utilization by using alternate carbon supports. The results of this study are summarized in Table B-5. As indicated, FC-30 remains the best carbon support for this system yielding a limiting current utilization of 33 ma/mg Pt. However, Cabot's Regal330R carbon may also be a useful support. It is interesting to note that platinum utilization increased with increased platinization. Some of this improvement is probably due to a reduction in electrode thickness. However, the utilization improvements with Regal 330R and XC-[illegible] carbons are much too large to be attributed to these small changes in thickness alone. Indeed, the FC-30 carbon's utilization increased despite a thickness increase. Thus it appears that each carbon has a minimum platinization level below which it does not function properly. This may be due to an electronic conduction problem.

Table 5-5

Effect of Carbon Type and Platinization Level on Butane Performance

(Co-Pt on C, 14.7 M H_3PO_4, 150°C)

Carbon	Pt wt %	Thickness mils	Crystallite size Å	Catalyst Utilization ma/mg at 0.4 volts polarized	Catalyst Utilization ma/mg at Limiting Current
FC-30(1)	1.8	21	--	12.5	15
	2.09	31	28.4	29	29
	5.76	13	40.5	30.2	33
Regal 330 R	3.27	31	48.7	2	3
	5.64	26	47.3	25	25
XC-72 R	2.5	34	--	6.4	--
	5.05	26	42.6	9.1	13.6
	8.13	20	48.7	18.2	20.5

(1) 28% CO_2 Treat

Attempts to prepare a Co-Pt catalyst on ozonized FC-20 carbon have thus far been unsuccessful. It appears that this may be due to the ozone treatment since incomplete reduction and desorption of cobalt ion was found on subsequent adsorptions. This would indicate that the cobalt and platinum adsorb on widely separated locations on this carbon since cobalt will not be reduced by 200°C H_2 except in the presence of platinum. Tests with untreated FC-20 carbon have not as yet been completed. However, cobalt desorption stops after the first or second intermediate reduction. This is important since by that point most of the ozonized sites have been re-reduced. Additional work with FC-20 carbon is anticipated.

Phase 2 - Electrode Structure Studies

Previous studies have shown that the interplay of electrolyte, catalyst and electrode structure can markedly affect the overall performance of a catalyst system. The necessity for structure optimization for each electrolyte has already been established. The development of the supported Co-Pt catalyst system will necessitate some structural re-evaluation. Consequently, this system was examined to determine the effect of catalyst loading, thickness, electrolyte and temperature parameters. In addition, the advent of highly platinized catalysts has necessitated a re-examination of our existing structure concepts since these materials will probably require very thin (1-3 mil) conductive structures mounted on a conductive, porous interface controlling matrix.

Part a - Supported Cobalt Platinum Catalysts

Earlier studies (7,8) with platinized carbon electrodes indicated that for a given catalyst loading, the thinest electrode (highest platinization) gave the best catalyst utilization. The thickness-loading response of the new supported Co-Pt alloy catalysts was examined to determine if thickness was also an important parameter in this system. For this study a Co-Pt on FC-30 Carbon (5.8 wt% Pt) was prepared by the multiple adsorption technique (phase 1, part a). As indicated in Figure B-5, a maximum current density of 80 ma/cm^2 at 0.4 volts polarized was obtained at the intermediate (3.2 mg/cm^2) platinum loading, thus demonstrating a marked electrode thickness dependence. In fact, the limiting current utilization decreases linearly with thickness between 13 and 31 mils. This indicates that increased platinization will also be required with this catalyst system.

Figure B-5

Effect of Loading and Thickness on Butane Performance

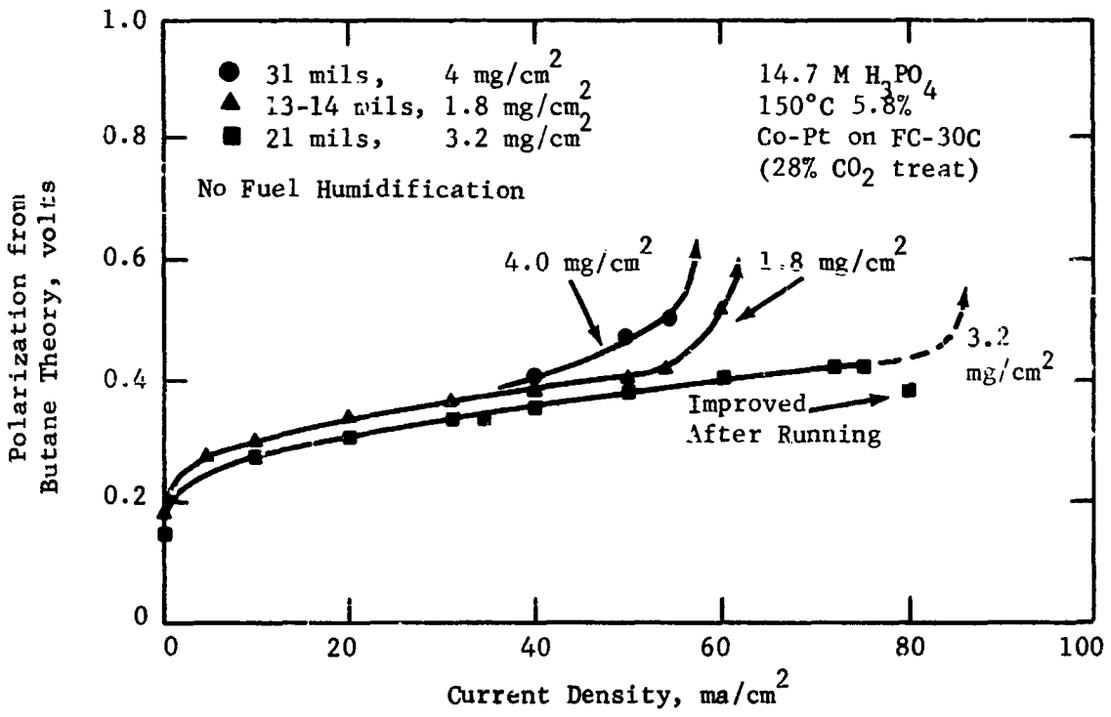

The effect of electrolyte composition and temperature was examined using a highly loaded (4 mg Pt/cm^2) electrode. Tests with unhumidified Butane (Figure B-6), indicate that increasing temperature from 150 to 200°C results in a three fold increase in current density despite the reduced electrolyte water activity. Above 175°C the current density-polarization curve appears to have a real Tafel slope ranging between 160 to 180 mv/decade. This is somewhat higher than obtained

with supported platinum (100 mv/decade). However, this is consistent with the methanol data which showed a Tafel slope of 85 mv/decade compared to 60 for platinum black.

Figure B-6

Effect of Electrolyte and Temperature on Butane Performance

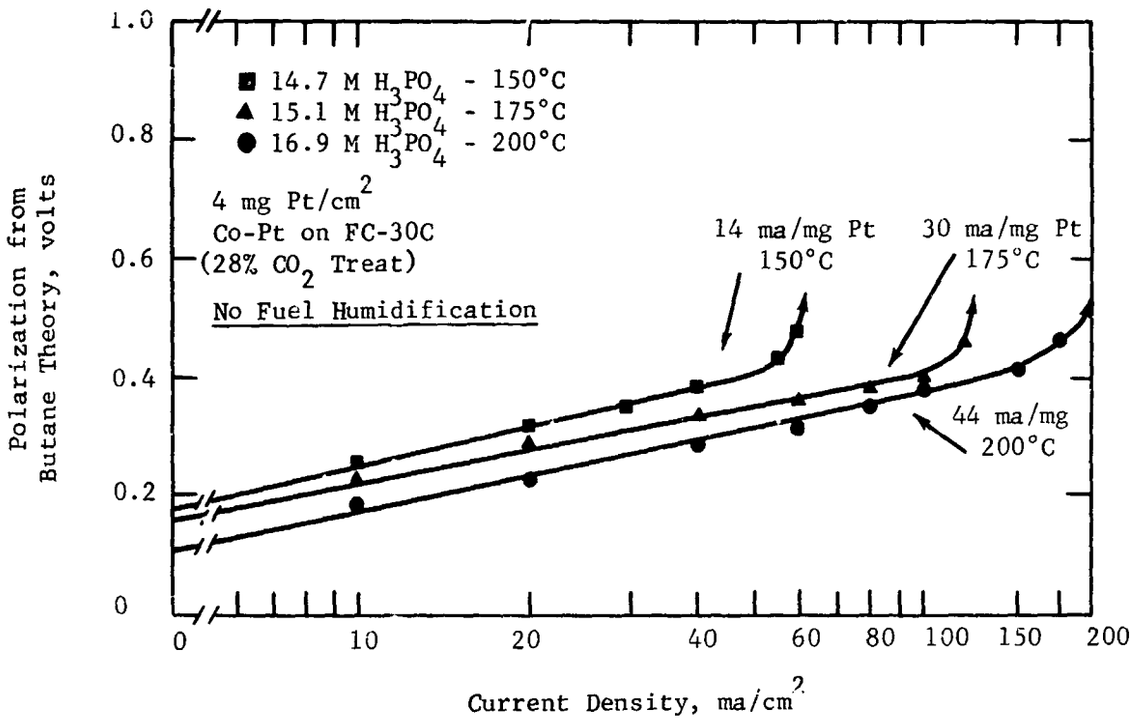

The activation energy at limiting current was only 8.5 Kcal/mole, considerably lower than that normally obtained with supported platinum catalysts. Furthermore, the activation energy in the Tafel region (0.3 volts polarized) was only 5.9 Kcal/mole, considerably lower than that encountered with unsupported platinum. This may be due to the fact that electrolyte water content was not maintained constant in this experiment. This will bear further investigation. However, it may also be due to the porous nature of the support. Attempts to increase the operating temperature above 225°C (using an appropriate electrolyte) resulted in a permanent performance loss with this electrode.

In view of the relatively high current capability at the 4 mg/cm^2 Co-Pt electrode at 200°C and the relative thickness of this electrode, it was felt that increased utilization and performance could be obtained by resorting to thinner low loaded electrodes. To test this hypothesis, a series of low loaded (1.6 to 2.0 mg/cm^2) electrodes were prepared and run at 200, 225 and 275°C. The results of this experiment are summarized in Figure B-7. Although these data were obtained

Figure B-7

Butane Performance
Low Loaded Anodes

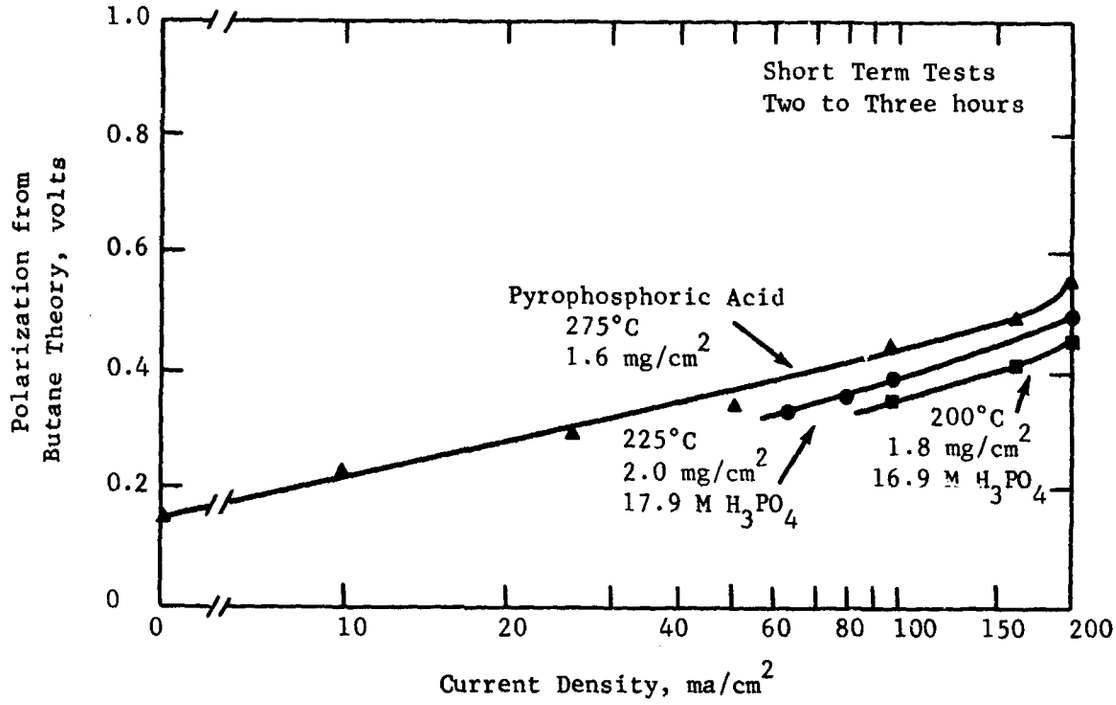

in short term tests they do indicate the potential of these systems. As shown in Table B-6 the utilization reached 110 ma/mg. However, there appeared to be a reduction in utilization at 275°C. This is probably due to the increased thickness of the 2.1% platinized catalysts. In addition, the electrodes prepared from the 5.8% Co-Pt catalyst showed some performance deterioration after running for three hours. This deterioration is still unexplained but it could be due to a lack of water at the active catalyst sites. Structure studies should clarify this latter point. Loss in intrinsic catalyst activity at elevated temperatures has not been ruled out as yet. However, the 2.1% catalyst has shown good performance in 275°C pyrophosphoric acid (humidified fuel) with no apparent deterioration.

Part b - Performance in Intermediate Temperature Electrolyte

Since most low loaded platinized carbon electrodes are limited by activation rather than transport phenomena, operation with intermediate temperature (200-300°C) electrolytes should result in substantial increases in current capability Consequently, tests were conducted to evaluate the anode and cathode performance of potential structural types. The catalyst used for this study was the 11.2% Pt on FC-20 Carbon (0.1 gm O3/gm Cwhich has previously (8) shown good butane activity

Table B-6

Platinum Utilization-Low Loaded
Carbon Supported Co-Pt Anode
(Butane, FC-30 Carbon)

Electrode	Temp, °C	Electrolyte	Platinum Utilization at Indicated Polarization, ma/mg Pt	
			0.4 Volts	0.45 Volts
2.1% Co-Pt 1.6 mg/cm^2	275	Pyrophosphoric Acid	41	75
5.8% Co-Pt 2.0 mg/cm^2	225	17.9 M H_3PO_4	50	100
5.8% Co-Pt 1.8 mg/cm^2	200	16.9 M H_3PO_4	83	110

in phosphoric acid. A thin 1.6 mg Pt/cm^2 sintered carbon Teflon electrode was the trial structure. Performance data summarized in Table B-7 indicates that active low loaded anodes and cathodes can be developed for this electrolyte. Cathode performance at 100 ma/cm^2 is quite acceptable. However, anode repeatability appears to be a problem.

Table B-7

Performance of Catalyzed Carbon(1)
Anodes and Cathodes

(1.6 mg Pt/cm^2-275°C)
(Pyrophosphoric Acid)

Current Density, ma/cm^2	Polarization from Butane Theory, volts	Polarization from Oxygen Theory, volts	
	Pt/FC-20C(2)	Oxygen	Air
0	0.15	0.12	0.15
10	0.15	0.13	0.17
50	0.20	0.18	0.26
100	0.24	0.23	0.32
200	0.32	0.29	0.40
300	--	0.32	0.44

(1) 11.2% Pt on FC-20C ozone treated 0.1 gm O_3/gm C
(2) Anode performance obtained in three hour run, duplicate electrodes could not sustain 150 ma/cm^2

Nevertheless, these electrodes represent practical anodes and cathodes which can markedly effect systems concepts. The effect of these low loaded electrodes on fuel cell design will be considered in Task C.

Part c - New Electrode Structures

The development of active carbon catalysts with high platinization will ultimately require a new type of electrode structure to allow adequate interface control and current collection within a one to three mil catalyst bed. The use of the 6 mil support screen as the primary current collection mode is therefore ruled out. Consequently, exploratory studies were conducted to determine if a gas-porous, conductive substrate could serve as the primary current collection device and also provide the required interface control.

To test this concept a three mil porous Teflon film (10 micron pores) was gold coated by a proprietary electrodeposition technique to a loading of 5 mg Au/cm^2. The resulting porous Teflon substrate was hydrophilic allowing direct application of the catalyst Teflon gel. However, the hydrophobic property of the film is restored on sintering to produce the finished electrode. A comparison of hydrogen and oxygen performance with coated and uncoated substrates is shown in Table B-8. The catalyst selected was a 24% Pt-Ir, on Regal 330R carbon, prepared by impregnation. This material is typical of our first generation catalyst systems and yields only 8 ma/mg on Butane and 40 ma/mg on oxygen.

Table B-8

Comparison of Porous Teflon Substrates(1)

(14.7 M H_3PO_4, 150°C)

Substrate	Reactant	Polarization at Indicated ma/cm^2, volts					
		0	10	50	100	200	300
Porous Teflon	O_2	0.15	0.28	0.48	0.65	--	--
	H_2	0.012	0.012	--	0.031	0.051	0.066
Gold coated Porous Teflon	O_2	0.16	0.33	0.42	0.47	--	--
	H_2	0.010	0.010	--	0.026	0.043	0.067

(1) 1.25 mg Pt/cm^2 prepared from 24% Impregnated Pt-Ir on 330R carbon Basic Blank thickness: 1 mil. sintered at 329°C, 2200 psi for 30 seconds.

The use of the gold coated matrix improved both the hydrogen and oxygen performance. However, the butane performance was quite poor (2-4 ma/cm^2), considerably more work is required to develop this into a hydrocarbon electrode structure. For comparison, a commercial Chemcell electrode, similar in structure to the uncoated porous Teflon electrode was also evaluated. This 2 mg Pt/cm^2 electrode also behaved poorly on butane yielding only 4 ma/mg. However, its oxygen and hydrogen performance was significantly better than the 1.25 mg/cm^2 Pt-Ir on Carbon electrode. (Appendix B-4)

Phase 3 - Conclusions

Supported platinum catalysts continue to show promise of significant hydrocarbon activity improvements in both the low and intermediate temperature electrolytes. These studies have shown that improvements can best be obtained through alteration in platinum deposition selectivity and increased platinization.

In this regard, the multiple adsorption procedure continues to be a potent tool for increasing platinum content without loss in catalyst utilizations.

Research has shown that platinum selectivity can be altered significantly through substrate pretreatment (ozone) and carbon and adsorbate selection. Studies indicate that the present ozone treatment procedure is far from optimum. Initial tests using a fluidized bed technique indicated that the original fixed bed technique led to poor ozone distribution. This in turn could result in poor platinum deposition selectivity. Attempts to improve selectivity through the use of intermediate porosity carbons meet with only partial success. Although these preparations gave the best performance of any previous synthetically prepared carbon, butane utilization was only 10 ma/mg Pt. Thus it appears that a distribution of macro and micro pore adsorptions sites is required for good hydrocarbon activity.

Attempts to alter platinum deposition selectivity by varying adsorbate composition failed to produce any marked change in crystallite size. However, these studies led to the development of a new Co-Pt catalyst system. Indeed a Co-Pt on FC-30 carbon has shown significant utilization in electrolytes ranging in temperature from 150 to 275°C. Although performance at 150°C is comparable to our best platinized carbon 80 ma/cm^2 at 3.2 mg/cm^2, utilization at elevated temperatures have reached as high as 44 ma/mg at 200°C for thick 23 mil electrodes. A reduction in thickness to 13 or 14 mils resulted in more than double the current capability. For example, a 1.8 mg Pt/cm^2 electrode sustained 200 ma/cm^2 at 0.45 polarized at 200°C (110 ma/mg Pt). Increasing the temperature caused some loss in performance but even at 275°C the electrode sustained 75 ma/mg Pt. However, some electrode deterioration was noted at elevated temperatures. Additional work is required to determine the source of this deactivation.

2.3 Task C New Electrolytes

The activity of hydrocarbon anodes has been shown to be limited by chemical (adsorption) rather than transport limitations. Thus, operation at elevated temperatures, consistent with engineering requirements, should result in substantial increase in anode and cathode performance. Preliminary studies indicated that operation at the lower end of the intermediate fuel cell range (200 to 300°C) would result in only minor increases in engineering problems. Unfortunately, this region is beyond the limit of aqueous electrolytes and below the area in which molten oxide-carbonate electrolytes operate. Previous studies (7,8) have shown that pyrophosphoric acid is an effective electrolyte for this temperature range. However, its extreme corrosiveness has led to the development of a second electrolyte system, the mixed alkali metal dihydrogen phosphate melts (phosphate melts). This latter material is unique in that it is both carbon dioxide rejecting and non-corrosive.

Previous studies have established that substantial improvements in hydrocarbon anode and cathode activity can be obtained in 250°C to 275°C pyrophosphoric acid electrolytes. Recent data, reported in Task B, indicates its effectiveness with low loaded (1.6 mg/cm^2) butane anodes and cathodes. Additional studies have been conducted to determine the range of applicability of this system with various fuels and materials of construction. Systems studies were initiated to determine if the improved performance levels observed are reflected in increased "system" power density (lbs/kw).

Work on the phosphate melts has centered about the evaluation of potential non-noble metal anode and cathode catalysts and the alteration of system pH to improve cathode performance. In addition the performance of low catalyst density noble metal electrodes was briefly examined.

Phase 1 - Pyrophosphoric Acid Electrolyte Studies

Pyrophosphoric acid meets all of the electrochemical requirements for an intermediate temperature hydrocarbon fuel cell electrolyte (7). As illustrated in Table C-1, it melts at 60°C and is stable at temperatures to 427°C. Although, the material is not liquid at room temperature, once melted it remains a super cooled liquid for several weeks. At operating temperatures it is as conductive as 3.7 M sulfuric acid, and has more than adequate buffering capacity. These properties, coupled with the performance improvements previously noted make this an extremely interesting electrolyte, corrosion problems not withstanding.

Table C-1

Properties of Pyrophosphoric Acid Electrolytes

Liquid Phase Region	60-427°C
Specific Resistance, ohm-cm 100°C 250°C	 15 2.6
Buffering Capacity	>1000 ma/cm^2 anodic and cathodic
Corrosion Resistant Materials	Pt, Au, Metal-Tungsten-oxides, Possibly Hastaloy B

Part a - Hydrocarbon Performance

In view of these good electrochemical properties, studies are under way to determine the range of fuels which can be effectively used in a 250 to 275°C electrolyte. Consequently, the anodic performance of a 50 mg/cm^2 sintered platinum Teflon electrode was determined with butane, hexane, octane and decane as the fuel. Initial experiments (7) used 0.88 mole water/mole of fuel. This mole ratio was chosen as a starting point because it was found to be optimum for butane activity in this electrolyte.

Evaluation of octane performance at 275°C (Appendix C-1) indicate that current densities as high as 400 ma/cm^2 can be obtained and no irreversible activity loss was noted. Periodic oscillation were noted at most steady state load conditions but this may have been a reflection of fuel flooding conditions rather than electrode behavior since this electrode was run at low fuel conversion (differential reactor). Figure C-1, summarizes these results along with data on other hydrocarbon fuels obtained previously. Notice that for a given water-fuel ratio, current capability decreases with increasing carbon number falling from 400 ma/cm^2 (0.30 polarized) on butane to 25 ma/cm^2 on hexane.

Figure C-1

Hydrocarbon Activity in Pyrophosphoric Acid

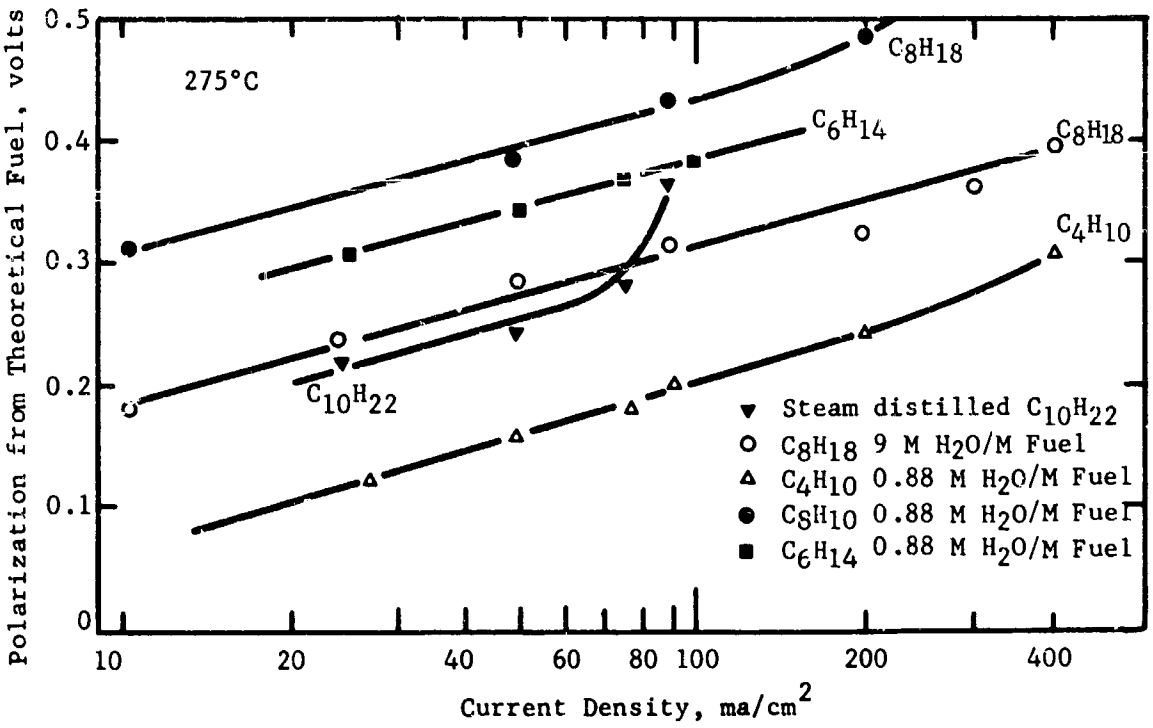

A series of experiments were conducted to determine if better reactant control would reduce anode polarization. In these experiments, pre-metered vaporized reactant feeds were used to control the electrode flooding (schematic in Appendix C-2) tendency which was presumed to be the cause of the "oscillation" inhabilities. As indicated in Figure C-1 performance with controlled reactant feed is significantly better than that obtained with steam vaporized fuel. This is probably due to the fact that the improved feed control allowed better optimization of reactant partial pressures. It appears that the water-fuel mole ratio will depend on carbon number. This response is similar to that found in reforming. This latter contention is confirmed by the fact that steam distilled decane (7 mole H_2O/mole decane) gave a lower polarization than either hexane or octane when these fuels were run with low water ratios.

All of the octane electrodes tested in the material reactant runs showed a 50% performance loss after two hours operation. This loss coincided with the onset of severe electrode leakage, probably due to mechanical deterioration of the electrode structure. Efforts to eliminate this problem through the use of a porous Teflon barrier have not been successful. While prolonging life, limiting currents were reduced to 100-150 ma/cm^2 as the barrier probably serves to impede reactant transport. Changes in electrode structure can also improve mechanical stability. Thus far, performance debits have been encountered with this approach. No performance deterioration was observed in the low water ratio runs.

Some additional studies to ascertain the source of this deterioration are contemplated. However, this appears to be an electrode structure problem, and work in this area is not anticipated unless it re-occurs with low loaded supported platinum electrodes.

Part b - Reformer Effluent Gas Performance

Steam reformer fuel cell systems suffer from two important problems; (1) systems integration with low temperature hydrogen-air fuel cells and (2) they require an expensive palladium diffuser for hydrogen purification. The pyrophosphoric acid electrolyte system could result in better reformer-fuel cell thermal compatability. In addition, the palladium diffuser might not be required if the elevated temperatures minimized the carbon monoxide "poisoning" effects encountered when operating on an unpurified hydrogen stream. A series of experiments were conducted to determine if the anticipated "poisoning" resistance actually existed. Tests were conducted on two synthetic reformer effluents containing 2 and 10% carbon monoxide plus other constituents typical of the range of reformer operating conditions. The results of this program are summarized in Table C-2.

Table C-2

Comparative Activity Reformer
Effluent vs Pure Hydrogen

Pyrophosphoric Acid at 275°C

Current Density, ma/cm^2	Polarized From Theoretical Hydrogen, volts				
	50 mg Pt/cm^2			5 mg Pt/cm^2	
	Pure H_2	2% CO	10% CO	Pure H_2	10% CO
100	0.005	0.010	0.005	0.01	0.005
200	0.015	0.020	0.015	0.015	0.010
400	0.020	0.025	0.015	0.035	0.030
500	0.030	0.020	0.020	(4)	(4)
1000	0.07	0.07	(3)		

(1) 72 vol% H_2, 23 vol% CO_2, 2 vol% CO, 3 vol% CH_4
(2) 90 vol% H_2, 10 vol% CO
(3) Not tested at 1000 ma/cm^2
(4) Not tested beyond 400 ma/cm^2, which is well below the limiting current

These data show no performance debit due to carbon monoxide "poisoning", even at levels as high as 10 mole percent. The anodic activity of pure hydrogen cannot be distinguished from that of reformer gas even with low loaded (5 mg/cm^2) platinum on carbon electrode structures. The minimum operating temperature required for complete absence of CO poisoning in this electrolyte has not been established as yet.

Part c - Materials of Construction

Pyrophosphoric acid is a highly corrosive material at its normal fuel cell operating temperature. Thus far, only platinum, gold and quartz are satisfactory materials of construction. However, the literature indicates that Hastalloy B should also show substantial corrosion resistance. In addition, plastic composites have also been examined as potential cell structural materials. Unfilled Teflon has satisfactory corrosion stability at this temperature, but it is structurally poor, being at the limit of its useful range. Although Rulon(1) was a satisfactory material for the 150°C phosphoric acid system, tests in 275°C pyrophosphoric acid indicate that this material was unsatisfactory. Structural stability was maintained for 500 hours. However, serious swelling was observed by 550 hours and the material failed by 600 hours. A similar filled Teflon plastic, Fluorosint(2) failed in less than 80 hours. These experiments indicated that the proper choice of filler would provide a suitable structural material.

(1) Commercial Filled Teflon, Dixon Corporation, Bristol, Rhode Island
(2) Commercial Filled Teflon, Polymer Corporation, Pennsylvania

In view of the corrosion resistance of mixed metal-tungsten-oxides (Task A Phase 4), this type of material was considered as a potential filler for a Teflon bonded composite. Two trial composites containing fifty weight percent $CdO.2WO_3$ were prepared using Teflon 42 BX emulsion. Initial sintering conditions were chosen arbitrarily. The first specimen was sintered at 330°C at 10,000 psi for ten minutes, while the second specimen was sintered under more severe conditions, 15,000 psi for ten minutes. These finished composites were tested in 275°C pyrophosphoric acid for 740 hours. No structural failure or dimensional change was observed and weight variation during this test under 15 mgs for the .584 and 1.371 gm sample tested.

These results bode well for the development of suitable plastic cell components for the pyrophosphoric acid system. Consequently, this structural material was used as a basis for systems weight considerations. However, further development of these composites are outside the scope of this program.

Phase 2 - Preliminary Systems Evaluation - Intermediate Temperature (Pyrophosphoric Acid) Fuel Cell

At this stage in the development of the pyrophosphoric acid electrolyte fuel cell system, a systems evaluation was initiated to determine if improvements in anode and cathode performance can actually result in a more compact hydrocarbon air battery with increased power per pound. In addition, the relation between platinum group metal content and system weight was also considered. In view of the absence of carbon monoxide sensitivity at these temperatures, both the direct and reformer hydrocarbon-air fuel cell systems were included in this preliminary analysis.

Part a - Total Cell Performance

Performance curves have been constructed from the numerous anodic and cathodic half cell performance curves reported in this and previous reports (7,8). The IR loss in the cell was also estimated using conductivity measurements and a typical electrolyte chamber space of 20 mils. Current collection loss was also estimated from past experience. Thus, the total IR loss was set at 50 mv at 100 ma/cm^2. Predicted cell potentials for the hydrogen, butane and octane-air cells are illustrated in Figure C-2 and C-3. Figure C-2 presents the current-density potential data for a total cell loading of 100 mg Pt/cm^2, while Figure C-3 presents similar performance data for a total platinum loading of 2.9 to 3.2 mg Pt/cm^2. The triangles mark the reference design points at 0.75 volts for hydrogen and 0.5 volts for hydrocarbon-air systems. These relative voltages were selected so that the resultant reformer system would be operating at about the same thermal efficiency as the direct hydrocarbon system.

Figure C-2

Predicted Performance Pyrophosphoric Acid

(High Loaded Electrodes)

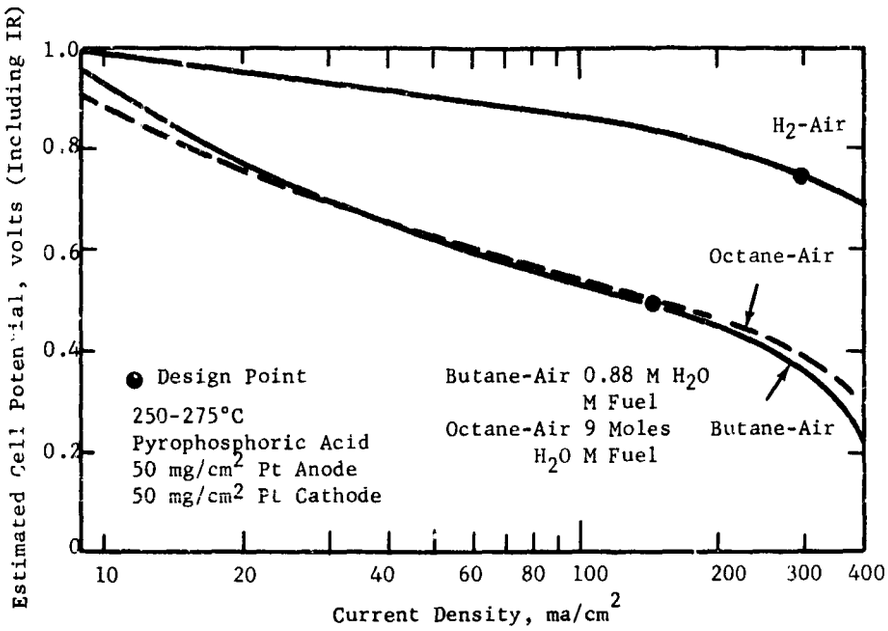

Figure C-3

Predicted Performance Pyrophosphoric Acid Cell

(Low Catalyst Loading Electrodes)

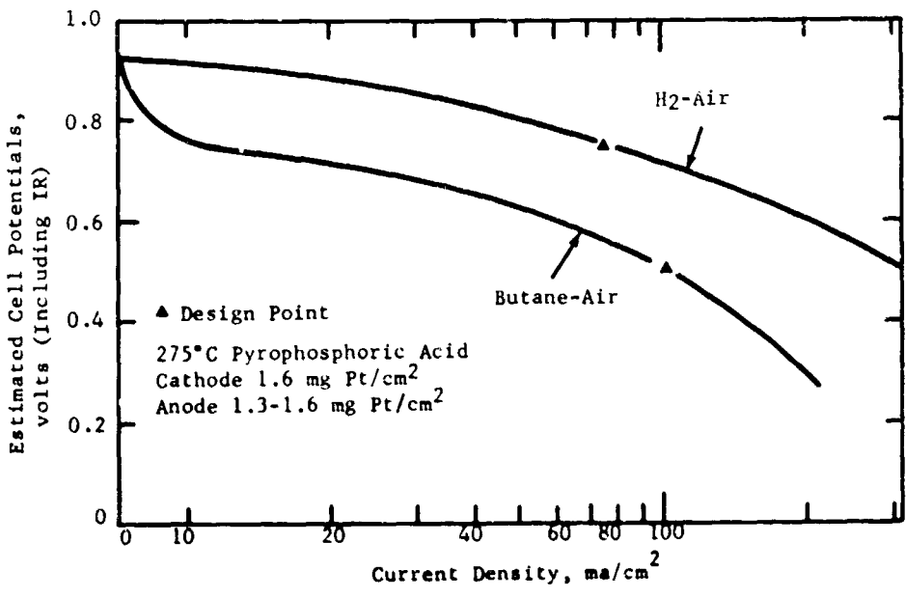

Table C-2 compares the power density and platinum utilization of the supported (low loaded) and unsupported (high loaded) hydrogen fuel cells. Notice that the low catalyst density electrodes gave a 9 to 10 fold increase in catalyst utilization over the unsupported catalyst electrodes, however, the power density is

reduced by a factor of four. It is interesting to note that the hydrogen-air utilization was 56.2 gm/kw, less than a factor of three from the military target of 20 gms/kw. Indeed the ex IR utilization for the H_2-O_2 system was 15.7 gm/kw, somewhat below the design target. Design hydrocarbon performance is summarized in Table C-3. Again the supported system shows a distinct (20 fold) utilization advantage, and the power density debit is substantially less. Indeed the utilization for the butane air system at 0.5 volts is comparable to that of hydrogen air at 0.75 volts. Octane performance was available only with the 50 mg/cm^2 electrodes.

Table C-3

Hydrogen or Reformer Gas Cell
(250-275°C Pyrophosphoric Acid)

Oxidant	Pt Loading, ma/cm^2 Anode	Cathode	Total	Power Density At 0.75 volts/cell	Platinum Utilization gm/kw
Oxygen	50	50	100	340	294.0
Oxygen	1.3	1.6	2.9	109	26.4(1)
Air	50	50	100	220	454.0
Air	1.3	1.6	2.9	53	56.2(1)

(1) Includes IR loss in cell, ex IR value for low loaded system 15.7 gm/kw on O_2, 32.5 gm/kw on air

Table C-4

Hydrocarbon Performance
275°C Pyrophosphoric Acid Cell

Oxidant	Platinum Loading, mg/cm^2 Anode	Cathode	Total	Power Density At(1) 0.5 Volts/cell, mw/cm^2	Platinum Utilization gm/kw
			Butane		
Oxygen	50	50	100	125	800.0
Oxygen	1.6	1.6	6.2	75	42.5
Air	50	50	100	70	1430.0
Air	1.6	1.6	3.2	53	60.5
			Octane		
Oxygen	50	50	100	140	710
Air	50	50	100	90	1380

(1) 47.2% Thermal Efficiency

However, as indicated in Figure C-2, octane gives about the same performance curve as butane so that it would be safe to estimate the supported catalyst octane performance from comparable butane data.

These performance curves will be used to estimate the requirements for a 5.63 kw(gross) hydrocarbon-air battery.

Part b - Direct Hydrocarbon-Air System

Heat transfer studies have indicated that the major problem in vapor feed hydrocarbon-air fuel cells is the necessity for vaporizing and condensing from the fuel stream. This is particularly important in the pyrophosphoric acid system since water ratios can run as high as nine moles H_2O/mole liquid fuel. The ideal thermal system is one in which only the required electrochemical water and fuel are vaporized and CO_2 rejection is accomplished without significant heat loss.

The system illustrated schematically in Figure C-4, meets this requirement by using a regenerable carbonate bicarbonate adsorption cycle,

$$CO_3^{=} + CO_2 + H_2O \longrightarrow 2H\ CO_3^{-}$$

Indeed, proprietary catalysts are available which can markedly speed up the adsorption and desorption step.

In this system, the effluent stream from the fuel cell stack is passed through a carbonate-bicarbonate scrubber humidifier where the carbon dioxide is removed simultaneously. The fuel stream humidity is raised so that the desired water fuel mole ratio is obtained after fresh fuel addition. After passing from the scrubber humidifier, the stoichiometric quantity of fuel is vaporized into the reactant stream which then returns to the fuel cell stack.

Figure C-4

Schematic Noncondensing Vapor Feed Hydrocarbon Fuel Cell

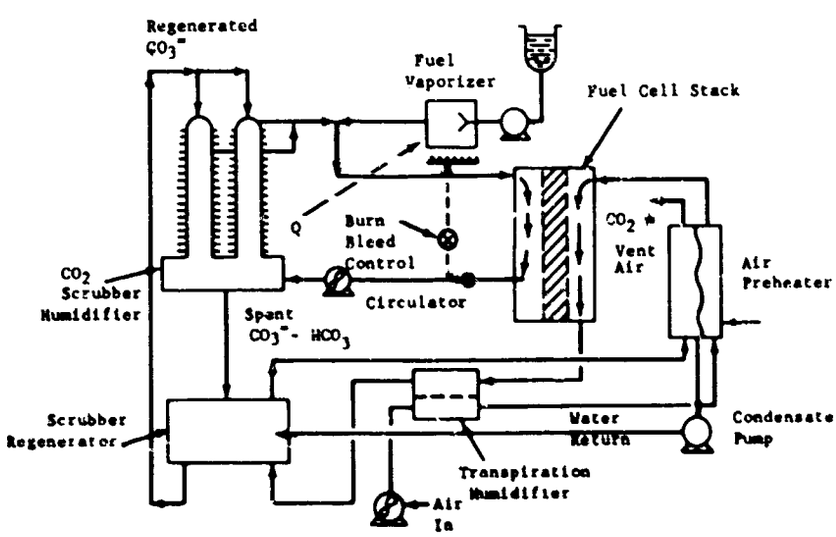

The spent carbonate solution can be regenerated by stripping with exhaust air, heating, or both. Thus the carbon dioxide is ultimately vented with the exhaust air. Water economy is maintained with a transpiration humidifier in the air exhaust stream.

This basic system has been used in the analysis of the direct bydrocarbon air system, and 9"x5 3/4" cell configuration has been assumed. Further, the cell is presumed to be made from a metal-tungsten-oxide filled Teflon (density 2.6 gm/cm^3).

Primary fuel cell component weights are detailed in Appendix C-3, while weight details of the three hydrocarbon-air systems are summarized in Appendix C-4 and 5. These weights were based upon experience in the methanol air, and decane-air systems designed previously.

Table C-4 summarizes the results of this design estimate. As indicated, power densities ranging from 71 to 91 lbs/kw were obtained. This is equal to or better than some of the present generation reformer fuel cell systems.

Table C-5

Weight and Platinum Requirements
Hydrocarbon-Air Fuel Cell System

(275°C Pyrophosphoric Acid,
5.63 kw Gross, 5.0 kw Net)

Electrical	Butane-Air		Octane-Air
	Unsupported Pt	Pt on Carbon	Unsupported Pt
Number of cells	243	320	192
Number of stacks	3	4	3
Stack voltage, volts	40	40	32
Platinum Requirements, Kg	8.05	0.340	7.77
Weights			
Stack Weight, lbs	207.0	273.2	178.5
Auxiliary Weight, lbs	175.5	179.7	174.4
Total System, lbs	382.5	452.7	353.2
Power Density lbs/kw	76.5	90.5	70.7

Notice also that a factor of 25 reduction in platinum requirement can be achieved with only a 70 pound increase in system weight (14 lb/kw). Thus, despite the added weight of cell components, the pyrophosphoric acid system can result in an overall improvement in direct hydrocarbon-air fuel cell power density.

Part c - Reformer-Air Fuel Cell

In view of the insensitivity to CO observed previously, a reformer-air fuel cell system was also considered in this preliminary systems analysis. Reformer weight information was taken primarily from a scaled-up version of the 3.7 kw P&W design (86) with the approximate weight of the palladium diffuser backed out. These weight estimates were checked against other inhouse reformer designs. The weight estimate for this hydrogen generator is summarized in Appendix C-6, while the weight and platinum requirements are summarized in Table C-5 and Appendix C-7. From these data, it appears that the reformer case is weighted in favor of the unsupported catalyst since a ten fold reduction in catalyst loading results in a two fold reduction in power density. Indeed, a comparison of data in Table C-4 and C-5 indicate that at the same apparent thermal efficiency, the low catalyst density reformer system is heavier than the comparable direct feed system (101.1 vs 90.5 lbs/kw). However, the low catalyst density reformer system gave about the same power density as the 3.7 kw Pratt and Whitney Unit (88).

Table C-6

Weight and Platinum Requirements
Reformer-Air Fuel Cell System

(275°C Pyrophosphoric Acid)
(5.63 kw Gross, 5.0 kw net)

Electrical	Unsupported Platinum	Platinum on Carbon	P&W 3.7 kw
Number of cells	80	320	
Number of stacks	1	4	
Stack voltage, volts	30	40	
Platinum Requirements, kg	2.6	0.317	
Fuel cell stack	68.3	273.2	
Fuel cell auxiliaries	95.0	104	
Hydrogen generator	128.8	128.3	
Total System	292.1	505.5	410.0
Power Density #/kw	58.4	101.1	110.8

Phase 3 - Mixed Alkali-Metal Dihydrogen Phosphate Melts

Alkali-metal dihydrogen phosphate melts have shown some promise as carbon dioxide rejecting electrolytes for intermediate temperature fuel cells (9). They are easily synthesized, stable non-corrosive systems with good anodic and cathodic buffering capacity. However, their resistance at operating temperature, 20 ohm-cm, is higher than desirable, and water must be supplied with both the anodic and cathodic reactants. Hydrocarbon activity was demonstrated previously using 50 mg/cm^2 sintered platinum Teflon electrodes. This is illustrated in Figure C-5, which illustrates the butane and oxygen half cell performance in this electrolyte. The estimated (IR free) cell potential, also shown, indicates a power capability of about

106 mw/cm^2 for this butane oxygen cell. This is the first indication of hydrocarbon fuel activity in a CO_2 rejecting buffer electrolyte. Previous studies with low temperature aqueous phosphate or carbonate buffers failed to show any hydrocarbon activity at all.

Figure C-5

Performance of Butane Oxygen System

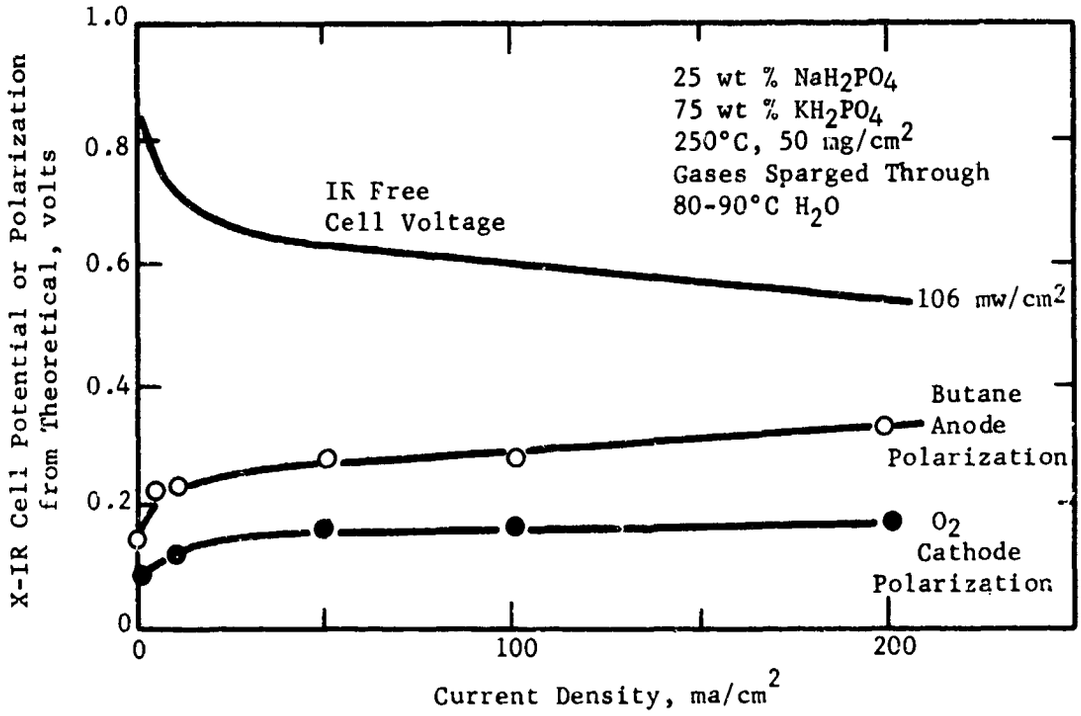

Part a - Supported Platinum Electrode

In view of the significant activity levels exhibited by butane and oxygen in this electrolyte, with high loaded (50 mg/cm^2) S.P.T.E. anodes, a study was initiated to determine if increased platinum utilization could be obtained with carbon supported catalyst systems. Consequently, a 2 mg/cm^2 sintered carbon teflon electrode was prepared using 4-5% platinized FC-50 carbon. Table C-6 summarizes the anode performance obtained with this electrode. Performance was improved when the fuel stream humidity was increased, and the electrode performance became more stable and less subject to voltage oscillations.

Table C-7

Performance of Butane on Catalyzed Carbon-Phosphate Melt at 250°C

Electrode 5% Pt on FC-50 Carbon(1)
2 mg Pt/cm^2

Current Density, ma/cm^2	Polarization From Theoretical Butane, volts	
	(2)	(3)
0	0.26	--
10	0.41-0.49	0.38
25	0.50-0.60	0.47
50	0.59-0.80	0.51
75	0.58-0.79	--
100	0.60-0.70	0.60

(1) This electrode attained a limiting current density of 45 ma/cm^2 in 85% H_3PO_4 at 150°C
(2) Butane pre-humidified with water at 80°C
(3) Butane pre-humidified with water at 90°C

Unfortunately, the anticipated utilization improvement was not observed with this electrode.

Oxygen activity was also poorer than anticipated despite a 4 mg Pt/cm^2 cathode prepared with 5% Pt on FC-50C yielded an oxygen limiting current of only 100 ma/cm^2 (Table C-7). However, the cathode was considerably thicker than conventional or supported anode or cathode systems. Thus, electrode structure effects could cancel the benefits of increased catalyst loading. Electrode structure problems could be confounding these measurements since electrode structure has not been optimized for this electrolyte as yet.

Table C-8

Performance of Oxygen on Catalyzed Carbon Electrodes, Phosphate Melt at 250°C

Electrode: 10% Pt on FC-50C
Carbon 4 mg Pt/cm^2

Current Density, ma/cm^2	Polarization from Theoretical Oxygen, volts	
	(1)	(2)
0	0.28	0.25
5	0.37	0.34
10	0.45	0.37
25	0.74	0.46
50	--	0.56
100	--	0.61

(1) Oxygen pre-humidified with water at 80°C
(2) Oxygen pre-humidified with water at 90°C

A commercial low catalyst loading (2 mg/cm^2) Chemcell electrode was also evaluated in the phosphate melt on hydrogen, butane and oxygen. These electrodes use an unsupported platinum catalyst and therefore provide an opportunity to examine the activity of low catalyst loaded structures in the absence of a carbon support. The steady state performance data are given in Table C-8.

Table C-9

Performance on Chem-Cell Electrode Phosphate Melt at 250°C

Electrode: 2 mg Pt/cm^2

Current Density, ma/cm^2	Polarization From Theoretical, volts,		
	Hydrogen	Oxygen(1)	Butane(1)
0	0	0.06	--
1	0	0.27	1.2
5	--	0.40	--
10	--	0.41	--
25	0.04	0.42	--
50	0.09	0.45	--
75		0.50	--
100	0.12	0.53	--
150	0.14	--	--

(1) Both oxygen and butane were pre-humidified with water at 80°C

The advantage of the unsupported catalyst can be seen at the oxygen electrode. The difference in oxygen open circuit between the Chem-Cell and the catalyzed carbon electrodes can be attributed to the lack of a mixed potential on the former electrode. As a consequence, the oxygen open circuit polarization of the Chem-Cell structure is almost 0.2 volts lower. However, the 80 mv difference at 100 ma/cm^2 may be mainly a reflection of a non optimized carbon electrode structure.

The low butane activity with this Chem-Cell structure parallels the results obtained in 85% H_3PO_4 at 150°C. Apparently, regardless of electrolyte, the Chem-Cell electrodes are not structurally suitable for hydrocarbon oxidation.

Part b - Non-Noble Anode Catalysts

Phosphate melts do not have the same corrosive properties as other carbon dioxide rejecting electrolytes. Previous studies for example have shown that nickel, cobalt and tantalum are stable in this electrolyte. Consequently, a preliminary study of potential non-noble anode catalysts was initiated. The first catalyst evaluated on a Raney 75 nickel-25 cobalt alloy, (at 75 nickel-25 cobalt). This catalyst previously described (9), was fabricated into an unsintered teflon bonded electrode having a catalyst density of 50 mg/cm^2.

This electrode was tested on hydrogen in the phosphate melt at 250°C, the results shown in Table C-9. The activity, although low, is probably real. There was no evidence of nickel or cobalt ion in the electrolyte after several hours of testing despite the severe polarization at current densities beyond 10 ma/cm^2. Electrode response and recovery upon open circuiting was rapid. Furthermore, electrode itself did not exhibit any signs of physical damage or chemical corrosion. It remained highly conductive, and when re-run on hydrogen (6 M KOH) it yielded 240 ma/cm^2 at 160 millivolts polarized.

Table C-10

Hydrogen Activity-Raney Nickel-Cobalt Alloy

(250°C Phosphate Melt)

Current Density, ma/cm^2	Polarization From Theoretical Hydrogen, Volts
0	0.03
2	0.08
5	0.18
7.5	0.30
10	0.38

Although rather significant activity improvements are required, these initial results are extremely encouraging in that a non-noble metal catalyst system is active in a relatively non-corrosive intermediate temperature electrolyte. These systems will be investigated in more detail as it is expected that structural variations will improve the anodic activity.

Commercial porous nickel powder electrodes made by Clevite Corporation, were also investigated as possible electrodes for the melt. These electrodes are 10 mils thick, 70% porous, with a mean pore size of six microns. As this structure did not hold an interface in aqueous KOH, a base case performance standard on hydrogen could not be obtained. This structure did maintain an interface in the phosphate melt and exhibited a polarization of 50 millivolts at 1 ma/cm^2. However, Clevite electrodes are quite brittle and several attempts to get performance data were aborted due to mechanical structure failure. For this reason, no further work is contemplated with Clevite electrodes.

Part c - Non-Noble Cathode Catalysts

Tests have shown that silver does not corrode in the phosphate melt. Accordingly, it should be possible to develop silver based cathodes for this medium. Therefore, a program to develop non-noble cathode systems utilizing silver was initiated.

Sintered silver-Teflon electrodes were fabricated by the same procedure used in making the standard sintered platinum-Teflon electrodes. The silver used was a 325 mesh powder. One of these electrodes was tested on oxygen in 3 M KOH at 80°C to determine if active silver electrodes can be prepared by this technique. A duplicate was tested in the phosphate melt at 250°C. The results given in Table C-10, show that while high activity can be obtained in aqueous KOH, activity in the melt is poor.

Table C-11

Silver Cathode In Phosphate Melt

50 mg Ag/cm^2

Current Density, ma/cm^2	Polarization from Theoretical Oxygen, volts	
	3 M KOH at 80°C	Phosphate Melt at 250°C
5	0.26	0.55
10	0.28	0.58
50	0.34	0.65
100	0.37	0.69
200	0.42	0.75

After running, the melt had a slight yellowish cast. Silver ion is known to impart a yellow color to the melt. However, tests for silver ion in the melt were negative. Furthermore, no changes could be detected, electronic conductivity was unimpaired, nor were any physical changes discernible. In view of the lower activities obtained in the melt relative to that obtainable in lower temperature KOH electrolyte, alternate approaches were examined. These included alterations in melt alkalinity and catalyst composition.

Previous studies with aqueous electrolytes (7) indicate that cathodic activity increases with increased pH. If this could be extended to the phosphate melts, then increasing melt alkalinity should also improve the oxygen activity of the silver cathode. Cesium carbonate addition was used to increase melt alkalinity. Buffering capacity measurements were required with this modified melt to insure that inadequate buffering capacity would not obscure the cathode measurements.

Table C-12

Buffering Capacity of Modified(Alkaline) Phosphate Melt - 250°C

($6.5\%\ Cs_2CO_3$, $23.5\%\ NaH_2PO_4 \cdot H_2O$)
($70.0\%\ KH_2PO_4$)

Current Density, ma/cm^2	Polarization From Theoretical Hydrogen, Volts		
	Anodically	Cathodically	
	(1)	(1)	(2)
5	--	0.01	0.03
10	--	0.02	0.04
25	0.06	0.03	0.07
50	0.08	0.07	--
75	0.08	--	--
100	0.12	--	--

(1) Dry H_2
(2) H_2 pre humidified with water at 80°C

As indicated in Table C-11, the anodic buffering capacity is essentially similar to that of the unmodified system, but the cathodic buffering capacity was considerably decreased (9). However, the residual cathodic buffering is adequate up to a current density of 50 ma/cm^2. This buffering capacity is sufficient to allow evaluation of the effect of increased melt alkalinity on silver cathode activity. As shown in Table C-12, the increased melt alkalinity failed to improve silver cathode activity.

Table C-13

Oxygen Performance-Modified Phosphate Melt (Sintered Silver Electrodes, 250°C)

Current Density, ma/cm^2	Polarization from Theoretical Oxygen, Volts
0	0.43
1	0.63
5	0.78
10	0.94

Mixed silver-silver oxide electrodes were examined as cathodes in both unmodified phosphate melt, and carbonate treated phosphate melts. The electrodes were prepared by the standard sintering technique and contained 30 mg/cm^2 each of silver and silver oxide. No activity improvements were noted with either melt and pre-humidification of the oxygen had little effect on performance. The steady state performance data is given in Table C-13.

Table C-14

Oxygen Activity On Sintered Ag/Ag_2O Electrodes at 250°C(3)

Current Density, ma/cm^2	Polarization From Theoretical Oxygen, Volts			
	Phosphate Melt		Carbonate Treated Melt	
	O_2(1)	O_2(2)	O_2(1)	O_2(2)
0	0.40	0.38	0.39	0.37
5	0.74	0.78	0.74	0.74
10	0.81	0.85	0.78	0.82

(1) Dry oxygen
(2) Oxygen pre-humidified with 80°C water
(3) Standard Phosphate Melt

The activity of the silver-silver oxide electrode is considerably poorer than that of the silver cathodes. The poor showing of the silver-silver oxide and the silver cathodes may be due to the operating temperature rather than the melt properties. Silver cathodes are believed to function through a silver-silver oxide route and silver oxide is not stable (89) at 250°C. Consequently, a program was initiated to improve the oxygen performance by alloying silver with B subgroup elements and to use silver in conjunction with more stable oxide systems.

Part d - Silver Alloys or Co-Catalyst Systems

Production of silver alloys by borohydride reduction, high temperature hydrogen reduction, and combinations of the two reduction processes was attempted. It was not expected in all cases that complete reduction to the metals would occur, or that alloys would be formed. However, a possible result of the co-reduction could be the formation of a stable surface oxide-silver redox system that could be more active than silver for the oxygen dissolution reaction.

Solutions containing equimolar amounts of silver and cupric ion, silver and manganous ion, and silver ion were borohydride reduced. The precipitates were washed, dried, and only that fraction passing through 325 mesh sieve was used.

The precipitates from the silver and silver-cupric ion solution were conductive, but the precipipate resulting from the co-reduction of silver and manganous ion in solution was non conductive. These powders were fabricated into electrodes using the standard technique for making 50 mg/cm^2 sintered Teflon electrodes. Raney gold (50 mg/cm^2) was used to augment electronic conductivity. The electrodes were tested in 3 M KOH at 80°C and in the phosphate melt at 250°C, the results are given in Table C-14.

Table C-15

Oxygen Activity of Borohydride
Co-Reduced Silver-Group B Metal Cathodes

Current Density, ma/cm^2	Polarization From Theoretical Oxygen, Volts					
	Ag		Ag-Cu		Ag-Mn	
	KOH	Melt	KOH	Melt	KOH	Melt
0	0.19		0.26	0.31	0.28	0.25
5	0.28	0.62	0.50	--	0.33	--
10	0.30	0.65	0.56	--	0.35	--
50	0.40	0.72	--	--	0.45	--
100	0.46	0.77	--	--	0.51	--

The co-catalyst systems exhibited lower open circuit polarizations in the melt than silver electrodes, the decreases ranging from 0.14 to 0.2 volts. However, polarization even at low current density was very severe.

Some additional silver based catalysts were prepared and tested. Precipitates of silver tungstate, silver molybdate, and silver vanadate, prepared by titration of silver nitrate with the appropriate oxyanion, were treated with excess borohydride. The resultant solids were poor electronic conductors. Again (50 mg/cm^2) Raney gold electrodes were used to increase conductivity.

Table C-16

Cathode Activity of Borohydride Reduced
Silver Salts of Group IV and V Anions

Current Density, ma/cm^2	Polarization From Theoretical Oxygen, Volts					
	Reduced Silver Molybdate		Reduced Silver Tungstate		Reduced Silver Vanadate	
	3 M KOH	Melt	3 M KOH	Melt	3 M KOH	Melt
0	0.16	0.47	0.19	0.49	0.21	0.34
5	0.26	1.18	0.27	--	0.31	1.03
10	0.28	--	0.30	--	0.33	--
50	0.34	--	0.34	--	0.40	--
100	0.37	--	0.37	--	0.45	--
200	0.41	--	0.41	--	0.57	--

The cathodic activities of the reduced silver molybdate and silver tungstate catalysts in potassium hydroxide (Table C-15) are identical to that of active silver cathodes. This suggests that the reduced material is primarily silver and that the poor conductivity is probably due to a coating of molybdenum or tungsten oxides. As shown in Table C-15, these systems performed very poorly in the melt.

High temperature hydrogen reduction of the silver molybdates, tungstates and vanadates was carried out. It was hoped that more intense reducing conditions would produce more active systems. The oxygen activity of these catalysts is given in Table C-16.

Table C-17

Oxygen Performance of High Temperature (800°C)
Hydrogen Reduced Silver Salts of Group IV and V Anions

Current Density, ma/cm^2	Polarization From Theoretical Oxygen, Volts					
	Silver Molybdate		Silver Tungstate		Silver Vanadate	
	3 M KOH	Melt	3 M KOH	Melt	3 M KOH	Melt
0	0.43	0.35	0.41	0.56	0.32	0.50
1	0.43	0.53	0.48	>1	0.33	0.87
5	0.45	1.06	0.63	--	0.36	>1
25	0.46	--	>1	--	0.39	--
50	0.51	--	--	--	--	--
100	0.59	--	--	--	--	--

The activity of the hydrogen reduced silver co-catalysts is less than that of the borohydride reduced systems, both in aqueous potassium hydroxide and in the phosphate melt. No further work with the silver alloy or co-catalyst system is planned for the present.

Part e - Unsaturated Fuels

Ethylene was tested in the phosphate melt at 250°C to determine whether this electrolyte functions as an olefin polymerization catalyst in the same way that phosphoric acid does. Analysis of the melt after running on ethylene for seven hours, showed that hydrocarbon species are present. Presumably these compounds are similar to what is produced in phosphoric acid. The amount of this material is considerably less than that which would be produced in phosphoric acid for the same time interval at temperatures 100°C or more lower than the melt temperature. This difference is attributed to a melt hydrogen ion concentration that is several orders of magnitude lower than that of phosphoric acid. Fuel cells employing phosphate melt electrolytes could therefore tolerate higher levels of olefinic contaminants in the hydrocarbon feed. This in turn would lead to simplified fuel purification problems.

Phase 4 - Conclusions

Part a - Pyrophosphoric Acid Electrolyte Studies

Pyrophosphoric acid has been shown to be an effective electrolyte for the electro-chemical oxidation of butane, hexane, octane and decane. However, fuel humidification is important, and it appears that the optimum water-fuel ratio will vary with carbon number. Furthermore, at low water-fuel ratio's (0.88 mole H_2O/ mole fuel) current capability decreases markedly with carbon number dropping sharply between C_4 on a C_6. Higher water-fuel ratios could change this picture. For example, octane half cell data indicates that system power densities as high as 100 mw/cm^2 at 0.45 volts can be obtained with humidification using high loaded electrodes. This electrolyte system is also potentially useful in hydrocarbon reformer fuel cell systems since no carbon monoxide poisoning is noted at the 250-275°C operating temperature, even with 10% carbon monoxide in the reformer gas effluent. The absence of CO poisoning is also noted with low loaded supported platinum catalysts.

Extensive applications of the electrolyte to both the direct and indirect hydrocarbon fuel cell systems is hampered by its extreme corrosiveness. However, recent studies have demonstrated that suitable plastic composites can be developed which can tolerate this material. A 50 Wt% $Cd_{0.2}Wo_3$ Teflon composite has been subjected to 740 hours in 275°C pyrophosphoric acid with no evidence of mechanical or chemical deterioration. Teflon-graphite fiber composites should also be effective. Thus, it appears that suitable Teflon bonded cell components can be prepared.

The enhanced anodic and cathodic performance observed has led to an assessment of overall systems capability to determine if these improvements are reflected in system weight and catalyst economy. This study indicates that a butane or octane-air system can be designed with a significant reduction in catalyst loading (1400 vs 61 gm/kw) at a weight increase of only 14 lbs/kw. On the other hand, an approximate ten fold reduction in catalyst loading (454 to 56.2 gms/Kw) in the reformer air fuel cell requires a two fold weight increase (58.4 to 101.0 lbs/kw). Thus, in this electrolyte, low catalyst loaded direct hydrocarbon systems may have a weight advantage over comparable reformer systems. It is interesting to note that from a catalyst standpoint, both of low catalyst loaded systems (reformer and direct) are within a factor of three of the military target of 20 gm Pt/kw. Development of these systems concepts will continue.

Part b - Mixed Alkali-Metal Dihydrogen Phosphate Melts

The phosphate melt shows promise as an alternate intermediate temperature electrolyte for hydrocarbon-air systems. Tests with unsupported (50 mg/cm^2) anodes and cathodes indicate that a butane-oxygen system performance of 100 ma/cm^2 is possible. However, low catalyst density carbon supported anodes and cathodes do not show the anticipated utilization improvements. This is probably due to the fact that the sintered carbon electrode structure was optimized for aqueous electrolyte.

Raney Ni-Co alloy catalyst show some hydrogen activity (10 ma/cm^2) in this electrolyte with no evidence of corrosion. This bodes well for potential development of more active non-noble anode catalyst systems. Attempts to prepare active catalysts based upon silver and silver-silver oxides systems have thus far been unsuccessful even when the alkalinity of the electrolyte was increased by cesium carbonate addition. Efforts to improve cathodic performance of silver based systems

by incorporation of molybdenum, copper, vanadium and tungsten oxides have resulted in less active materials. Work on both non-noble anode and cathode catalysts for this system will continue.

SECTION 3

REFERENCES

(1) Heath, C. E., Tarmy, B. L., et al, Soluble Carbonaceous Fuel-Air Fuel Cell, Report No. 1, Contract DA 36-039 SC-89156, 1 Jan 1962 - 30 June 1962.

(2) Tarmy, B. L., et al, Soluble Carbonaceous Fuel-Air Fuel Cell, Report No. 2, Contract DA 36-039 SC-89156, 1 Jan 1962 - 31 Dec 1962.

(3) Tarmy, B. L., et al, Soluble Carbonaceous Fuel-Air Fuel Cell, Report No. 3, Contract DA 36-039 AMC-00134(E), 1 Jan 1963 - 30 June 1963.

(4) Tarmy, B. L., et al, Soluble Carbonaceous Fuel-Air Fuel Cell, Report No. 4, Contract DA 36-039 AMC-00134(E), 1 Jan 1963 - 31 Dec 1963.

(5) Heath, C. E., Holt, E. L., Horowitz, H. H.., Levine, D. G., Tarmy, B. L., et al, Hydrocarbon-Air Fuel Cell, Report No. 5, Contract DA 36-039 AMC-03743(E), 1 Jan 1964 - 30 June 1964.

(6) Heath, C. E , Holt, E L., Horowitz, H. H., Levine, D. G., Tarmy, B. L., et al, Hydrocarbon-Air Fuel Cell, Report No. 6, Contract DA 36-039 AMC-03743(E), 1 July 1964 - 31 Dec 1964.

(7) Epperly, W. R., Holt, E. L., Horowitz, H. H., Levine, D. G., et al, Hydrocarbon-Air Fuel Cell, Report No. 7, Contract DA 36-039 AMC-03743(E), 1 Jan 1965 - 30 June 1965.

(8) Heath, C. E., et al, Hydrocarbon-Air Fuel Cell, Report No. 8, Contract No. DA 36-039 AMC-03743(E), 1 July 1965 - 31 Dec 1965.

(9) Heath, C. E., et al, Hydrocarbon-Air Fuel Cell, Report No. 9, Contract No. DA 36-039 AMC-03743(E), 1 Jan 1966 - 31 July 1966.

(10) W. Ostertag, Inorg. Chem., 5, 758 (1966).

(11) C. V. Collins and W. Ostertag, J. Am. Chem. Soc. 88, 3171 (1966).

(12) S. Andersson and A. D. Wadsley, Acta Cryst. 15, 201 (1962).

(13) H. J. Borchardt, J. Chem. Phys. 39, 504 (1963).

(14) A.S.T.M. X-Ray Powder Diffraction Card 5-0431.

(15) K. Nassau, H. J. Levinstein, and G. M. Loiacono, J. Phys. Chem. Solids 26, 1805 (1965).

(16) A.S.T.M. X-Ray Powder Diffraction Cards 5-0392,3.

(17) A.S.T.M. X-Ray Powder Diffraction Cards 5-0386,7.

(18) S. Geller, Acta Cryst., 10, 248 (1957).

(19) M. J. Sienko, Advances in Chemistry Series No. 39, American Chemical Society, Washington, D. C., 1963, Paper 21.

(20) D. Vandeven, M. Pouchard, and P. Tagenmuller, Compt. Rend., 263C, 228 (1966).

(21) H. T. Tien, M. A. Thesis, Temple University, 1959.

(22) L. E. Conroy and T. Yokokawa, Inorg. Chem., 5, 994 (1965).

(23) A. R. Sweedler, J. K. Hulm, B. T. Matthias, and T. H. Getalle, Physics Letters, 19, 82 (1965).

(24) M. J. Sienko and P. F. Weller, Inorg. Chem., 1, 324 (1962).

(25) M. J. Sienko and B. R. Mazumder, J. Am. Chem. Soc., 82, 3508 (1960).

(26) M. J. Sienko and S. M. Morehause, Inorg. Chem., 2, 485 (1963).

(27) L. E Conroy and M. J. Sienko, J. Am. Chem., Soc., 79, 4048 (1957).

(28) F. T. Jones, Ph.D. Dissertation, Polytechnic Institute of Brooklyn (1960). Also see Diss. Abs. 21, 1390 (1960).

(29) E.O. Brimm, J. C. Brantley, J. H Lorenz and M. H. Jellinek, J. Am. Chem. Soc., 73, 5427 (1951).

(30) A. W. Sleight, Acta Chem. Scand. 20, 1102 (1966); S. Andersson, W G. Mumme and A. D. Wadsley, Acta Cryst. 21, 802 (1966).

(31) R. S. Roth and J. L. Waring, J. of Res. N.B.S. 70A 281 (1966).

(32) A. Magneli, Acta Cryst., 6, 495 (1953).

(33) P Gado, B. Holmberg and A. Magneli, Acta Chem. Scand. 19, 2010 (1965).

(34) A. D. Wadsley, Reviews Pure and Applied Chem., 5, 165 (1965).

(35) J. Marucco and P. Gerdanian, Compt. Rend., 262C, 1037 (1966).

(36) J. O'M. Bockris Private Communicate.

(37) B. W. Brown and E. Banks, J. Am. Chem. Soc., 76, 963 (1954).

(38) M. E. Straumanis and A. Dravnicks, J. Am. Chem. Soc. 71, 683 (1949).

(39) J. A. Shropshire, Electrochim. Acta, In Press.

(40) A. D. Wadsley, Chapter 3 in "Non-Stoichiometric Compounds" L. Mandelcorn, Ed., Academic Press, New York, 1964.

(41) W. Prandtl, Berichte 38, 657 (1905).

(42) W. Prandtl and H. Murschhauser, Z. anorg. u. allg. Chem., 56, 173 (1907).

(43) W. Prandtl and H. Murschhauser, Z. anorg. Chem 60, 441 (1908).

(44) H. Flood and H. Sorum, Tidsskrift For Kiemi, Bergvessen Og Metallurgi 3, 55 (1943); 5, 59 (1946).

(45) J. Galy, A. Casalot, M. Pouchard, and P. Hagenmuller, Compt. Rend., 262C, 1055 (1966).

(46) J. Galy and A. Hardy, Acta Cryst., 19, 432 (1965).

(47) B. V. Slobodin and A. A. Fortiev, Eng. Translation of J. Appl. Chem. USSR., 38, 799 (1965).

(48) A. A. Fotievand, B. V. Slobodin, Eng. Translation of J. Appl. Chem. USSR., 38, 512 (1965).

(49) A. M. Bystrom and H. T. Evans, Jr., Acta Chem. Scand., 13, 377 (1959).

(50) A. D. Wadsley, Acta Cryst., 8, 695 (1955).

(51) H. Flood, Th. Krog and H. Sorum, Tidsskrift For Kiemi Bergvessen Og Metallurgi 3, 33 (1945).

(52) S. Andersson, Acta Chem. Scand., 19, 137 (1965).

(53) M. J. Sienko and J. B. Sohn, J. Chem. Phys., 44, 1369 (1966).

(54) V F. Volfson, L. N. Ganyuk and E. F. Totskaya, Eng. Translation of Kinetics and Catalysis, 5, 974 (1964).

(55) M. Kestigian, J. G. Dickenson and R. Ward, J. Am. Chem. Soc., 79, 5598 (1957).

(56) A. Magneliand B. M. Onghton, Acta. Chem. Scand., 5, (1951).

(57) A. Magneli and B. Blomberg, Acta. Chem. Scand., 5, 585 (1951).

(58) N. Strupler and A. Morette, Compt. Rend., 260, 1971 (1965).

(59) G. Tridot, J. Tudo, G. Leman-Delcour and M. Nolf Compt. Rend. 260, 3410 (1965).

(60) H. A. Eick and L. K. Hiborg, Nature 211, 515 (1966).

(61) A. D. Wadsley and S. Andersson, Nature 192, 551 (1961).

(62) S. Andersson and A. D. Wadsley, Acta Cryst., 15, 201 (1962).

(63) A. D. Wadsley, Z. Krist., 120, 396 (1964).

(64) M. Kestigian and R. Ward, J. Am. Chem. Soc., 77, 6132 (1955).

(65) H. D. Megaw, Proc. Phys., Soc., 58, 133 (1955).

(66) D. Ridgley and R. Ward, J. Am. Chem. Soc., 77, 6132 (1955).

(67) F. S. Galasso and L. Katz, Acta Cryst., 14, 647 (1961).

(68) A. D. Wadsley, Acta Cryst., 17, 623 (1964).

(69) F. S. Galasso, L. Katz, and R. Ward, J. Am. Chem. Soc., 80, 1762 (1958).

(70) F. S. Galasso, L. Katz and R. Ward, J. Am. Chem. Soc., 81, 5898 (1959).

(71) F. S. Galasso and W. Darby, J. Phys. Chem., 68, 1253 (1964).

(72) A. Wald, W. Kunnmann, R. J. Arnott and A. Ferretti, Inorg. Chem., 3, 545 (1964).

(73) T. A. Bither, J. L. Gillson and H. S. Young, Inorg. Chem., 5, 559 (1966).

(74) J. Graham, N. C. Stephenson, A. D. Wadsley, and A. Wola Nature 206, 924 (1965).

(75) J. Graham and A. D. Wadsley, Acta. Cryst. 20, 93 (1966).

(76) N. C. Stephenson, Acta Cryst. 20, 59 (1966).

(77) W. H. McCarroll, R. Ward and L. Katz, J. Am. Chem. Soc., 78, 2909 (1956).

(78) W. H. McCarroll, L. Katz and R. Ward, J. Am. Chem. Soc., 79, 5410 (1957).

(79) F. A. Cotton, Inorg. Chem. 3, 1217 (1964).

(80) G. B. Ansell and L. Katz, Acta Cryst. 21. 482 (1966).

(81) Masatero Fukuola, Komei Asai and Tadayasu Mitsumata.

(82) Pourbaix, M., Atlas of Equilibie Electro-Chemique, Garthia-Villan.

(83) Latimer, W., Oxidation Potentials, 2nd edition Prentice-Hall, N.Y. 1952.

(84) O. Glamser and C. Naumann, Z. Quorg. Allgem. Chem., 265, 288 (1951).

(85) Heath, C. E., et al, Methanol-Air Fuel Cell, First Quarterly Report, Contract DA 28-043 AMC-02387(E), June - September 1966.

(86) Dubinin, Dokl. Acad Nank. SSSR 84, 93 (1952).

(87) Pope, N. J. and Peachey S. J., The alkyl Compounds of Platium, Proc. Regal Soc. Vol. 94, p. 571.

(88) S. J. Keating, Interum Technical Report on Silent Liquid Hydrocarbon-Air Fuel Cell Power Plant, October 8, 1965.

(89) Otto, E. M., J. Electro Chem. Soc. 113, 643, (1966).

(90) Heath, C. E., et al, Methanol-Air Fuel Cell, Second Quarterly Report, Contract DA 28-043 AMC-02387(E), 15 September - 15 December 1966.

APPENDIX A-1

ANODIC ACTIVITY OF THE RARE EARTH TUNGSTEN BRONZES

(Data Obtained in 3.7 M Sulfuric Acid Unless Otherwise Noted)

Volts From Reversible Hydrogen Potential	ma/5 cm^2	Gas
$Ce_{0.04}WO_3$		
0.40	0.03	N_2
0.40	0.08	H_2
0.94	0.01	N_2
0.94	0.08	H_2
$Ce_{0.1}WO_3$		
0.20	0.00	N_2
0.20	0.10	H_2
0.30	0.00	N_2
0.30	0.25	H_2
0.40	0.00	N_2
0.40	1.10	H_2
0.60	0.00	N_2
0.60	1.50	H_2
0.80	0.00	N_2
0.80	1.80	H_2
$Ce_{0.15}WO_3$		
0.94	0.05	N_2
0.94	0.18	H_2
$Sm_{0.1}WO_3$		
0.70	0.00	N_2
0.70	0.09	H_2
$Eu_{0.1}WO_3$		
0.40	0.01	N_2
0.40	0.36	H_2
0.94	0.01	N_2
0.94	0.97	H_2

APPENDIX A-1 (CONT'D)

ANODIC ACTIVITY OF THE
RARE EARTH RUNGSTEN BRONZES

(Data Obtained in 3.7 M Sulfuric
Acid Unless Otherwise Noted)

Volts From Reversible Hydrogen Potential	ma/5 cm^2	Gas
$Gd_{0.1}WO_3$		
0.40	0.00	N_2
0.40	0.26	H_2
0.94	0.01	N_2
0.94	1.00	H_2
$Dy_{0.1}WO_3$		
0.94	0.01	N_2
0.94	0.10	H_2
$Ho_{0.1}WO_3$		
0.70	0.01	N_2
0.70	0.05	H_2
0.94	0.01	N_2
0.94	0.25	H_2
$Yb_{0.1}WO_3$		
0.40	0.00	N_2
0.40	0.30	H_2
0.60	0.00	N_2
0.60	0.40	H_2
0.94	0.00	N_2
0.94	0.20	H_2
$Ce_{0.1}WO_3$ in 14.7 M Phosphoric Acid at 150°C		
0.40	0.00	N_2
0.40	0.50	H_2
0.94	0.80	N_2
0.94	1.40	H_2

APPENDIX A-2

X-RAY LINES OF $Cr_{0.05}WO_3$

a = 3.85 Å c = 3.80 Å

d Spacing, Å	Possible hkl
3.82	100
3.70	001
2.71	110
2.645	101
2.215	111
1.905	200
1.835	002
1.69	210 or 201
1.555	211
1.342	270
1.278	300
1.265	221
1.253	212
1.234	003
1.213	310
1.704	201
1.140	311

APPENDIX A-3

ANODIC ACTIVITY OF THE ACTIVE TRANSITION METALS IN THE TRANSITION METAL-TUNGSTEN-OXYGEN SYSTEM

Data Obtained in 3.7 M
Sulfuric Acid at 90°C

Volts From Reversible Hydrogen Potential	ma/5 cm^2	Gas
$Ti_{0.2}WO_3$		
0.40	-0.05	N_2
0.40	+0.10	H_2
0.80	+0.065	N_2
0.80	+0.13	H_2
$V_{0.2}WO_3$		
0.10	-0.60	N_2
0.20	+0.70	H_2
0.30	0.00	N_2
0.30	1.30	H_2
0.40	0.10	N_2
0.40	3.00	H_2
	Corrosion Occurs at 0.6 Volts Polarized	
$Mn_{0.2}WO_3$		
0.60	0.05	N_2
0.60	0.20	H_2
0.94	0.20	N_2
0.94	0.40	H_2
$Cr_{0.4}WO_3$		
0.94	0.20	N_2
0.94	0.24	H_2
$Fe_{0.2}WO_3$		
0.40	0.01	N_2
0.40	6.00	H_2
After 16 Hours		
0.40	0.01	N_2
0.40	2.80	H_2

APPENDIX A-3 (CONT'D)

ANODIC ACTIVITY OF THE ACTIVE TRANSITION METALS IN THE TRANSITION METAL-TUNGSTEN-OXYGEN SYSTEM

Data Obtained in 3.7 M Sulfuric Acid at 90°C

Volts From Reversible Hydrogen Potential	ma/5 cm^2	Gas
$Ni_{0.237}WO_3$		
0.40	0.00	N_2
0.40	0.22	H_2
0.60	0.075	N_2
0.60	0.265	H_2
0.80	0.08	N_2
0.80	0.40	H_2
$NiWO_3$		
0.60	0.60	N_2
0.60	1.15	H_2
0.94	3.40	N_2
0.94	3.90	H_2
$Zn_{0.2}WO_3$		
0.40	0.00	N_2
0.40	1.40	H_2
$Zr_{0.2}WO_3$		
0.94	0.12	N_2
0.94	0.22	H_2

APPENDIX A-4

SLURRY ELECTRODE CELLS

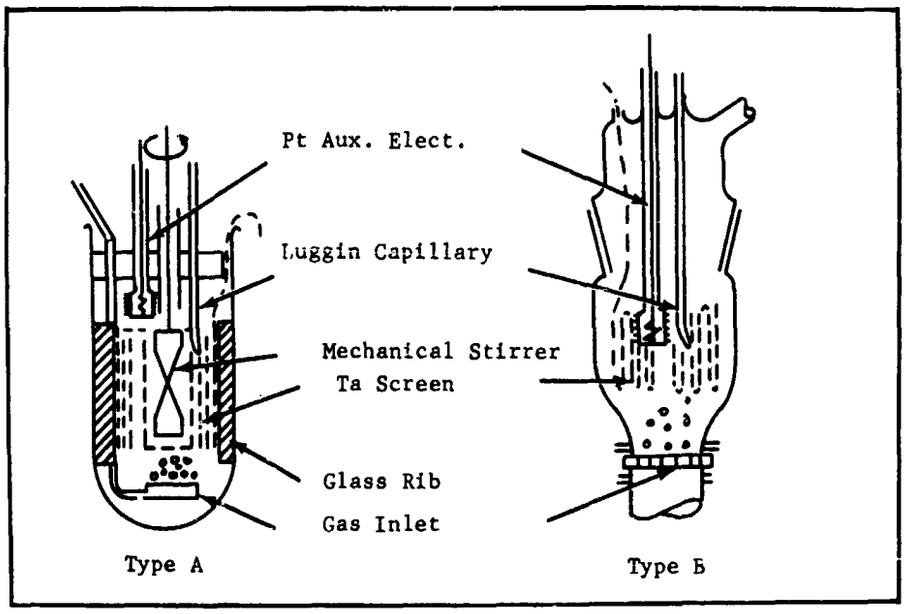

APPENDIX A-5

CORROSION OF $TiWO_3$ BY VOLTAGE SCAN

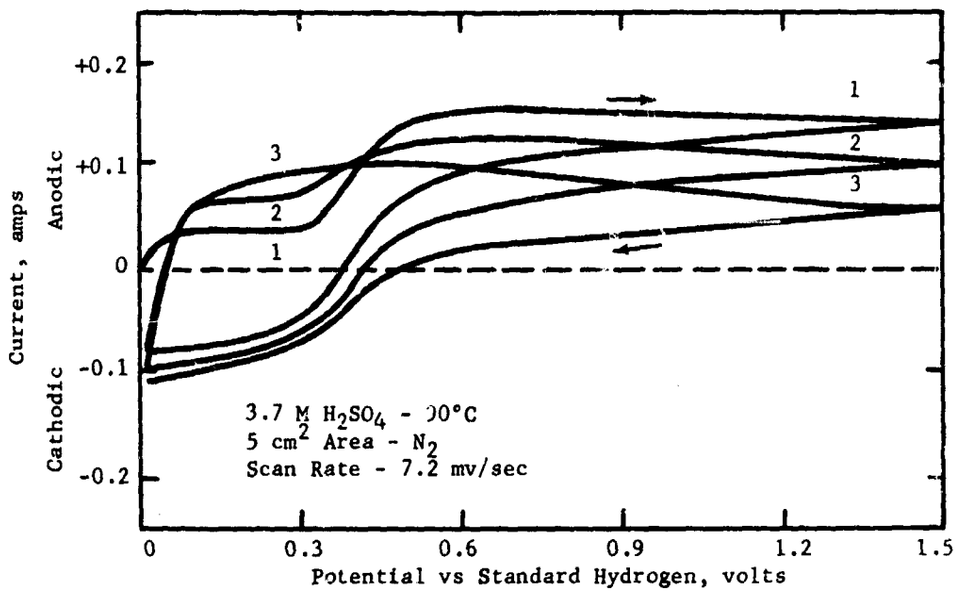

APPENDIX A-6

CORROSION OF $Mo_{0.2}WO_3$ BY VOLTAGE SCAN

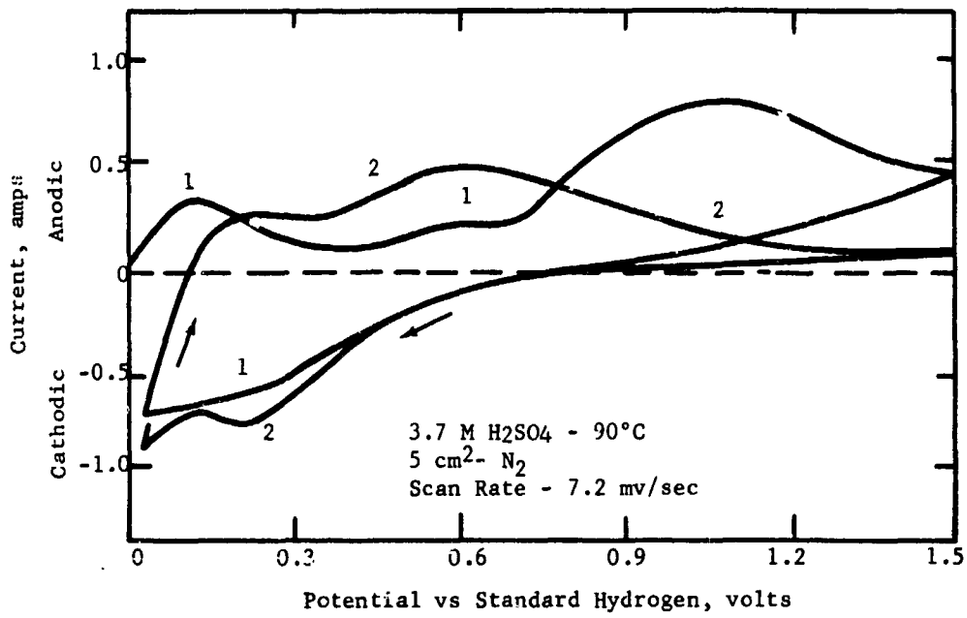

APPENDIX A-7

CORROSION OF $W_{0.2}WO_3$ BY VOLTAGE SCAN

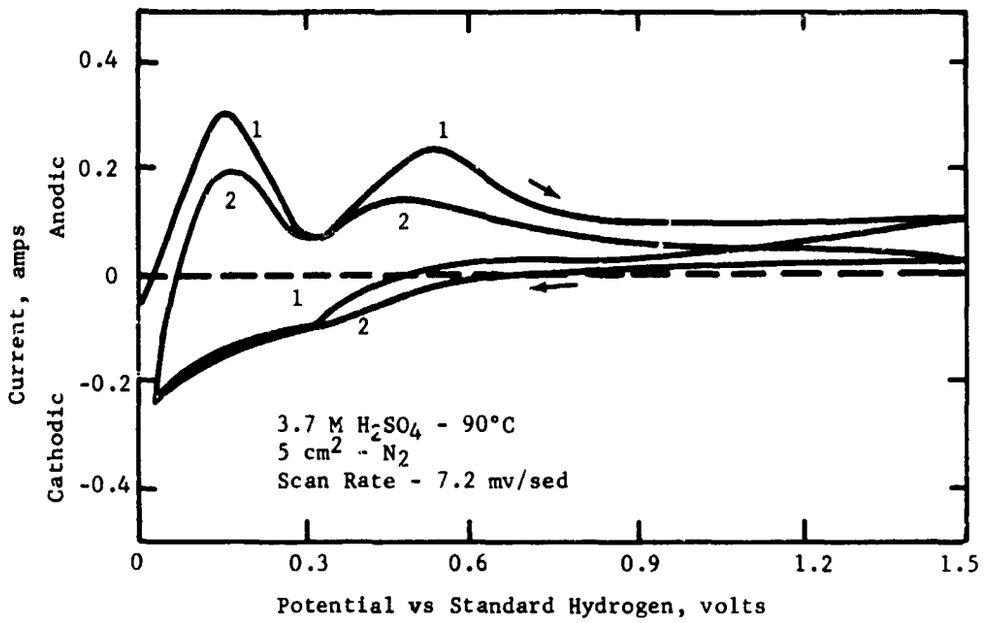

APPENDIX A-8

OPTIMUM PERFORMANCE OF Ga.IN BACKED CATHODES IN PYROPHOSPHORIC ACID AT 275°C

Current Density, ma/cm^2	Raney Gold(1)	Polarization From Oxygen Theory, Volts														
		$Fe_{0.2}WO_3$	$Sn_{0.8}WO_3$	$Mo_{.1}WO_3$(2)	$As_{0.01}WO_3$	$Co_{0.1}WO_3$	$Ni_{0.23}WO_3$	$Co_{0.2}WO_3$	$In_{0.2}WO_3$	$Mn_{0.2}WO_3$	$Sr_{0.2}WO_3$	$Y_{0.2}WO_3$	$La_{0.8}TiO_3$	NaO_5V	$Na_{0.33}V_2O_5$	$Ag_{0.33}V_2O_5$
0	0.44	0.53	0.86	0.52	0.45	0.43	0.47	0.51	0.57	0.48	0.56	0.75	0.74	0.04	0	0
1	0.54	0.57	1.17	0.62	0.73	0.64	0.62	0.56	0.65	0.69	0.62	0.75	1.0	0.24	0	0.11
5	0.65	0.63	--	0.72	0.84	0.74	0.74	0.63	0.79	0.79	0.68	0.81	--	--	0.31-0.4	--
10	0.72	0.66	--	0.76	0.87	0.79	0.80	0.66	0.90	0.83	0.73	0.90	--	--	1.0	--
15	--	0.68	--	0.78	1.0	0.83	0.84	0.67	1.0	--	--	--	--	--	--	--
25	0.77	0.70	--	0.82	--	0.89	0.86	0.69	--	0.88	--	1.04	--	--	--	--
50	0.83	0.77	--	--	--	1.04	0.95	0.74	--	--	0.88	--	--	--	--	--
75	1.01	0.77	--	--	--	--	--	0.79	--	--	--	--	--	--	--	--
100	--	0.78	--	--	--	--	1.04	0.83	--	--	--	--	--	--	--	--

(1) Catalyst density 150 mg/cm^2.
(2) Catalyst density 200 mg/cm^2

APPENDIX A-9

BUTANE PERFORMANCE OF OXIDE BRONZE ANODES IN PYROPHOSPHORIC ACID AT 275°C

Current Density, ma/cm²	Polarization from Butane Theory, volts — Butane Pre-humidified with Water at 80°C										
	$Fe_{0.2}WO_3$ (2)	$Ce_{0.1}WO_3$	$W_{0.1}WO_3$	$Ni_{0.237}WO_3$	$Sn_{0.2}WO_3$	$Ag_{0.1}WO_3$	$Co_{0.2}WO_3$	$In_{0.2}WO_3$	$Mn_{0.2}WO_3$	$Y_{0.2}WO_3$ (2)	$Sn_{0.8}NbO_3$
0	0.18	0.50	0.10	0.28	0.35	0.2	0.36	0.32	0.4	0.16	0
0.1	0.26	--	--	--	--	--	--	--	--	--	--
0.5	0.28	--	--	--	--	--	--	--	--	--	--
1.0	0.31	>1	0.96	>1	>1	>1	>1	>1	>1	0.28 (1)	>1
5.0	--	--	--	--	--	--	--	--	--	>1	--

(1) Polarization increases very slowly.
(2) This apparent activity may be due to trace platinum and is being checked.

APPENDIX B-1

BUTANE PERFORMANCE CARBON SUPPORTED CATALYSTS

(150°C - 14.7 M H_3PO_4 Sintered Carbon Teflon Electrodes)

Fabrication Symbol A - Teflon 42 BX, 2200 psi, 1 minute, 329°C, 85 C/15 TFE
B - Teflon 41 BX, 2200 psi, 1 minute, 349°C, 85 C/15 TFE

Catalyst Number	Electrode Number	Carbon Type	Wt % Platinum	Platinum Crystallite Size, Å	Catalyst Loading, mg Pt/cm²	Electrode Thickness, mils	Fabrication Symbol(1)	Butane Performance at 0.4 volts Polarized: Current Density, ma/cm²	Butane Performance at 0.4 volts Polarized: Utilization, ma/mg Pt	Limiting Butane Performance (0.45-0.48 v): Current Density, ma/cm²	Limiting Butane Performance (0.45-0.48 v): Utilization, ma/mg Pt	Remarks
328-45	328-85-2E	PC-20	11.47	--	2.48	23	A	15.0	6.2	20.0	8.3	10% O_3 treat.
328-66	328-85-3E	PC-20	10.91	--	2.30	23	A	10.0	4.3	10.0	4.3	10% O_3 treat + 10% SiO_2.
328-66	328-85-1E	PC-20	11.51	--	2.60	23	A	20.0	8.3	25.0	10.4	10% O_3 treat.
328-126-1	330-17	PC-20 hand ground through 100 on 250 mesh	4.57	18.4	1.90	24	A	25.0	13.1	30.0	13.8	10% O_3 treat.
328-134-1	330-18	PC-20 colloid milled	4.37	<18.0	1.82	24	A	30.0	16.4	35.0	19.2	10% O_3 treat
328-126-1	330-22	PC-20, hand ground	4.57	18.6	1.90	23	A	25.0	13.1	45.0	23.6	Repeat of electrode 330-17.
328-126-2	330-23	PC-30, hand ground	9.14	23.3	1.90	14.5	A	12.5	6.6	12.5	6.6	10% O_3 treat
328-134-2	330-24	PC-20, colloid milled	8.93	21.3	1.86	11-11.5	A	5.0	2.7	5.0	2.7	10% O_3, Teflon problem.
328-128-1	330-27	PC-20 ballmilled	4.38	19.3	1.82	--	A	5.0	2.7	5.0	2.7	Teflon problem.
328-140-4	330-30	PC-30, 20% CO_2 Treat	1.86	--	2.30	--	A	2.0	<1	3.0	<2.0	Pt trimethyl benzylchloride Ammonium
328-126-3	330-31	PC-20	12.15	37	2.50	11.5	B	12.5	5.0	15.0	6.0	
328-140-1	330-35	PC-30, 20% B.O.	2.09	28.4	1.13	31	A	32.5	29.0	32.5	29.0	Co-Pt.
328-140-2	330-36	PC-30 20% B.O.	1.50	23.0	1.25	32	A	40.0	32.0	40.0	32.0	Not stable.
							Fluid Oxomizer Study					
328-142-2	330-37	PC-20, hand ground	4.27	53.2	1.77	23	A	12.5	7.0	15.0	8.5	10% O_3 treat
328-142-1	330-38	PC-20, hand ground	6.44	85.0	2.70	23	A	17.5	6.4	20.0	7.4	5.0% O_3 treat
328-142-4	330-39	"	5.77	77.5	2.40	23	A	15.0	6.2	17.5	7.2	7.5% O_3 treat

APPENDIX B-1 (CONT'D)

BUTANE PERFORMANCE CARBON SUPPORTED CATALYSTS

Catalyst Number	Electrode Number	Carbon Type	Wt % Platinum	Platinum Crystallite Size, Å	Catalyst Loading, mg Pt/cm²	Electrode Thickness, mils	Fabrication Symbol (F)	Butane Performance at 0.4 volts Polarized Current Density, ma/cm²	Butane Performance at 0.4 volts Polarized Utilization, ma/mg Pt	Limiting Butane Performance (0.65-0.68v) Current Density, ma/cm²	Limiting Butane Performance (0.65-0.68v) Utilization, ma/mg Pt	Remarks
328-142-6	330-60	PC-20, hand ground	6.78	150	2.82	23	A	7.5	2.6	10.0	3.6	0% O_3 treat
328-142-5	330-62	"	4.48	63	1.86	23	A	7.5	4.0	10.0	5.4	15% O_3 treat
328-142-3	330-63	"	5.83	94.7	2.84	23	A	12.5	4.5	12.5	4.5	2.5% O_3 treat
328-142-2	330-65	"	4.27	53.2	2.37	30	B	17.5	7.4	17.5	7.4	10% O_3 treat
328-142-2	330-66	"	4.27	53.2	2.37	31	B 90/10	12.5	5.3	15.0	6.3	
328-142-2	330-67	"	4.27	53.2	2.37	--	B 95/5	16.6	7.0	20.0	8.4	
328-142-5	330-49	"	6.83	94.7	3.79	31	B	7.5	2.0	7.5	2.0	
328-142-6	330-50	"	6.78	100	3.76	32	B	14.0	3.7	15.0	3.8	
328-142-6	330-51	"	6.78	100	3.76	30	B 95/5	14.0	3.7	15.0	3.8	
328-142-4	330-52	"	5.77	77.4	3.20	31	B 95/5	10.0	3.1	10.0	3.1	
328-142-4	330-53	"	5.77	77.4	3.20	30	B	10.0	3.1	15.0	4.7	
328-142-5	330-54	"	4.48	63	2.50	30	B	8.0	3.2	10.0	4.0	
328-142-1	330-55	"	6.44	85	3.60	30	B	15.0	~ 2	20.0	5.5	
328-142-1	330-56	"	6.44	85	3.60	30	B 95/5	11.0	3.0	15.0	4.2	
328-142-3	330-57	"	6.83	94.7	3.80	30	B 95/5	10.0	2.6	10.0	2.6	
328-142-5	330-58	"	4.48	63	2.50	29	B	7.5	3.0	7.5	3.0	
						Co-Pt on Carbon Electrodes						
328-145-1	330-59	BC-72	23.00	--	2.50	9	A	---------- Unstable ----------				Pt-Co Structure feasibility test.
328-145-2A	330-60	"	2.50	(2)	1.11	34	A	7.0	6.4	--	--	
328-145-2A	330-61	"	2.50	(2)	1.11	34	A 95/5	3.0	2.7	--	--	
328-145-2B	330-62	"	5.05	42.6	2.2	26	A 80/20	20.0	9.1	25.0	11.4	
328-147-2B	330-64	"	5.05	42.6	1.10	16	A 80/20	10.0	9.1	15.0	13.6	
328-147-1B	330-65	PC-20, 10% O_3	11.50	(2)	2.31	14	A	4.0	1.7	5.0	2.1	
328-147-1A	330-66	"	3.56	(2)	1.43	24	A	12.5	8.7	15.0	10.5	
328-147-3B	330-68	BC-72	5.00	47.3	2.00	20	A 80/20	12.5	6.3	15.0	7.5	

APPENDIX B-1 (CONT'D)

BUTANE PERFORMANCE CARBON SUPPORTED CATALYSTS

Catalyst Number	Electrode Number	Carbon Type	Wt % Platinum	Platinum Crystallite Size, Å	Catalyst Loading, mg Pt/cm²	Electrode Thickness, mils	Fabrication Symbol(1)		Butane Performance at 0.4 volts Polarized: Current Density, ma/cm²	Butane Performance at 0.4 volts Polarized: Utilization, ma/mg Pt	Limiting Butane Performance (0.45-0.48v): Current Density, ma/cm²	Limiting Butane Performance (0.45-0.48v): Utilization, ma/mg Pt	Remarks
328-145-3B	330-69	Regal 330R	5.64	47.3	1.00	26	A		25.0	25.0	25.0	25.0	
328-147-1B	330-72	FC-20, 10% O_3	11.50	(2)	2.30	13	A		10.0	4.3	10.0	4.3	
328-147-1A	330-73	"	3.56	(2)	1.78	27	A		23.0	12.9	25.0	12.9	
328-147-3C	330-74	XC-72	8.13	48.7	2.19	20	A		40.0	18.2	45.0	20.5	
328-147-2C	330-75	FC-30, 28% B.O.	5.76	40.5	1.82	13	A		50.0	27.8	55-60	30.8	
328-147-2C	330-78	"	5.76	40.5	1.82	14	A		55.0	30.2	60.0	32.9	
328-147-2C	330-79	"	5.76	40.5	3.20	21	A		80.0	25.0	--	25.0	
328-147-2C	330-79	"	5.76	40.5	3.20	21	A		150.0	46.9	200.0	62.5	Co-Pt 200°C.
328-147-4C	330-76	Regal 330R	3.27	48.7	(2)	31	A		2.0	--	5.0	--	Catalyst ignited prior to activation.
328-147-3C	330-77	XC-72	8.13	48.7	2.20	20	A	80/20	30.0	13.6	33.0	15.1	
328-147-2A	330-83	FC-30	1.80	(2)	1.00	21	A		12.5	12.5	15.0	15.0	
328-147-3A	330-84	C-72	2.55	(2)	0.90	24	A		1.0	1.1	--	--	
328-147-4A	330-85	Regal 330R	--	(2)	--	27	A		2.0	--	--	--	
328-147-2C	330-86	FC-30 28% B.O.	5.76	40.5	4.00	30	A		45.0	11.0	55.0	13.0	
328-147-2C	330-86	"	5.76	40.5	4.00	30	A		100.0	25.0	110.0	27.5	15.1M H_3PO_4, 175°C.
328-147-2C	330-86	"	5.76	40.5	4.00	30	A		150-175	43.5	175.0	43.5	16.9M H_3PO_4, 200°C.
328-147-2C	330-86	"	5.76	40.5	4.00	30	A		120.0	30.0	140.0	35.0	18.9M H_3PO_4, 240°C. deteriorated after 1 hour

(1) Numbers denote change in Teflon content.
(2) Analytic data not yet complete.

APPENDIX B-2

BUTANE PERFORMANCE OF EXPERIMENTAL SUCROSE CARBONS

($150°C$ - 14.7 M H_3PO_4)

Catalyst Number	Electrode Number	Composition Sucrose: $ZnCl_2$	Carbon Surface Area, m^2/gm	Wt % Platinum	Platinum X-Ray Crystallite Size, Å	Loading, mg Pt/cm²	Butane Performance 0.4 volts Polarized: Current Density, ma/cm²	Butane Performance 0.4 volts Polarized: Utilization, ma/mg Pt	Limiting Butane Performance (0.45-0.48 v): Current Density, ma/cm²	Limiting Butane Performance (0.45-0.48 v): Utilization, ma/mg Pt
328-76	328-92-1E	2:1 Double Leached	929	7.24	60-65	3.1	30	9.7	45	14.5
328-78	328-92-3E	4:1 Double Leached	617	5.84	54-55	2.5	25	10	30	12
328-77	328-92-2E	4:1 Single Leached	667	7.18	54-55	3.06	15	3.9	30	9.8
328-75	328-92-5E	2:1 Single Leached	988	6.92	60-65	2.96	30	10	45	15
328-107	328-116-1E	2:1 10% O_3 Treat	--	6.0(1)	--	2.56(1)	20	--	25	--
328-108	328-116-2E	2:1 10% O_3 - 10% SiC_2	--	6.0(1)	--	2.56(1)	25	--	25	--
328-111	328-119-1E	1:1	--	8.9	--	3.8	25	6.6	30	7.9
328-112	328-119-3E	1:1	--	8.9	--	3.8	40	10.5	50	13.1
328-114	328-119-2E	2:1 ($FeCl_3$)	--	5.7	--	2.4	15	6.2	15	6.2
328-115	328-119-5E	3:1:1 $FeCl_3$, $ZnCl_2$	--	5.0(1)	--	2.2(1)	30	--	30	--
328-79	328-92-4E	8:1	215	2.56	25	1.1	3	2.9	4	3.8

(1) Nominal % Pt analytic data not yet available.

APPENDIX B-3

POTENTIAL ADSORBATES

Inorganic Salts	Comment
Nickelous Chloroplatinate	Alloy attacked by acid could be used if Ni is leached out to produce increased surface area or smaller crystallites, not examined further at present.
Cobaltous Chloroplatinate	Alloy corrosion resistant to 3.7 M sulfuric and 14.7 M phosphoric acid. Analogous d bond occupancy to optimum Ni-CO hydrogen catalyst.
Ammonium Chloroplatinate	Neutral salt presumably same as that made by neutralizing H_2PtCl_6 with amonia to pH 6.
Tetra amino platinum (IV) chloride	Cationic platinum salt.
Organic Salts	
Platinum trimethyl benzl Ammonium Chloride	Benzene soluble
$(CH_3)_3PtI$	Thermally decomposes to Pt, I, C,+ H_2 prepared, initial performance poor.
$(CH_3)_4Pt$	Material in preparation decomposes thermally to Pt, carbon and hydrogen.

APPENDIX B-4

PERFORMANCE OF POROUS TEFLON SUPPORTED ELECTRODES

(14.7 M H_3PO_4 150°C)

Electrode	Loading, mg/cm^2	Reactant	Polarization At Indicated ma/cm^2, volts							
			0	1	5	10	50	100	200	300
Uncoated		O_2	0.15	--	--	0.28	0.48	0.65	--	--
Porous TFE	1.25	H_2	0.012	--	--	0.012	--	0.031	0.051	0.066
Support	Pt-10 IR	Butane	0.21	0.29	0.64	(4 ma/cm^2 @ 0.40 volts)				
Gold Coated		O_2	0.16	--	--	0.33	0.42	0.47	--	--
Porous TFE	1.25	H_2	0.010	--	--	0.01	--	0.026	0.043	0.067
Support		Butane	0.12	0.38	0.64	--	--	--	--	--
Chemcell	2.0	O_2	0.12	--	--	0.22	0.29	0.33	0.37	--
		H_2	0.001	--	--	0.021	--	0.026	0.027	0.027
		Butane	0.26	0.34	38	(8 ma/cm^2 @ 0.44 volts)				

APPENDIX C-1

OCTANE PERFORMANCE IN PYROPHOSPHORIC ACID WITH PRE-METERED FEED

Current Density, ma/cm^2	Polarization From Theoretical Octane, Volts		
	Steam Vaporized 1 mole H_2O/mole Octane	Electrode #1 9 moles H_2O/mole Octane	Electrode #2 9 moles H_2O/mole Octane
0	0.18	0.09	0.10
10	0.31	0.18	0.25
25	--	0.24	0.28
50	0.38	0.28	0.30
100	0.43	0.31	0.35
200	0.48	0.32	0.37
300	0.59	0.36	0.47
400	0.58	0.39	--

APPENDIX G-2

SCHEMATIC FEED PREPARATION SYSTEM - PYROPHOSPHORIC ACID TESTS

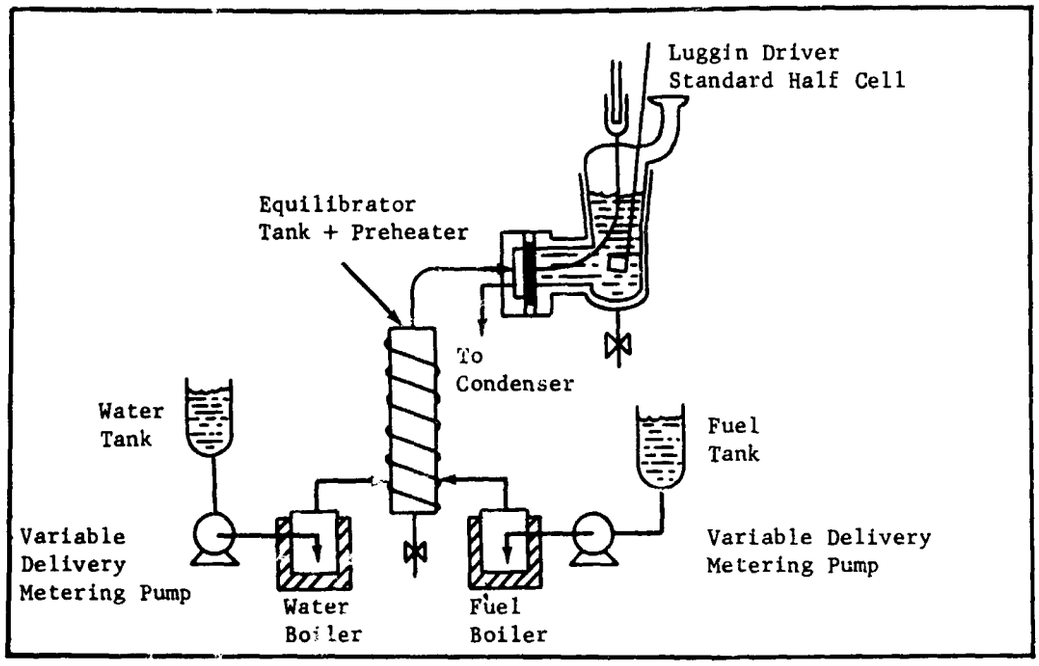

APPENDIX C-3

WEIGHTS OF VARIOUS FUEL CELL COMPONENTS
WEIGHT BURDEN PER STACK(1)

	lbs
Dual purpose end plates(3)	9.2
Spring tension units (10 ea)	0.13
Stainless steel bolts(2)	1.1-2.2
Bussing connections	0.8
Feed lines	0.4
	11.63-12.13

(1) Maximum stack-length 24" including end plates (92 cell maximum)
(2) 1.1 for 1/2 length 2.2 for 14" stack
(3) Could be reduced to 5 lbs

CELL COMPONENT WEIGHTS

	lbs
Air chamber (102 mils)(2) + electrode + current collector	0.24
Fuel chamber (102 mils)(2) + electrode + current collector	0.24
Electrode chamber (20 mils) + electrolyte	0.10
Cell separator (20 mils)	0.015
Bussing	0.10
Total	0.695

(2) Cell spaced 0.25" per cell

APPENDIX C-4

SUMMARY SHEET-BUTANE AIR FUEL CELL

	High Loaded Electrodes 150 ma/cm^2	Low Loaded Electrodes 2.9 mg/cm^2
Number of cells	243.0	320.0
No of stacks	3.0	4.0
Stack voltage, volts	40.0	40.0
Fuel cell stack	207.0	273.2
Air loop + CO_2 scrubber regenerator	76.0	78.0
Heat exchangers + coolant loops	30.0	30.0
Fuel loop + circulator	6.5	9.5
Blower	3.0	3.0
Voltage regulator	15.0	15.0
Battery	10.0	10.0
Insulation	25.0	25.0
Fuel tankage lpg	10.0	10.0
Total wt	382.5	452.7
lb/kw	76.5	90.5

APPENDIX C-5

SUMMARY SHEET-OCTANE-AIR

	High Loaded Anode & Cathode 100 mg/cm^2
Number of cells	192.0
Number of stacks	3.0
Stack voltage	32.0
Fuel cell stack	178.5
Air loop and CO_2 scrubber regenerator	76.0
Heat exchange and collant loops	30.0
Fuel loop circulator	6.5
Vaporizer fuel	9.2
Blower	3.0
Voltage regulator	15.0
Battery	10.0
Insulation	25.0
Total wt	353.2
lb/kw	70.7

APPENDIX C-6

HYDROGEN GENERATOR WEIGHTS

5.63 kw Electrical Load

	Lbs
Reformer (Reactor + shift converter, no diffusor)	37.0
Boiler	12.8
Burner + Feed pumps	12.5
Piping, controls + insulator tanks	55.0
Liquid fuel	6.0
Weight	123.3

APPENDIX C-7

SUMMARY SHEET REFORMER-AIR FUEL CELL

	Unsupported Pt High Loaded 100 mg/cm^2	Pt on Carbon 2.9 mg/cm^2
Number of cells	80.0	320.0
Number of stacks	1.0	4.0
Voltage	30.0	40.0
Fuel cell stack	68.3	273.2
Fuel and oxidant loop	6.5	9.5
Heat exchangers	18.7	18.7
Controls	5.3	11.0
Coolant loop + pumps	14.5	15.5
Insulation	25.0	25.0
Voltage regulator	15.0	15.0
Battery	10.0	10.0
	163.3	377.9

Security Classification

DOCUMENT CONTROL DATA - R&D

(Security classification of title, body of abstract and indexing annotation must be entered when the overall report is classified)

1. ORIGINATING ACTIVITY *(Corporate author)*
Esso Research and Engineering Company
Government Research Laboratory
Linden, New Jersey

2a. REPORT SECURITY CLASSIFICATION
Unclassified

2b. GROUP

3. REPORT TITLE

HYDROCARBON-AIR FUEL CELL

4. DESCRIPTIVE NOTES *(Type of report and inclusive dates)*
Semi-Annual - 1 August 1966 - 31 December 1966

5. AUTHOR(S) *(Last name, first name, initial)*

Heach, Carl E.; Okrent, Eugene H.; Beltzer, Morton; Broyde, Barret

6. REPORT DATE
June, 1967

7a. TOTAL NO. OF PAGES
94

7b. NO. OF REFS
90

8a. CONTRACT OR GRANT NO.
DA 36-039 AMC-03743(E)

b. PROJECT NO.
AMC Code: 1C622001A053-04

c.

d.

9a. ORIGINATOR'S REPORT NUMBER(S)

9b. OTHER REPORT NO(S) *(Any other numbers that may be assigned this report)*
ECOM-03743-10

10. AVAILABILITY/LIMITATION NOTICES
Each transmittal of this document outside the Department of Defense must have prior approval of CG, U.S. Army Electronics Command, Fort Monmouth, N.J.
ATTN: AMSEL-KL-PE

11. SUPPLEMENTARY NOTES

12. SPONSORING MILITARY ACTIVITY
U.S. Army Electronics Command
Fort Monmouth, New Jersey 07703
ATTN: AMSEL-KL-PE

13. ABSTRACT

Studies aimed at the development of a direct hydrocarbon-air fuel cell system for moderate temperature and pressure operation indicates that anode electrocatalysis is the key problem area. Research emphasized (1) improving platinum catalyst utilization and (2) developing a non-noble hydrocarbon catalyst. Studies aimed at defining the range of catalytically active non-noble metal-tungsten oxides have shown that a wide variety of metals can produce electrochemically active anodes and cathodes. Most of the first row transition metal-tungsten oxides and magnetic rare earth tungsten bronzes show both anodic and cathodic activity. All of these materials were active as cathodes. This appears to be a general property of the conductive tungsten oxides. These metal tungsten oxygen systems also show promise for use in 275°C pyrophosphoric acid electrolytes. No significant corrosion was observed even though the $Fe_{0.2}WO_3$ could sustain 100 ma/cm^2 on oxygen.

Supported platinum catalysts continue to show promise of significant hydrocarbon activity improvement. A new Co-Pt on FC-30 carbon catalyst has shown significant utilization at temperatures ranging from 150 to 275°C. For example, a 1.5 mg Pt/cm^2 electrolyte (13 mils thick) yielded 200 ma/cm^2 of 0.45 volts polarized on butane (110 ma/mg Pt) in 200°C phosphoric acid.

Pyrophosphoric acid electrolyte was shown to be an effective intermediate temperature electrolyte. Octane half cell data indicate that power density of up to 100 mw/cm^2 can be obtained and operation with unpurified reformer gas would not result in performance debit. Phosphate melts continue to show promise as an alternate electrolyte for this temperature range.

DD FORM 1 JAN 64 1473

Security Classification

Security Classification

14. KEY WORDS	LINK A ROLE	LINK A WT	LINK B ROLE	LINK B WT	LINK C ROLE	LINK C WT
Hydrocarbon Oxidation						
Adsorption Mechanism						
Catalyst Utilization						
Electrochemical Activity						
Non-Noble Catalysts						
Buffer Electrolytes						
Limiting Currents						
Noble Metal Alloy Catalysts						
Electrode Structure						
Catalyst Supports						

INSTRUCTIONS

1. ORIGINATING ACTIVITY: Enter the name and address of the contractor, subcontractor, grantee, Department of Defense activity or other organization *(corporate author)* issuing the report.

2a. REPORT SECURITY CLASSIFICATION: Enter the overall security classification of the report. Indicate whether "Restricted Data" is included. Marking is to be in accordance with appropriate security regulations.

2b. GROUP: Automatic downgrading is specified in DoD Directive 5200.10 and Armed Forces Industrial Manual. Enter the group number. Also, when applicable, show that optional markings have been used for Group 3 and Group 4 as authorized.

3. REPORT TITLE: Enter the complete report title in all capital letters. Titles in all cases should be unclassified. If a meaningful title cannot be selected without classification, show title classification in all capitals in parenthesis immediately following the title.

4. DESCRIPTIVE NOTES: If appropriate, enter the type of report, e.g., interim, progress, summary, annual, or final. Give the inclusive dates when a specific reporting period is covered.

5. AUTHOR(S): Enter the name(s) of author(s) as shown on or in the report. Enter last name, first name, middle initial. If military, show rank and branch of service. The name of the principal author is an absolute minimum requirement.

6. REPORT DATE: Enter the date of the report as day, month, year; or month, year. If more than one date appears on the report, use date of publication.

7a. TOTAL NUMBER OF PAGES: The total page count should follow normal pagination procedures, i.e., enter the number of pages containing information.

7b. TOTAL NUMBER OF REFERENCES: Enter the total number of references cited in the report.

8a. CONTRACT OR GRANT NUMBER: If appropriate, enter the applicable number of the contract or grant under which the report was written.

8b, 8c, & 8d. PROJECT NUMBER: Enter the appropriate military department identification, such as project number, subproject number, system numbers, task number, etc.

9a. ORIGINATOR'S REPORT NUMBER(S): Enter the official report number by which the document will be identified and controlled by the originating activity. This number must be unique to this report.

9b. OTHER REPORT NUMBER(S): If the report has been assigned any other report numbers *(either by the originator or by the sponsor)*, also enter this number(s).

10. AVAILABILITY/LIMITATION NOTICES: Enter any limitations on further dissemination of the report, other than those imposed by security classification, using standard statements such as:

(1) "Qualified requesters may obtain copies of this report from DDC."

(2) "Foreign announcement and dissemination of this report by DDC is not authorized."

(3) "U. S. Government agencies may obtain copies of this report directly from DDC. Other qualified DDC users shall request through _____."

(4) "U. S. military agencies may obtain copies of this report directly from DDC. Other qualified users shall request through _____."

(5) "All distribution of this report is controlled. Qualified DDC users shall request through _____."

If the report has been furnished to the Office of Technical Services, Department of Commerce, for sale to the public, indicate this fact and enter the price, if known.

11. SUPPLEMENTARY NOTES: Use for additional explanatory notes.

12. SPONSORING MILITARY ACTIVITY: Enter the name of the departmental project office or laboratory sponsoring *(paying for)* the research and development. Include address.

13. ABSTRACT: Enter an abstract giving a brief and factual summary of the document indicative of the report, even though it may also appear elsewhere in the body of the technical report. If additional space is required, a continuation sheet shall be attached.

It is highly desirable that the abstract of classified reports be unclassified. Each paragraph of the abstract shall end with an indication of the military security classification of the information in the paragraph, represented as *(TS)*, *(S)*, *(C)*, or *(U)*.

There is no limitation on the length of the abstract. However, the suggested length is from 150 to 225 words.

14. KEY WORDS: Key words are technically meaningful terms or short phrases that characterize a report and may be used as index entries for cataloging the report. Key words must be selected so that no security classification is required. Identifiers, such as equipment model designation, trade name, military project code name, geographic location, may be used as key words but will be followed by an indication of technical context. The assignment of links, rules, and weights is optional.

Security Classification